SUPPORTING STUDIES IN CLOUD IMAGE PROCESSING FOR PLANETARY FLYBYS OF THE 1970'S

A REPORT

from the space science and engineering center
the university of wisconsin-madison
madison, wisconsin

SUPPORTING STUDIES IN CLOUD IMAGE PROCESSING FOR PLANETARY FLYBYS OF THE 1970'S

A Semi-Annual Progress Report
on
NASA Grant NGR 50-002-189

for the period
1 July 1976 through 30 December 1976

Verner E. Suomi, Principal Investigator
Robert J. Krauss, Program Manager

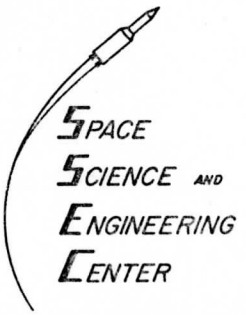

University of Wisconsin-Madison
1225 W. Dayton Street
Madison, Wisconsin 53706

30 March 1977

The six month period starting with July 1976 has been quite productive. Many of the tasks begun earlier in the year are now completed, the major scientific results have been disseminated to the scientific community, and a Ph.D. thesis supported by this grant is nearing completion and will be finished by late Spring. Most of the work concerning interpretation of the general circulation of the Venus stratosphere based on our existing measurements of Mariner 10 data should be completed by the end of Summer. We hope to report on this at the Ottawa Symposium on Planetary Atmospheres, 16-19 August 1977. In essence, we have to date identified the existence on Venus of: hemispheric vortices, solid rotation at the poles accompanied by a significant difference in cloud albedo, near conservation of angular momentum at low latitudes, small meridional flow probably due to near cyclostrophic balance, and spiral streaks shaped by shear. In October 1974 at the GISS Conference on Venus, these were presented as mere speculations. Evidence now exists to support all of them.

We have, in addition, found evidence for possible eddy transport, possible global scale waves, possible phase transitions, vertical wind shear, and optically active light and dark regions. During the next year we must work to quantitatively define the magnitude and extent of these phenomena, characterize the organization and lifetimes of smaller scale cloud systems, and attempt to better understand what is becoming more and more a highly complex and finely structured cloud system. Clearly, more work must be done in analyzing the Mariner 10 data. With our newly developed precision navigational tools and the ability to properly organize the data in the time domain, we are ready to proceed. The key to our future progress lies in the fact that we can now remove both the effects of varying illumination and of the mean zonal flow from the images, so that it is possible to detect and accurately measure the order of magnitude smaller motions which contain the key information about fluctuations in the large-scale dynamic structure.

The power of these techniques is best illustrated in a 20 minute long 16 mm color sound movie which we produced in December. The movie describes the image navigation techniques and measuring procedures we use and shows some of the Venus UV cloud features in motion in perspective, mercator, and polar stereographic projections. This movie was shown at the annual meeting

of the Division of Planetary Sciences of the American Astronomical Society in January 1977, and to the Mariner Jupiter/Saturn imaging science team, to the Pioneer Venus Atmospheric Working Group, and to groups at the Jet Propulsion Lab, University of Arizona, and Ames Research Center. The overall response from the scientific community has been highly positive, even though the movie was a somewhat crude "in-house" test of our techniques and does not have professional scripting, editing, and polish. At some later date, we will produce a final version. It is evident that this is a very good way to communicate subtleties of atmospheric structure and motion. A copy of the existing movie has been sent to Dr. Robert Fellows at NASA Headquarters.

COMPLETED WORK

Besides the 16 mm movie of Venus, a number of reports were prepared covering various aspects of work under this grant. They are attached as appendices to this report, and we will give a brief explanation of each one here:

1. The measurement of absolute cloud motions in the first 36 hours worth of Venus flyby images has been made possible by completion and testing of a new image navigation program developed by Kuhlow and Phillips and described in Appendix A. The navigation program we have been using for cloud motion measurements up to now depends on a least squares fit to the bright limb of Venus to define the planet center. If there is not sufficient arc length in an image, the planet center is not adequately defined, so that the navigation and resulting cloud motion measurements are inaccurate.

   Those early Mariner 10 images are extremely important to our research for several reasons: a) they add about 40% of additional time base to permit study of global scale wave phenomena with periods >2 1/2 days; b) they are the only source of high resolution details of a scale height or smaller and are needed to adequately discriminate and measure phase velocities, vertical wind shear, and convective phenomena; and c) they are needed to fully characterize atmospheric motions and dynamic organization over the entire range

of observable scales. The high resolution data may be of great value in allowing us to measure dynamic features superimposed on the mean flow. This new navigation scheme will make such measurements possible.

2. Appendix B is a report by Krauss on a streak line analysis of the Venus global cloud motion field. Belton, et al. (JAS 33, 1394 , 1976) published mercator projections of Mariner 10 images of the Venus clouds. In the pictures, one can see correlation of spiral streak curvature, latitude position of the bright polar cloud band, and albedo of large scale low latitude cloud features. In our previous semi-annual report, we indicated that all of the correlated visual changes in the mercator projections were also correlated with the time variation of our large scale velocity measurements. This paper shows that there is a direct quantitative relation between curvature of the spiral streaks and the global scale motion field. It is possible to invert that relation to infer the velocity field from the streak shape. Then, one obtains a correlation of velocity field fluctuations with position of the polar band and with cloud albedos at low latitude. One interpretation of such a correlation is that a large wave with a 4 1/2 day period encircles the planet. One can speculate that such a wave, coupled to mean global albedo, serves as a means of driving the global vortex and also a means of maintaining its dynamic stability.

3. The existence of large scale waves in the stratosphere of Venus, embedded in the hemispheric vortices, is further examined by Limaye in Appendices C, D, and E. Inertial waves on Earth are relatively small and not of much practical use to a meteorologist. On Venus, such waves can have a global extent and periods of several days or more, varying with latitude. Up to now, they have not been seriously considered in connection with Venus. In Appendix C, an abstract read at the DPS meeting in January 1977, Limaye makes the point that inertial waves are possibly quite important in interpreting the stratospheric motions on Venus.

Appendix D is a reprint from the Journal of Atmospheric Sciences, of a paper originally given by Suomi and Limaye at the April 1976 DPS meeting at Austin, Texas. It is possible to remove the effect of lighting

conditions (solar zenith angle) on the sphere of Venus by using the observed fact that the stratosphere of Venus is almost completely isotropic in its scattering properties. As a result, Suomi and Limaye find a much higher cloud albedo at the poles, indicative of a different cloud structure or scattering property.

In Appendix E, they now carry the work one step further by remapping the brightness normalized images onto a series of polar stereographic projections. These projections demonstrate the differential rotation of the stratospheric clouds in graphic form and supply further evidence of vortex structure in the stratosphere. It is impossible to match up pie-shaped wedges along any straight radial cut at all latitudes. Instead, one must cut the abutting regions along curved lines defined by the latitudinal gradient of zonal velocity. This produces a polar mosaic with a structure very reminiscent of a hurricane on Earth. Moreover, the bright polar cloud is shown to depart from axial symmetry, having an elliptical shape suggesting wave number two at high latitudes.

PROPOSED FUTURE WORK

In any planetary atmosphere the general circulation is constrained by the requirement to transfer heat from regions of excess to regions of deficiency, but the motion must satisfy overall momentum balance. These requirements can be satisfied with a specific steady or symmetric flow or with wave motions. On the Earth we have both, but mainly wave motion, while on Venus we also have both, but mainly steady motion. It would be very helpful to establish a better estimate of the fraction each type of motion contributes to the overall momentum and heat budgets. We now have a carefully navigated data set where this is possible. Therefore we have proposed to provide:

1. Descriptions of global scale wave phenomena, e.g. polar wave phenomena, mid latitudes, and tropical wave phenomena.

   This will primarily involve extending our observation time base to earlier and higher resolution images, and stratifying the data by latitude, longitude, and time. By using enough measurements, it may be possible to uniquely define amplitudes and phase relationships in the velocity measurements.

2. Details of small scale wave motions, e.g. phase velocities, wavelengths, lifetimes, interactions with mean flow, etc.

   Our new navigation scheme will permit us to gain access to an entirely new domain of scales in time and space. We can see evidence of small scale waves, but need better observations to quantify them.

3. Estimates of vertical wind shear and relative cloud heights.

   If we can quantify horizontal motions as a function of height, we gain access to information concerning latitudinal temperature gradients and vertical cloud structure. These are crucial aspects of study if we intend to examine radiative balance and global energy transport.

4. Organization of cloud streets, convection, spiral bands.

   In the high resolution mosaics of Venus, there are many examples of organization of cloud forms not necessarily related to waves. These too should be examined in detail.

5. Estimates of lifetimes of cloud systems as functions of scale.

   The estimation of lifetimes of cloud features is extremely important to interpretation of the motion field for two reasons: first, it permits scale analysis of the motion field which will help us select valid dynamic mechanisms and estimate their strengths, and secondly, it may aid us in answering the perplexing question of how we can see so many clear examples of wave phenomena in an atmosphere devoid of condensates.

6. Composite views of the entire planet's cloud system.

   An extremely useful way to understand atmospheric motions is to observe them in the proper Lagrangian frame of reference by remapping to different coordinates. This method of analysis needs more work, but in the case of our mercator and polar projections has already yielded evidence of substantially more complex structure in the motion field than even the sets of cloud motion measurement have heretofore indicated.

APPENDIX A

NAVIGATION OF VENUS MULTIFRAME MOSAICS

William W. Kuhlow and Dennis R. Phillips

Space Science and Engineering Center

University of Wisconsin-Madison

Madison, Wisconsin

November, 1976

I. INTRODUCTION

Accurate determination of Venus coordinates from Mariner 10 data image coordinates have been, until recently, restricted to single frames of resolution around 8 km in which a sufficient portion of the bright Venus limb was in view. Image coordinate measurements from this bright edge were necessary to uniquely determine the navigation transform from image to Venus coordinates.

Navigation of high resolution image frames is more difficult because most of the frames making up a Venus mosaic do not contain bright edges at which measurements can be made; furthermore, each frame has a slightly different perspective of the planet due to spacecraft motion.

A self-consistent iterative procedure has been developed in which multi-frame mosaic navigation is possible for any connected configuration of overlapping high resolution image frames from a Venus sequence providing that:

(1) some of the frames contain portions of the Venus limb from which edge measurements can be made and that these measurements (from either the same or different frames) span a reasonably large arc-angle along the limb;

(2) a Venus feature common to each pair of overlapping frames can be identified and the image coordinates measured.

The procedure accounts for changes in the spacecraft's position and results in a unique navigation transform for each of the frames. Once navigated, each frame contains all the information necessary for accurate image to coordinates transformations and may be dealt with on an individual basis.

II. VENUS NAVIGATION FOR A SINGLE IMAGE FRAME

This section discusses the equations used in the navigation of a single image frame; these equations also form the mathematical basis for the Venus multiframe-mosaic navigation.

1. Definitions

The following parameters† are available for each Venus image frame:

(θ_s, ϕ_s) = Venus latitude and longitude, respectively, of the sub-spacecraft point

(θ_H, ϕ_H) = Venus latitude and longitude of the sub-solar point

a = Venus radius at visible limb as determined from UV images (a = 6131 km)

h = height of spacecraft (km)

(θ_L, θ_E) = FOV angles in the scan line and element directions (degrees)

(T_L, T_E) = total number of scan lines per FOV image and total number of elements per FOV scan line.

In addition to these available parameters, the following are defined (refer to FIGURES II.1 and II.2):

(θ, ϕ) = Venus latitude and longitude of an arbitrary feature

(ρ_L, ρ_E) = angle in radians subtended per image scan line $(\pi\theta_L/180T_L)$ and per element $(\pi\theta_E/180T_E)$

(L, E) = line and element value of an arbitrary image point

(L_c, E_c) = image center line and element $(L_c = T_L/2;\ E_c = T_E/2)$

---

†The parameters (θ_s, ϕ_s), (θ_H, ϕ_H) and h are available from the JPL/Mariner 10 Supplementary Experimenter Data Records (SEDR).

(λ,δ) = angle between L and L_c at picture center and between E and E_c at picture center

$\vec{r}_v$ = vector pointing from Venus center to Venus feature ($\|\vec{r}_v\| = a$, where $\|\vec{r}_v\|$ is the vector norm of $\vec{r}_v$)

$\vec{b}$ = vector pointing from Venus center to spacecraft ($\|\vec{b}\| = h$)

$\vec{r}_h$ = vector from Venus center to Venus sub-solar point ($\|\vec{r}_h\| = a$)

$\vec{r}$ = vector pointing from the spacecraft to a Venus feature ($\vec{r}$ is expressed in Venus coordinates)

$\vec{r}'$ = vector pointing from the spacecraft to the image of the Venus feature associated with $\vec{r}$ ($\vec{r}'$ is expressed in image coordinates)

R = 3 x 3 orthogonal (rotation) matrix which transforms $\vec{r}$ into $\vec{r}'$. Finding the navigation transform for an image frame is equivalent to determining R.

The two basic coordinate systems (FIGURES II.1 and II.2) used in the navigation procedure are defined as follows:

(1) Venus-Centered Coordinate System

The $+X_v$, $+Y_v$ axes lies in the Venus equatorial plane. The longitude ϕ of a Venus feature is measured from the $+X_v$ axis (in the X_vY_v plane) in a counter clockwise sense about the $+Z_v$ axis which points into the northern celestial hemisphere and defines Venus north. (The planet Venus rotates in a clockwise sense about the $+Z_v$ axis.)

(2) Image Frame Coordinate System

The +X' axis points through the image center coordinates (L_c,E_c); the +Y' axis is parallel to the image scan lines and points towards decreasing element numbers (nominally west); the +Z' axis is perpendicular

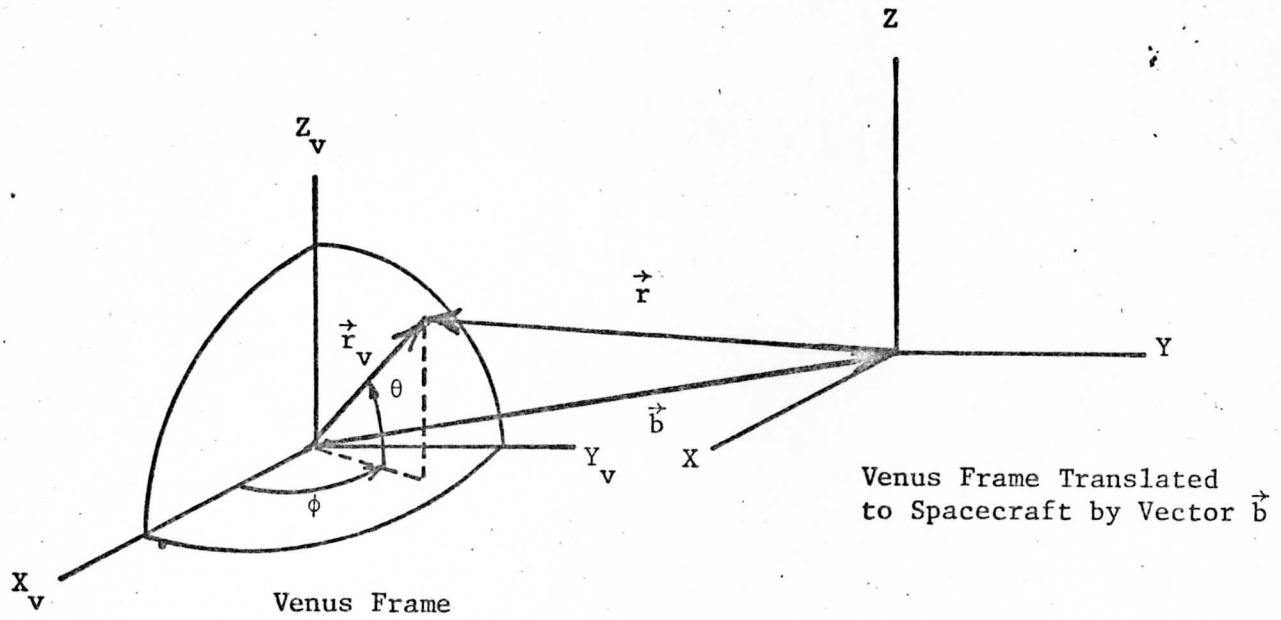

FIGURE II.1. Venus/Spacecraft Geometry. The vector $\vec{r}$ points from the spacecraft center to a Venus feature whose components are expressed in Venus coordinates ($\vec{r} = \vec{r}_v - \vec{b}$).

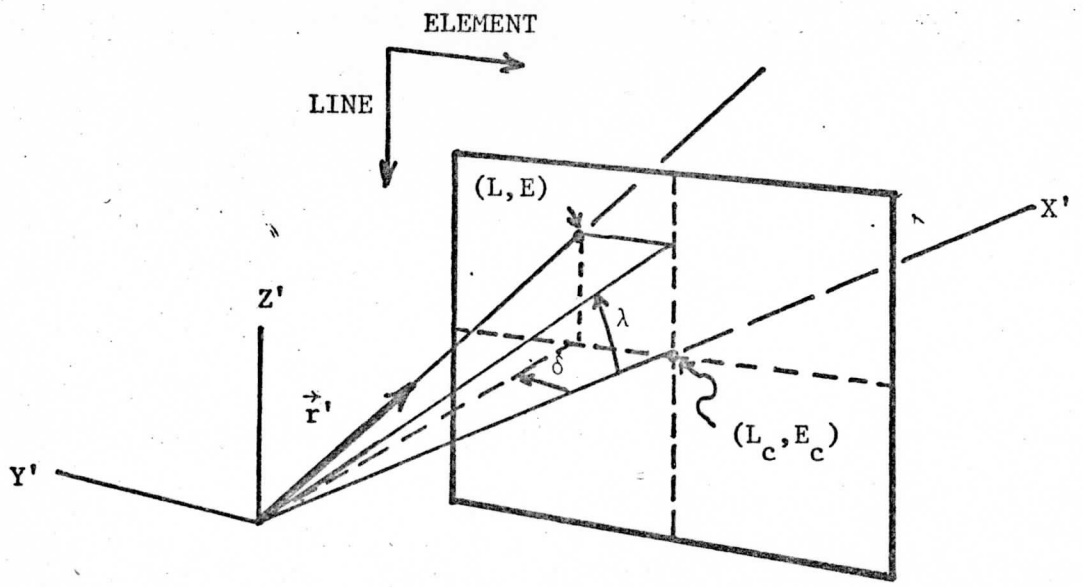

FIGURE II.2. Image Frame Geometry. The vector $\vec{r}'$ whose components are expressed in image coordinates is associated with the vector $\vec{r}$ in FIGURE II.1. The origins of the XYZ and X'Y'Z' coordinate systems are coincident.

to the scan lines and points towards decreasing line numbers (nominally north). The origin of this system is so situated such that the angles subtended at the image frame limits from the origin equals the FOV camera angles (θ_L, θ_E).

2. Basic Transformation Equations

The basic transformation equations between Venus and image coordinates and their relationship to the navigation procedure can now be written in terms of the definitions and conditions given above.

The vector $\vec{r}$, which points from the spacecraft to a Venus feature and is expressed in Venus coordinates, is given as $\vec{r} = \vec{r}_v - \vec{b}$. It is convenient to express $\vec{r}$ as a unit vector $\hat{r}$; thus,

$$\hat{r} = (\vec{r}_v - \vec{b})/\|\vec{r}_v - \vec{b}\| = [X,Y,Z]^T, \tag{1}$$

where "T" refers to the transpose of the column vector $\vec{r}$ and

$$\vec{r}_v = a[\cos\theta\cos\phi,\ \cos\theta\sin\phi,\ \sin\theta]^T = [X_v,Y_v,Z_v]^T, \tag{2}$$

$$\vec{b} = h[\cos\theta_s\cos\phi_s,\ \cos\theta_s\sin\phi_s,\ \sin\theta_s]^T. \tag{3}$$

The unit vector $\hat{r}'$ associated with $\hat{r}$ is defined in image coordinates as

$$\hat{r}' = [1,\ \tan\delta,\ \tan\lambda]^T/\sqrt{1 + \tan^2\delta + \tan^2\lambda} = [X',Y',Z']^T, \tag{4}$$

where

$$\left.\begin{aligned} \lambda &= (L_c - L)\rho_L = (L_c - L)(\pi/180)(\theta_L/T_L) \\ \delta &= (E_c - E)\rho_E = (E_c - E)(\pi/180)(\theta_E/T_E)\ . \end{aligned}\right\} \tag{5}$$

It should be emphasized at this point that the coordinate representations of $\hat{r}$ and $\hat{r}'$ are relative to orthogonal coordinate systems (the Venus frame

translated to the spacecraft and the image frame) and therefore are related to each other by a rotation matrix R, i.e.,

$$\hat{r}' = R\,\hat{r} \ . \tag{6}$$

With the explicit determination of R (shown in the following two subsections), the frame is said to be navigated and by convention R is called the navigation transform. Thus given R, any Venus coordinate (θ,ϕ) can be transformed to its corresponding image coordinate or vice-versa using equations (1) through (6). In symbols:

Venus → Image Coordinates

$$\left.\begin{aligned} &(\theta,\phi) \rightarrow \vec{r}_v \rightarrow \hat{r} \ , \\ &\hat{r}' = R\hat{r} \rightarrow (L,E) \ , \\ &\text{where} \\ &L = L_c - (\arctan\,(Z'/X'))/\rho_L \\ &E = E_c - (\arctan\,(Y'/X'))/\rho_E \ ; \end{aligned}\right\} \tag{7}$$

Image → Venus Coordinates

$$\left.\begin{aligned} &(L,E) \rightarrow \hat{r}' \ , \\ &\hat{r} = R^T\hat{r}' \rightarrow \vec{r}_v \rightarrow (\theta,\phi)^{\dagger} \ , \\ &\text{where} \\ &\theta = \arcsin\,(Z_v/a) \\ &\phi = \arctan\,(Y_v/X_v) \end{aligned}\right\} \tag{8}$$

---

†In transforming from image to Venus coordinates, the magnitude of $\vec{r}$ must be determined in order to determine $\vec{r}_v$ ($\vec{r}_v = \|\vec{r}\|\hat{r} + \vec{b}$; eq. (1)). This is easily accomplished by an iterative procedure with the convergence criteria that $\|\vec{r}_v\| - a < 10^{-2}$ km.

3. Conditions for Determining the Navigation Transform, R

The navigation matrix R for an image frame is uniquely determined from the equations given above by implementing the conditions that:

(1) the Venus coordinates (θ,ϕ) for at least one image point (L,E) in the frame are known;

(2) the scan lines of the image frame (nominally running in an east-west direction) are parallel to the plane formed by the centers of the sun, Venus, and the spacecraft.

Satisfying the first condition is the essence of image navigation and always implies the direct measurement of image coordinates from the image frame(s) under consideration. For low-resolution images navigated in the past in which a single frame contained most or a large portion of the bright Venus limb, the measurements consisted of edge point measurements along the limb. These image points were then used to calculate (in a least-squares sense) the Venus-center image coordinates. Since this point corresponds to the sub-spacecraft point for which the Venus coordinates are given, the first condition was then satisfied.

For the higher-resolution multiframe Venus mosaics, the frames making up the mosaic may each contain only a small arc-angle of the Venus limb or, indeed, no Venus edge at all. In order to satisfy the first condition for the determination of R for multiframe mosaic navigation, not only are edge point measurements required from each of the frames containing portions of the Venus limb, but in addition, link point measurements (image coordinates for a feature common to two overlapping frames) of the overlapping frames,

which connect the multiframes into a mosaic, are also necessary. By a self-consistent interative procedure discussed in the following section, the image coordinates for the sub-spacecraft point of one of the frames in the mosaic are found to satisfy the first condition. This condition is satisfied for the rest of the frames via the iterative procedure using the link point measurements.

For the purpose of this section, however, it is assumed that the Venus coordinates for at least one image point per frame are known. Let the known vector pair be denoted by $\hat{r}_1$, $\hat{r}_1'$ where $\hat{r}_1$ is the unit vector in Venus coordinates (eq. 1) and $\hat{r}_1'$ the unit vector derived from the associated image coordinates (eq. 4). Thus, the rotation matrix must satisfy the relationship

$$\hat{r}_1' = R\,\hat{r}_1 \quad . \tag{9}$$

The second condition that the image scan lines be parallel to the sun-Venus-spacecraft plane is a result of the stabilization/pointing procedure employed on the Mariner 10 during the Venus image acquisition period and is assumed to be accurate to within attitude error limits ($\pm$0.25 degrees). This condition is equivalent to imposing the constraint that the normal to this plane be perpendicular to the scan lines. A unit vector normal to this plane is obtained by crossing the sub-solar vector $\vec{r}_h$ into the sub-spacecraft vector $\vec{b}$ and normalizing

$$\hat{r}_2 = (\vec{r}_h \times \vec{b})/\|\vec{r}_h \times \vec{b}\| \tag{10}$$

(Note that $\hat{r}_2$ can be calculated directly from the SEDR parameters available for each image frame). That the normal of the plane be perpendicular to

the scan lines, is equivalent to stating that the Y-component of $\hat{r}_2$ (expressed in image coordinates equal zero, i.e.,

$$\hat{r}_2' = [X_2', Y_2', Z_2']^T = R\,\hat{r}_2, \qquad Y_2' = 0 \ . \tag{11}$$

4. Determination of R

The problem of determining R can now be restated as follows:

Given that R must be a 3 x 3 orthogonal matrix satisfying the equations

$$\hat{r}_1' = R\,\hat{r}_1,$$
$$\hat{r}_2' = R\,\hat{r}_2,$$

where $\hat{r}_1 = [X_1, Y_1, Z_1]^T$, $\hat{r}_1' = [X_1', Y_1', Z_1']^T$, $\hat{r}_2 = [X_2, Y_2, Z_2]^T$, $Y_2' = 0$ are known, determine R.

Use will be made of the properties of an orthogonal matrix that the scalar products and norms remain invariant under such a transformation, and that the transform of a vector product is equal to the vector product of the transform. Thus, for arbitrary vectors $\vec{r}_a$, $\vec{r}_b$, $\vec{r}$

$$(\vec{r}_a \cdot \vec{r}_b) = (\vec{r}_a' \cdot \vec{r}_b') \tag{12a}$$

$$\|\vec{r}\| = \|\vec{r}'\| \tag{12b}$$

$$(\vec{r}_a \times \vec{r}_b)' = \vec{r}_a' \times \vec{r}_b' \tag{12c}$$

where

$$\vec{r}' = R\,\vec{r} \ .$$

The first step in the determination of R is to compute $\hat{r}_2'$; in particular, to find X_2', Z_2' ($Y_2' = 0$). Applying the scalar product - invariant condition

expressed in eq. (12a) to $\hat{r}_1$, $\hat{r}_2$, we have

$$\hat{r}_1 \cdot \hat{r}_2 = X_1 X_2 + Y_1 Y_2 + Z_1 Z_2 = \hat{r}'_1 \cdot \hat{r}'_2 = X'_1 X'_2 + Z'_1 Z'_2 = \alpha, \qquad (Y'_2 = 0). \tag{13}$$

Similarly, as implied by eq. (12b),

$$\|\hat{r}_2\| = \|\hat{r}'_2\| = 1 = X'^2_2 + Z'^2_2 . \tag{14}$$

Thus, eqs. (13) and (14) constitute two equations in terms of the unknowns X'_2, Z'_2, the solutions of which are

$$Z'_2 = (\alpha Z'_1 + X'_1 \sqrt{X'^2_1 + Z'^2_1 - \alpha^2})/(X'^2_1 + Z'^2_1) \tag{15a}$$

$$X'_2 = \alpha / X'_1 \tag{15b}$$

$$Y'_2 = 0 . \tag{15c}$$

The choice of the positive sign in front of the radical in eq. (15a), guarantees that the +Z' axis of the image frame (FIGURE II.2) will lie in the northern celestial hemisphere. With $\hat{r}'_2$ completely determined, computation of R can proceed.

From $\hat{r}_1$, $\hat{r}_2$ a set of mutually orthogonal unit basis vectors can be constructed in the translated Venus frame (unprimed coordinate system) as follows:

$$\left.\begin{aligned} \hat{s}_1 &= \hat{r}_1 \\ \hat{s}_2 &= (\hat{r}_2 - (\hat{r}_1 \cdot \hat{r}_2)\,\hat{r}_1)/\|\hat{r}_2 - (\hat{r}_1 \cdot \hat{r}_2)\,\hat{r}_1\| \\ \hat{s}_3 &= \hat{s}_1 \times \hat{s}_2 , \end{aligned}\right\} \tag{16}$$

which are used to create an orthogonal matrix

$$S = [\hat{s}_1 | \hat{s}_2 | \hat{s}_3]^T, \tag{17}$$

where the $\hat{s}_i$ are column vectors. (That S is an orthogonal matrix can be easily shown by carrying out the multiplications $S^T S$ and $S S^T$, each product

of which equals the unit matrix. This result is necessary and sufficient to guarantee that S is orthogonal). Thus for an arbitrary vector $\vec{r}$,

$$S\vec{r} = [\hat{s}_1 \cdot \vec{r}, \hat{s}_2 \cdot \vec{r}, \hat{s}_3 \cdot \vec{r}]^T . \tag{18}$$

Expressing the $\hat{s}_i$ in the primed system (image coordinate frame) is easily achieved by operating on both sides of eqs. (16) with R ($\hat{s}'_i = R\hat{s}_i$, i = 1,3) using the conditions implied in eqs. (12) and the equations $\hat{r}'_1 = R\hat{r}_1$, $\hat{r}'_2 = R\hat{r}_2$. The result is

$$\left.\begin{aligned} \hat{s}'_1 &= \hat{r}'_1 \\ \hat{s}'_2 &= (\hat{r}'_2 - (\hat{r}'_1 \cdot \hat{r}'_2)\hat{r}'_1)/\|\hat{r}'_2 - (\hat{r}'_1 \cdot \hat{r}'_2)\hat{r}'_1\| \\ \hat{s}'_3 &= \hat{s}'_1 \times \hat{s}'_2 . \end{aligned}\right\} \tag{19}$$

The significance of eqs. (19) is that the basis vectors $\hat{s}'_i$ can be calculated directly from $\hat{r}_1$, $\hat{r}'_2$, which can then be used to generate the orthogonal matrix

$$S' = [\hat{s}'_1 | \hat{s}'_2 | \hat{s}'_3]^T . \tag{20}$$

Now because a scalar product remains invariant under an orthogonal transformation, the components $\hat{s}_i \cdot \vec{r}$ in eq. (18) are each equal to $\hat{s}'_i \cdot \vec{r}'$ and therefore the RHS of (18) is equal to

$$[\hat{s}'_1 \cdot \vec{r}', \hat{s}'_2 \cdot \vec{r}', \hat{s}'_3 \cdot \vec{r}'] = S'\vec{r}' . \tag{21}$$

Combining (18) and (21),

$$S\vec{r} = S'\vec{r}'$$

or

$$S'^T S\vec{r} = \vec{r}', \tag{22}$$

and since S and S' are each orthogonal, $S'^T S$ is orthogonal; thus from (22)

$$R = S'^T S \tag{23}$$

or expressing R in terms of its components R_{ij},

$$R_{ij} = \sum_{k=1}^{3} S'^{T}_{ik} S_{kj} = \sum_{k=1}^{3} S'_{ki} S_{kj} . \qquad (24)$$

Thus, since the S'_{ki}, S_{kj} are derived from their orthogonal basis vectors $\hat{s}_i$, $\hat{s}'^{\dagger}_i$ which in turn are calculated from $\hat{r}_1$, $\hat{r}_2$, $\hat{r}'_1$, $\hat{r}'_2$, the matrix R is completely determined.

---

†The relationship is $S_{ij} = (\hat{s}_i^{\,T})_j$.

III. VENUS MULTI-FRAME MOSAIC NAVIGATION

1. Basic Procedure

The procedure outlined in the previous section forms the basis for multiframe mosaic navigation. The following requirements for this general navigation procedure are:

(1) The configuration of frames making up a partial or full mosaic must be connected together with enough overlap between connecting frames such that at least one small Venus feature common to both frames can be identified and a link point measurement made. A link point measurement consists of the image point coordinates of the feature for each of the two overlapping frames.

(2) The multiframe mosaic must contain at least one frame from which Venus limb edge point measurements are available. (An edge point measurement consists of the image point coordinates on the limb where the gradient of the brightness values reaches a user-specified threshold; for the threshold used on the UV images this method has been proven to be very consistent resulting in a radius of 6131 km). For maximum accuracy in the navigation, it is best to have two frames containing Venus limbs each separated by as large an arc-angle along the limb as is practicable.

From the link and edge point measurements along with the available parameters for each image frame (see Section II, Subsection 1.), the multiframe configuration is navigated using the self-consistent procedure described below:

1. One of the frames is arbitrarily chosen as a reference frame. For ease of implementation, one furthest from the Venus limb or one occurring at frame branch point is chosen. This reference frame is navigated by making a first-guess of the sub-spacecraft image coordinates, then using the navigation equations for a single image frame as discussed in Section II, to determine the navigation transform for that frame. (The first-guess coordinates are computed by expressing the edge point measurements in reference frame coordinates. The assumption is made that all frames currently under consideration have the same resolution and are simply translated one from the other. Thus using the link and edge point measurements, the total displacement of the edge points in pixels from the reference frame can be obtained by simple addition. The two edge points with the largest arc-angle separation are then used (with the given radius of 6131 km converted to pixels) to compute the sub-spacecraft image coordinates of the reference frame. These values usually agree with the final convergence values to within a few pixels).

2. With the reference frame navigated, the Venus coordinates associated with the reference frame link point coordinates can be calculated. Since the image coordinates of this point associated with the linked frame are available from the measurements, this "link-to" frame can likewise be navigated. The navigation from this frame is in turn used to predict the Venus coordinates of the frame it is linked to so that the third frame can be navigated. This leap-frog method of frame navigation follows a path of linked frames (constraint path) until it terminates on a frame containing edge measurements.

3. From the navigation transform computed for this edge frame, the sub-spacecraft vector $\hat{r}'_c$ in image coordinates is computed using the SEDR-available Venus sub-spacecraft coordinates. The measured edge point image coordinates are converted to a unit vector $\hat{r}'_e$ in the image frame and used with $\hat{r}_c$ to compute $\sin\theta'$, where θ' is the approximate half-angle Venus subtends at the spacecraft (FIGURE III.1). In addition, a direct calculation of this half-angle (called θ) is made from the frame-available parameters a and h, the Venus radius and spacecraft height, respectively. Thus,

$$\sin\theta' = \|\hat{r}'_e \times \hat{r}'_c\|,$$

$$\sin\theta = a/h .$$

The squared difference, $(\sin\theta - \sin\theta')^2$, for this constraint path is accumulated as part of a sum, S, which is discussed below.

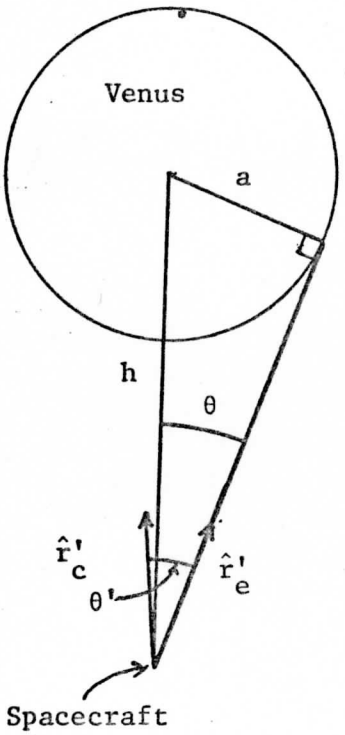

FIGURE III.1. The angle θ is the correct half-angle Venus subtends at the spacecraft; θ' is the half-angle derived from an edge measurement ($\hat{r}'_e$) and the mosaic model-computed sub-spacecraft point ($\hat{r}'_c$) expressed in image coordinates.

4. Steps 2 and 3 are repeated for all uniquely defined constraint paths producing for this first-iteration navigation: a navigation transform matrix for each of the frames and the sum, S, where

$$S = \sum_k (\sin\theta_k - \sin\theta'_k)^2 \ ,$$

where "k" is summed over all constraint paths.

5. The function of S is minimized relative to the reference frame sub-spacecraft image coordinates using a method of steepest descent and variable step size until the appropriate convergence criteria are met. Although steps 1 through 4 are repeated for each iteration in minimizing S (indeed, for each iteration the gradient of S is calculated using a difference technique which requires four additional computations of S), the CPU time required on the SSEC/McIDAS Datacraft minicomputer is relatively small (about 30 seconds for 50 iterations using 3 images, 2 link points and 3 edge points).

With the minimization of S, there results a unique navigation transform for each of the image frames involved in this self-consistent multiframe mosaic navigation. Thus, since each of these frames have been navigated, any of these individual frames may be employed in studies requiring accurate image to planet transformations without further reference to their parent mosaic.

2. Example and Results

FIGURE III.2 shows a pseudo 3-frame mosaic (fabricated from a single Venus frame) used in testing the mosaic navigation computer model. TABLE III.1 is the model output associated with the figure. Of these three frames, the one not containing a Venus edge (frame numbered one) was arbitrarily chosen as the reference frame (the frames, FM, are labeled by the encircled numbers in FIGURE III.2). With the two link points (LP - denoted by solid triangles)

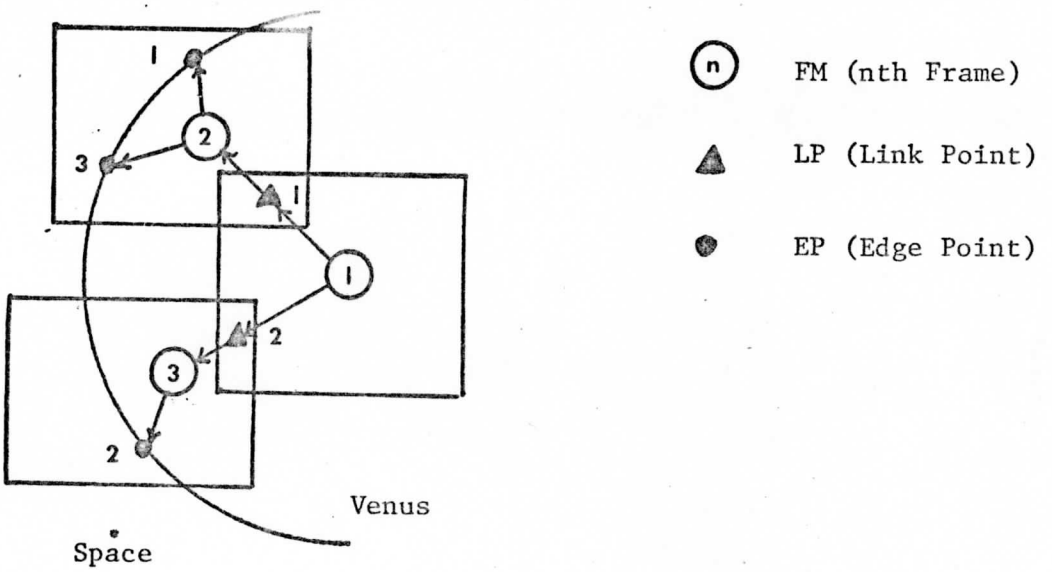

FIGURE III.2. A three-frame mosaic configuration demonstrating link points (LP), edge points (EP) and constraint paths.

and three earth edge points (EP-solid circles) labeled as shown in the figure, the three constraint paths used were

$$\text{FM-1} \xrightarrow{\text{LP-1}} \text{FM-2} \longrightarrow \text{EP-1}$$

$$\text{FM-2} \longrightarrow \text{EP-3}$$

$$\text{FM-1} \xrightarrow{\text{LP-2}} \text{FM-3} \longrightarrow \text{EP-2} \ .$$

The manner in which these measurements and constraint paths are entered into the computer model is discussed in the Appendix. The first block of output data in TABLE III.1 records these input values. In the second block, the "CALCULATED INPUT POINT" is the first estimation of the reference frame sub-spacecraft image coordinates (line, element) derived from edge points 1 and 2 in the manner discussed in Section III.1 (Step 1 of the algorithm). The "FINAL CONVERGENCE POINT" is the result of minimizing the functicn S relative to this sub-spacecraft point with a "CONVERGENCE

VENUS MOSAIC NAVIGATION

NO. OF FRAMES	NO. OF EDGE POINTS	NO. OF LINK POINTS	NO. OF CONSTRAINT PATHS
3	3	2	3

CALCULATED INPUT POINT		FINAL CONVERGENCE POINT		CONVERGENCE ACCURACY(PIXELS-RMS)	NO. OF ITERATIONS
LIN	ELE	LIN	ELE		
264.222	363.700	264.428	363.939	.370	50

EDGE POINTS USED IN NAVIGATION

NUMBER	FRAME ID	LIN	ELE
1	2	64	194
2	3	314	106
3	2	164	122

LINK POINTS USED IN NAVIGATION AND LINK POINT RESIDUALS

NUMBER	FRAME ID	LIN	ELE	DELTA LIN	DELTA ELE
1	1	150	250	-.007	.003
1	2	150	250	.006	-.010
2	1	300	200	.003	-.007
2	3	300	200	.002	-.006

NAVIGATED SUB-SPACECRAFT IMAGE COORDINATES

NFRAME	FRAME ID	LIN	ELE
1	1	264.441	363.949
2	2	264.426	363.979
3	3	264.441	363.950

TABLE III.1. This table shows multiframe mosaic navigation results for a three-frame mosaic derived from a single image frame and is associated with FIGURE III.2. See text for further explanation.

ACCURACY" given by

$$(\sqrt{S_f/N})(1/\sqrt{\rho_L \rho_E}) ,$$

where

S_f = final convergence value of S

N = total number of distinct edge points

ρ_L = radians/image scan line

ρ_E = radians/image element

Edge and link point number and measurements are recorded in the third and fourth blocks of data long their associated FRAME ID's (a number associated with and unique to each image frame). The "LINK POINT RESIDUALS" are differences between measured coordinates and the coordinates derived by transforming the measured image link point coordinates to Venus coordinates and back into image coordinates. These residuals are no gauge of absolute navigation accuracy, but serve to show that the transformations for each image frame are at least internally consistent and in addition, give a measure of the computational error associated with the transformations.

The final output block of data is the computed image coordinates of the sub-spacecraft point for each of the image frames. In this example, they are identical since all three frames were, in fact, derived from the same image frame. These navigation results (sub-spacecraft point image coordinates and components of the matrix R) were compared to those derived for this image frame (ID number 4901018) from the single frame navigation model currently running on SSEC's McIDAS.[†] (The formulation of this current

[†]Phillips, D. R. and S. Limaye, Annual Report, Space Science and Engineering Center, Madison, Wisconsin, 1976; NASA Contract Report No. NGR-50-002-189.

single frame navigation procedure was such that it could not easily be generalized to include multiframe navigation). The results were identical to within the round-off and truncation errors inherent in the system.

It is also noteworthy to mention that the linkage point measurements used in the example above were changed for the reference frame on the order of 10 pixels to effectively compress it relative to the two other fabricated frames. The function S converged to a final value without difficulties and the final results were what one would expect (sub-spacecraft image coordinates were least affected for the frame containing the two edge measurements). Tests on the model were also made by stretching and rotating the reference frame with the same successful results

Once it was ensured that the basic mosaic navigation program was working as conceived the procedure was tested on a true mosaic. Three frames with overlap and sufficient bright limb in each one of them (IDS #'s 4608397, 4610397, and 4617397) were chosen. The images had not been FICORed or GEOMed. Now usually the geometric distortions in a raw vidicon image are significantly large and increase away from the center of the frame. The bulk of the mosaic frames were not likely to be GEOMed and hence it was thought desirable to find out what the effect of geometric distortions would be on the mosaic navigation procedure. The check on the mosaic navigation was provided by the existing navigation scheme. FIGURE III.3 shows an overlapping view of all three frames displayed. TABLE III.2 shows the navigations obtained from the mosaic navigation scheme.

The convergence value of 3.4 pixels is in fact better than could be expected since the geometric distortions in the three frames were completely ignored. We surmise that the least squares scheme utilized in the mosaic

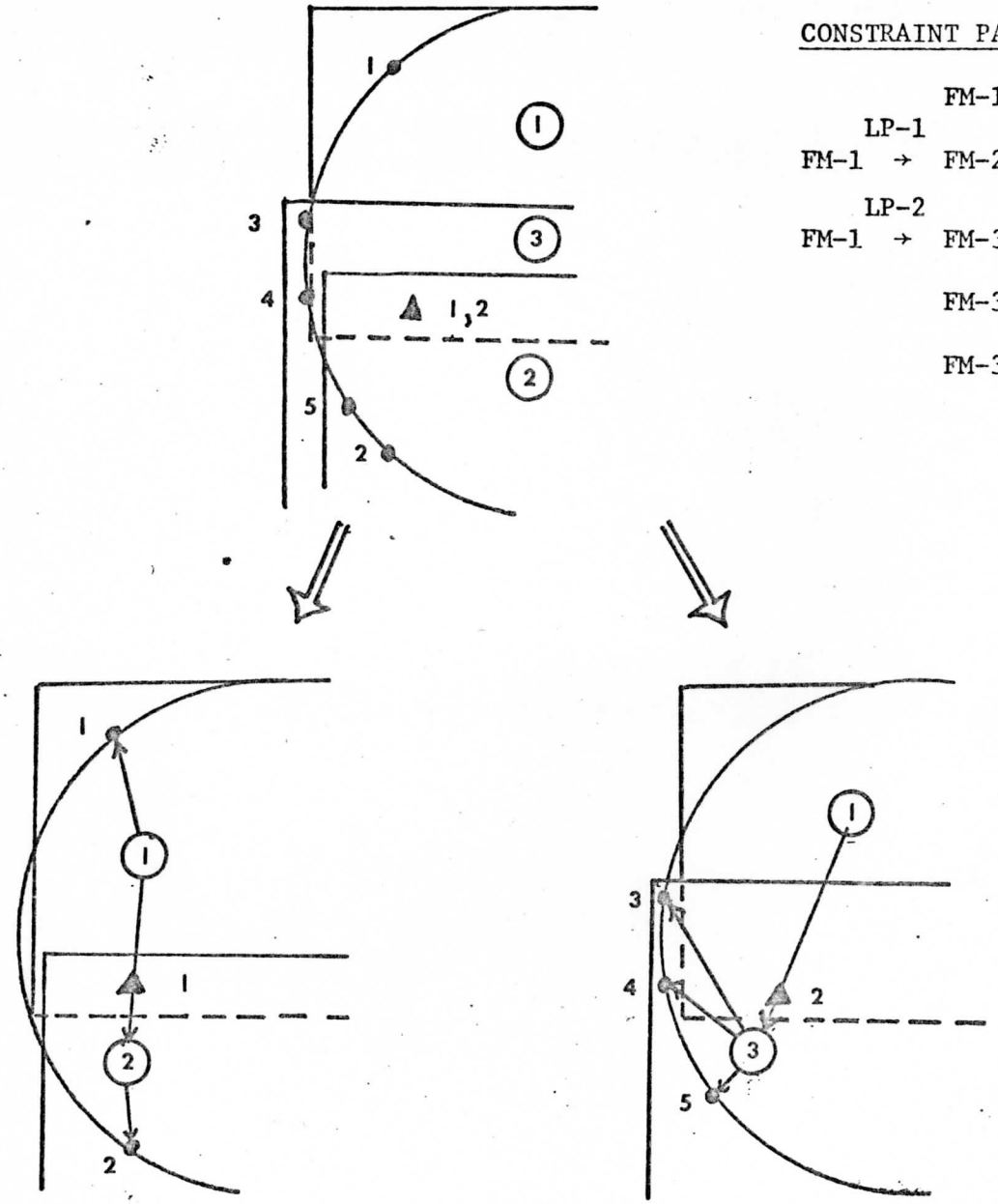

CONSTRAINT PATHS

FM-1 → EP-1

LP-1
FM-1 → FM-2 → EP-2

LP-2
FM-1 → FM-3 → EP-3

FM-3 → EP-4

FM-3 → EP-4

FIGURE III.3. Three-Frame Mosaic Used in Navigation. Uppermost figure shows the configuration of the frames, edge points and link points (same link point used in FM-1). The uppermost figure is decomposed for clarity into the two lower figures where the constraint paths used in the navigation are shown.

```
* * * * * * * * * * * * * * * * * * * * * * * * * * * * * * * * * * * * * * * *
*                                                                               *
*                          VENUS MOSAIC NAVIGATION                              *
*                                                                               *
* * * * * * * * * * * * * * * * * * * * * * * * * * * * * * * * * * * * * * * *
```

NO. OF FRAMES	NO. OF EDGE POINTS	NO. OF LINK POINTS	NO. OF CONSTRAINT PATHS
3	5	2	5

CALCULATED INPUT POINT		FINAL CONVERGENCE POINT		CONVERGENCE ACCURACY(PIXELS-RMS)	NO. OF ITERATIONS
LIN	ELE	LIN	ELE		
546.633	486.490	547.884	484.999	3.409	50

EDGE POINTS USED IN NAVIGATION

NUMBER	FRAME ID	LIN	ELE
1	4608397	137	156
2	4610397	348	110
3	4617397	10	64
4	4617397	202	60
5	4617397	442	164

LINK POINTS USED IN NAVIGATION AND LINK POINT RESIDUALS

NUMBER	FRAME ID	LIN	ELE	DELTA LIN	DELTA ELE
1	4608397	641	199	.006	-.014
1	4610397	57	181	.012	-.015
2	4608397	641	199	.006	-.014
2	4617397	197	276	.005	-.023

NAVIGATED SUB-SPACECRAFT IMAGE COORDINATES

NAVID	FRAME ID	LIN	ELE
1	4608397	547.880	485.012
2	4610397	-36.041	466.764
3	4617397	104.054	561.343

TABLE III.2. This table shows multiframe mosaic navigation results for three different Venus image frames and is associated with FIGURE III.3. See text for further explanation.

navigation to determine the best guess for image space sub-spacecraft point also tends to treat the vidicon geometric distoritons as true errors in planet limb locations. Future plans include using the Reseau-mark measurements available in the image data to correct for these distortions.

A second but much smaller source of error affecting the mosaic navigation accuracy is the assumption that a Venus feature common to two overlapping image frames, from which link point measurements are derived, has the same Venus coordinates in both images, i.e., the movement of the feature over the time interyal between the two frames in negligible.

In the case of the MVM-73 mission successive frames were shuttered 42 seconds apart. Given that the nominal speed of the UV features seen in these images is of the order of 100 $msec^{-1}$, the features move zonally approximately 4.2 km between two successive images. Thus as long as the resolution per pixel is nominally only of the order of a few kilometers, the assumption that the UV feature has the same planet co-ordinates in the two frames is a good one. In any case the motion of the UV features has been determined from lower resolution frames[†] and the results can be used to extrapolate the true planet co-ordinates of the same UV feature if a need arises. It seems very unlikely at this stage that this need will arise in the context of MVM-73 UV images of Venus though since the 8-bit data (6-bit in IM-3 format) is simply not sufficient to show any visible detail for resolutions greater than about 2-4/km/pixel.

[†]Krauss, R., Annual Report, Space Science and Engineering Center, Madison, Wisconsin, 1976; NASA Contract Report No. NGR-50-002-189.

ACKNOWLEDGMENT

We are pleased to thank Robert Krauss who provided the impetus for this work. We are especially grateful to Sanjay Limaye for providing the Venus mosaic measurements and for his helpful revisions of this report.

This research was supported by the National Aeronautics Space Administration under NASA Grant No. NGR-50-002-189.

APPENDIX - Brief FORTRAN Description of Venus Mosaic Navigation

This appendix documents the essential features of the FORTRAN program used for the Venus mosaic navigation and describes the current procedure and format for inputting the relevant measurements (link/edge point) for a navigation.

1. Single Frame Navigation

Associated with each image frame is the common block VENCOM consisting of 22 words. The first 10 words consist of the basic parameters available for each image (Section II.1); the remaining 12 words consist of the derived sub-spacecraft vector, $\vec{b}$, and the 3 x 3 navigation transform matrix, R. Listed below are these parameters in the order in which they appear in VENCOM and their FORTRAN equivalent. Reference should be made to Section II for the details.

VENCOM PARAMETERS

Algebraic Symbol	Definition	FORTRAN Equivalent
(θ_S, ϕ_S)	sub-spacecraft latitude and longitude (decimal degrees)	(SSPLAT, SSPLON)
(θ_H, ϕ_H)	sub-solar latitude and longitude (decimal degrees)	(SSLLAT, SSLLON)
a	Venus radius (km)	RADIUS
h	spacecraft height (km)	H
$(L_c, E_c)^\dagger$	picture center line and element	(PCLIN, PCELE)

†These parameters are actually derived from the tape-available parameters of the FOV angles (θ_L, θ_E) and the total lines and elements (T_L, T_E); see Sec. II.

Algebraic Symbol	Definition	FORTRAN Equivalent
$(\rho_L, \rho_E)^{\dagger}$	radians per line, radians per element	(RDPLIN, RDPELE)
$\vec{b}$	sub-spacecraft vector in Venus coordinates	B
R	navigation transform matrix	RM
	ADDITIONAL PARAMETERS	
(θ, ϕ)	latitude, longitude of a Venus feature	(XLAT, XLON)
(L,E)	line and element image coordinates associated with (θ, ϕ)	(XLIN, XELE)
$\hat{r}_1$	translated Venus vector used to determine R	R1V
$\hat{r}'_1$	image of $\hat{r}_1$ - used to determine R	R1S
$\hat{r}_2$	vector normal to spacecraft-sun-Venus plane - used to determine R	R2V

Subroutine FRMNAV, given a Venus feature in planet and image coordinates (XLAT, XLON), (XLIN, XELE), computes B and RM, and stores them in VENCOM.

FRMNAV calls three basic subroutines; their name, functional description, and equations associated with their function are given in the order they are called:

Name	Function	Equations (Sec. II)
VENVEC	Given XLAT, XLON,* computes R1V, R2V	(1),(2),(3),(10)
SATVEC	Given XLIN, XELE, computes R1S	(4),(5)
RMTRX	Given R1V, R1S, R2V, computes R	(13),(14),(15),(24).

---

†See page 19.

*These coordinates pairs are associated with each other.

When the image frame has been navigated, transformations between arbitrary image and planet coordinates are made with the subroutine

VENTRN(XLIN,XELE,XLAT,XLON,IDIR)

where if

IDIR = 1,

(XLAT,XLON) → (XLIN,XELE) (Eq. 7);

if

IDIR = 2,

(XLIN,XELE) → (XLAT,XLON) (Eq. 8).

2. Multi-frame Mosaic Navigation

This section's primary purpose is to describe the procedure and format for entering the link/edge point measurements and constraint paths for a multiframe mosaic navigation. Heavy reference will be made to Section III.

As indicated in the text of Section III and shown in FIGURES III.2 and III.3, distinct integer values NAVID, ILINK, INEDG are assigned to identify the frame number (FM-NAVID), the link point number (LP-ILINK) and the edge point number (EP-INEDG) for the configuration of image frames to be mosaic-navigated. The frame to serve as the reference frame may be arbitrarily chosen and for bookkeeping convenience should be assigned the value 1. In general

NAVID = 1, 2, 3, ..., total number of frames

ILINK = 1, 2, 3. ..., total number of link points

INEDG = 1, 2, 3, ..., total number of edge points.

After the assignment of the integer indices defined above, the constraint paths are determined. As will be recalled from the main text, one complete iteration of the multiframe mosaic navigation starts with the navigation of the reference frame (by using a calculated guess of the sub-spacecraft image coordinates), then navigates a frame linked to it using the information supplied by the link point measurement, and proceeds in such a manner from frame to frame via link point measurements and terminates on an "edge point" frame. The half-angle subtended by the Venus image is calculated, subtracted from the actual half angle, squared and accumulated in the function S. The path of frames and link points used in the computation is called a constraint path. The procedure is repeated until all the edge point measurements have been utilized in the computation of S. The integer indices of the link points (ILINK) and edge points (INEDG) are stored in the order in which they are encountered along each constraint path in the one dimensional array, ICNSTR.

ICNSTR consists of K + 1 segments where K is the number of constraint paths used in the navigation. Letting I_J be the index of ICNSTR which is the first value in the Jth segment, then

$$\text{ICNSTR}(I_J) = \text{number of link points in the Jth constraint path plus 1;}$$

if there are N link points in this Jth constraint path, then

$$\text{ICNSTR}(I_J + 1) = \text{ILINK for the 1st LP (link point),}$$

$$\text{ICNSTR}(I_J + 2) = \text{ILINK for the 2nd LP}$$

$$\vdots$$

$$\text{ICNSTR}(I_J + N) = \text{ILINK for Nth LP,}$$

ICNSTR(I_J + N + 1) = INEDG for Jth path.

If J = K, then

ICNSTR(I_K + N + 2) = 0,

and ICNSTR is terminated. (If J < K, then $I_J + N + 2 = I_{J+1}$, and a new segment or constraint path is begun.) Note that except for the last segment, the value of ICNSTR for the last element in each segment always equals an edge point number INEDG. Note also, that constraint paths don't have to start with the reference frame (except for the first constraint path); they may start with any navigated frame (frames through which previous constraint paths have passed). In fact, for the sake of computational efficiency, it is best to choose a navigated frame from which the minimal number of link points need be traversed to arrive at the edge point terminating the constraint path.

ICNSTR references directly or indirectly all the other arrays containing the information necessary for the navigation. These arrays and their definitions are given as follows:

IDCOR (1, ILINK) = NAVID of "link-from" frame

IDCOR (2, ILINK) = NAVID of "link-to" frame

IDEDG (INEDG) = NAVID of edge point, INEDG

ARYNAV (22, NAVID) = VENCOM (22)
common block associated with frame NAVID

$$\text{ARYCOR}\left(\begin{Bmatrix}1\\2\end{Bmatrix}, \text{ILINK}\right) = \begin{Bmatrix}\text{XLIN}\\\text{XELE}\end{Bmatrix} \text{ of link point, ILINK, of the "link-from" frame}$$

$$\text{ARYCOR}\left(\begin{Bmatrix}3\\4\end{Bmatrix}, \text{ILINK}\right) = \begin{Bmatrix}\text{XLIN}\\\text{XELE}\end{Bmatrix} \text{ of link point, ILINK, of the "link-to" frame}$$

$$\text{ARYEDG}\left(\begin{Bmatrix}1\\2\end{Bmatrix},\ \text{INEDG}\right) = \begin{Bmatrix}\text{XLIN}\\\text{XELE}\end{Bmatrix} \text{ of edge point, INEDG.}$$

3. An Example

Correctly filling these arrays is actually quite a simple task. The array value which appear below in FIGURE A are the array values used in navigating the three-frame mosaic discussed in Section III and are associated with FIGURE III.3 and TABLE III.2.

```
ICNSTR(1)=1          IDCOR(1,1)=1          IDEDG(1)=1
ICNSTR(2)=1          IDCOR(2,1)=2          IDEDG(2)=2
ICNSTR(3)=2          IDCOR(1,2)=1          IDEDG(3)=3
ICNSTR(4)=1          IDCOR(2,2)=3          IDEDG(4)=3
ICNSTR(5)=2          ARYCOR(1,1)=641       IDEDG(5)=3
ICNSTR(6)=2          ARYCOR(2,1)=199       ARYEDG(1,1)=137
ICNSTR(7)=2          ARYCOR(3,1)=57        ARYEDG(2,1)=156
ICNSTR(8)=3          ARYCOR(4,1)=181       ARYEDG(1,2)=348
ICNSTR(9)=1          ARYCOR(1,2)=641       ARYEDG(2,2)=110
ICNSTR(10)=4         ARYCOR(2,2)=199       ARYEDG(1,3)=10
ICNSTR(11)=1         ARYCOR(3,2)=197       ARYEDG(2,3)=64
ICNSTR(12)=5         ARYCOR(4,2)=276       ARYEDG(1,4)=202
ICNSTR(13)=0                               ARYEDG(2,4)=60
                                           ARYEDG(1,5)=442
                                           ARYEDG(2,5)=164
```

FIGURE A. Input Arrays Used for Venus Mosaic Navigation Discussed in Section III (refer to FIGURE III.3 and TABLE III.2).

From the constraint paths shown in FIGURE III.3 and the rules discussed above, the definition of ICNSTR is apparent. The definitions of IDCOR and IDEDG also follow immediately from the figure; the definitions of ARYCOR and ARYEDG follow from the figure and TABLE III.2.

ARYNAV is not shown since it has been discussed in detail in the first portion of this appendix and because the VENCOM common blocks, which make up

ARYNAV, are defined according to the convention used for the single-image-frame navigation program currently running on the McIDAS system.

The only remaining array not discussed thus far is IDFRAM which is used to define the "FRAMEID" in the TABLES,

IDFRAM (NAVID) = frame (or reel) ID.

For TABLE III.1,

IDFRAM (NAVID) = NAVID;

for TABLE III.2,

IDFRAM (NAVID) = reel number associated with each Mariner 10/JPL/SEDR data image tape.

IDFRAM merely provides labels and plays no direct role in the mosaic navigation.

APPENDIX B

A SHEAR MODEL FOR SPIRAL STREAKS IN THE VENUS CLOUDS

Robert J. Krauss

Space Science and Engineering Center

University of Wisconsin-Madison

Madison, Wisconsin

August, 1976

A SHEAR MODEL FOR SPIRAL STREAKS IN THE VENUS CLOUDS

Robert J. Krauss

ABSTRACT

Large spiral streak features are seen in Mariner 10 UV images of the upper level clouds on Venus. Measurements of the cloud velocities in and around the streaks indicates that the spiral streaks are unlikely to be either streamlines or jets in the atmosphere, since they have a comparatively small meridional velocity component. A hypothesis is developed that the shape of the streaks is caused by horizontal shear in the measured velocity field. This approach can be inverted to infer the global velocity field from the curvature of the streaks. Such an analysis reveals that a global scale wave with a 4 1/2 day period is likely to be superimposed on the predominant mean flow at high altitudes. The shear hypothesis also provides a means of correlating large scale cloud features and albedo changes on Venus with the global atmospheric flow patterns that have been measured. On the basis of the correlations, one can speculate what the upper level general circulation of Venus might be like.

INTRODUCTION

The bright spiral streaks in the Mariner 10 UV images are one of the most conspicuous features of the global cloud patterns on Venus. The appearance of the streaks changes superficially from day to day as the upper atmosphere rotates through the 8 day sequence of Mariner pictures. We can see variations in streak brightness, variations in streak width, and irregularities and blobs along the edges of the streaks. Several features of the spiral streaks are important, however, in that they do not change substantially over the 8 days: a) The streaks originate near the equator and spiral around the planet some 200-300 degrees in longitude before merging into a bright polar ring near 50 degrees latitude; b) More often than not, the streaks are coherent across the equator and a corresponding bright streak is also present in the other hemisphere; c) The streaks always diverge from the equator in a "V" pattern, with the arms of the "V" pointing in the direction of the retrograde mean zonal flow; d) The streaks do not change very fast in time, appearing to be virtually fixed on the rotating sphere, similar in character to the stripes on a barber pole, creating the illusion of motion without exhibiting true motion themselves.

The large scale organization and the temporal and spatial stability of the spiral streaks indicates some relation to the global scale motion field and to the general circulation of the upper atmosphere which also appears to exhibit large scale organization and stability in time over periods of days or weeks. The streaks may thus be of potentially greater significance in determining the large scale mass motion field than, say, the circumequatorial belts, which would be difficult to interpret in any other way than as a periodic wave phenomenon. Murray, et.al. (1974) offered several tentative explanations for the origin of the spiral

streaks. If the zonal motion is caused by periodic solar heating from above, then the streaks are likely to be wavelike disturbances caused by some interaction of the zonal flow with the subsolar convective zone. With no meridional flow, the streaks would have to be entirely wavelike. If meridional flow exists, the wavelike character would be strongest in the equatorial regions of maximum solar heating, but the streaks (at higher latitudes at least) are more likely to be streamlines in the fluid flow field. A third possibility was proposed which maximizes solar heating effects to the point where we have not only wavelike interactions and streamlines, but also large heat induced pressure gradients centered at the subsolar point. These pressure gradients generate large scale horizontal jets due to the cross-isobar flow. Both of the latter views require a subsequent moderate to strong meridional flow.

Detailed measurement of the small scale cloud motions (Suomi, 1975; and Krauss, 1976a&b) has shown very small meridional motions, well under 10 m/s everywhere. The only exception is the circumequatorial belts, which have a $\sim$ 20 m/s southward component. If the spiral streaks were either jets or streamlines, their angle to the equator as seen in the Mariner pictures, would require meridional velocities of 30-50 m/s. This is not observed. Moreover, a jet ought to exhibit horizontal shear at its edges. We have seen no velocity changes across the spiral streaks. The motion field is everywhere locally uniform, except for a 10-15 m/s measurement scatter due most likely to convection, turbulence, or vertical shear. Thus, the only remaining hypothesis is that the spiral streaks are wavelike in origin.

Now, the wave hypothesis is believable near the equator. Interaction of the mean zonal flow with the subsolar convection zone is bound to generate vertical oscillations in the atmosphere, especially in the presence of the very stable temperature lapse rate observed at 60-70 km altitude. Cloud streets or billow patterns might possibly remain even after a number of days and one or two revolutions around the planet. The cloud features need only to be preserved for several days after being formed by wave induced processes. In view of the unknown nature of the UV contrasts, persistence of some features for several days is a reasonable assumption.

Two characteristics of the spiral streaks require some added explanation before we attribute them exclusively to waves, however. The first unexplained characteristic is that the spiral streaks appear everywhere to move with the mean zonal and meridional flow. No organization whatsoever is observed anywhere along a spiral streak to indicate it has a propagation velocity relative to surrounding cloud features. To explain the streaks as waves thus requires combining origins and phase velocities in such a way as to produce a periodic standing wave train which remains fixed, not with respect to its source, but with respect to its medium. This seems highly unrealistic. The second unexplained characteristic of the streaks is that, in the mid-latitudes at least, the streaks are distorted by the increasing angular velocity of the mean zonal flow at higher latitudes. The "streak wave" thus moves with the mass field, tends to locally conserve angular momentum, and exhibits horizontal shear. If the spiral streaks are indeed waves, they are, in many respects, very unwavelike in character.

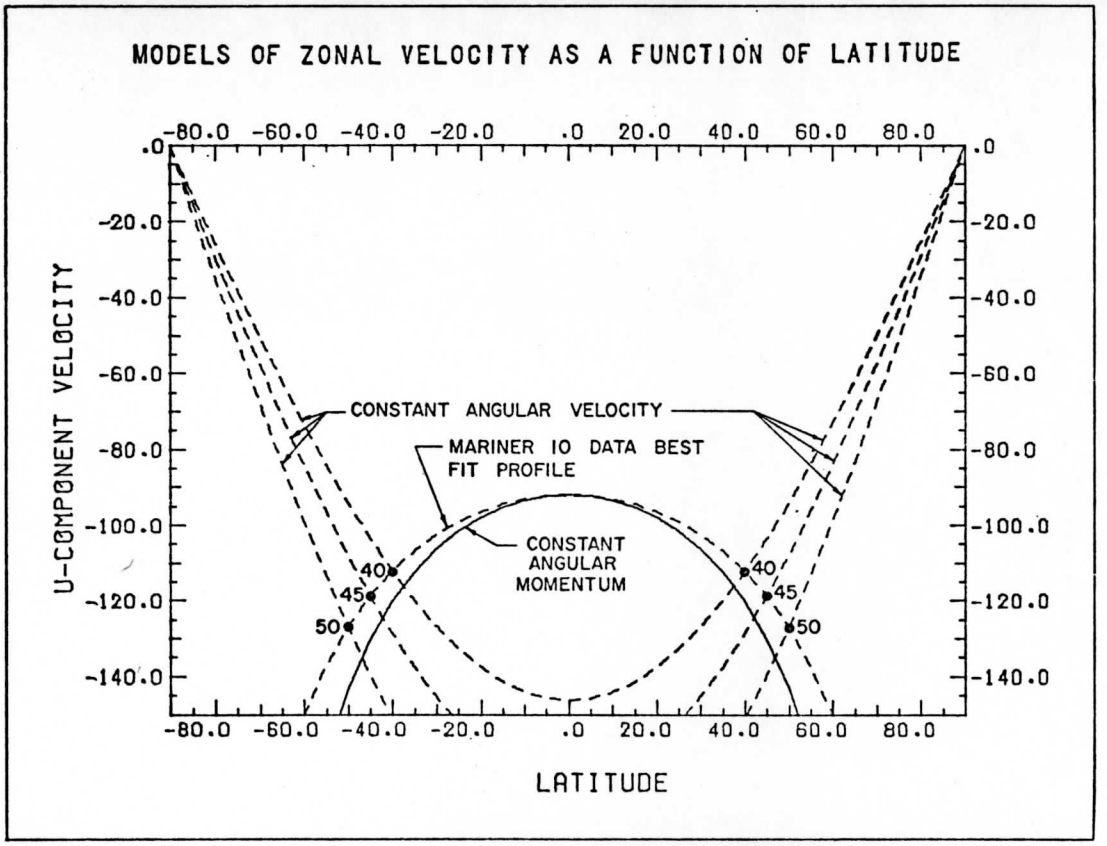

Figure 1a. The dependence of the zonal velocity as a function of latitude can be modeled by a profile of nearly constant angular momentum at low latitudes and a constant angular velocity at high latitudes. The transition between the two regimes seems to vary between 40 and 50 degrees (illustrated by solid dots). Of the three transition latitudes shown, 45 degrees was chosen for the streak model as a good average value.

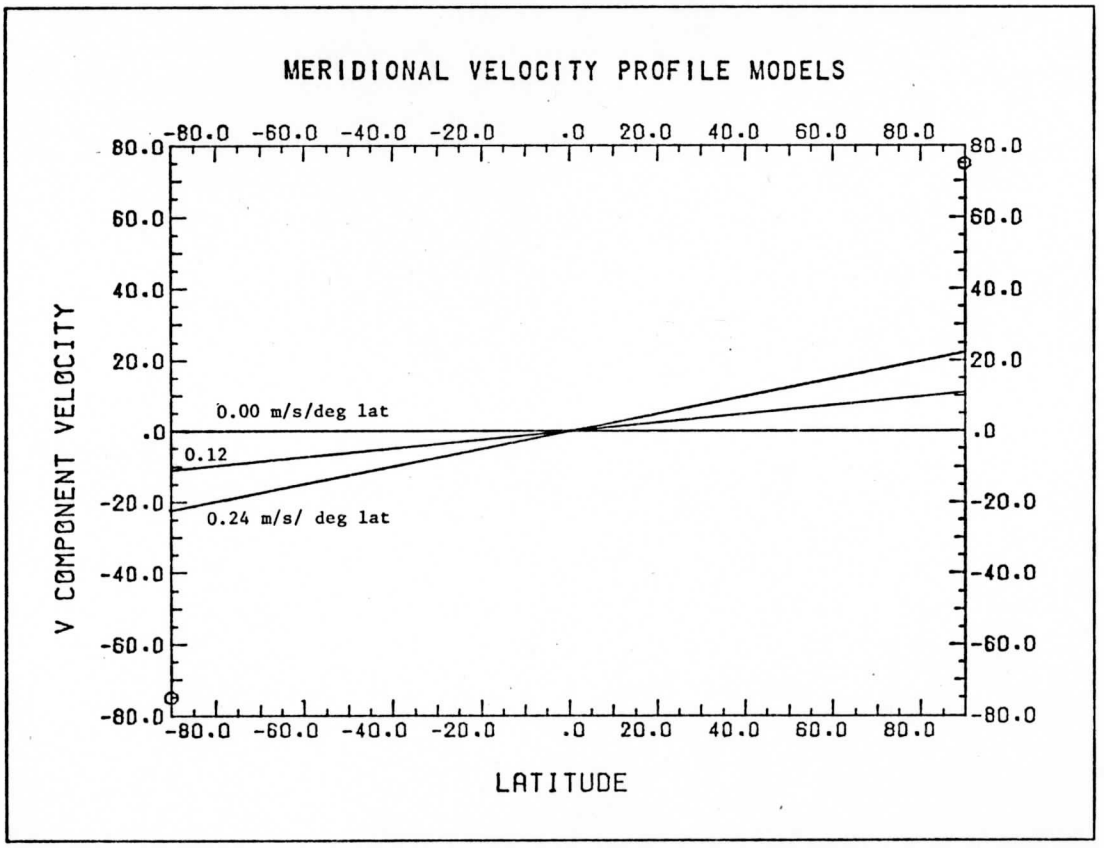

Figure 1b. The dependence of meridional velocity as a function of latitude is modeled by a constant velocity gradient. Scatter in the data prevents meaningful use of anything other than a linear approximation. The range of gradients shown here was used to generate the seven streak families shown in Figure 3.

The next obvious question is "Do we need a wave at all?" If the streaks tend to distort like the mass field at higher latitudes, maybe they also move with the mass field at lower latitudes where the distortion due to shear is too small to detect by direct velocity measurement. If that is the case, the streaks may have their origin in a wave, perhaps caused by an interaction of the mean zonal flow with the subsolar convective region. The waves generate and feed bright cloud material into the streaks, but the shape of the streaks would be due entirely to their being carried along with mass motion of the surrounding atmosphere. Since we have a measured global velocity field, it is easy to test the shear hypothesis by looking at the effects of horizontal shear in the zonal and meridional velocity fields as a function of latitude.

THE SHEAR MODEL

To test this hypothesis, we constructed a computer model using a zonal velocity profile with a -92 m/s equatorial velocity and a 120 m/s zonal maximum velocity at 45 degrees latitude (Figure 1a). The velocity profile was derived from our measurements of the Venus cloud motion in Mariner 10 images on day 39 (Krauss 1976a). Various meridional velocity gradients (Figure 1b) were used to generate a family of trajectories. Figure 2 illustrates schematically how a single mass element might spiral toward the pole under the combined influence of the u (zonal) and v (meridional) motion vectors. Note the shallow angle of the trajectory with respect to the equator, requiring several trips around the planet to reach higher latitudes. The v component of the measured velocity profiles is too small for the trajectories to have the same large angle relative to the equator as we see for the spiral streaks.

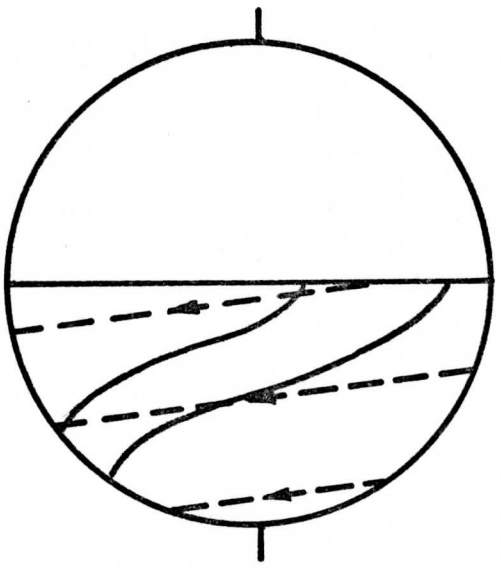

Figure 2. The dashed lines schematically illustrate the slow departure from the equator taken by a mass parcel under the influence of the velocity field defined by Figures 1a and 1b. Note that the spiral streaks, depicted by the solid lines, have a much larger angle with respect to the equator.

SPIRAL STREAK LINE MODEL

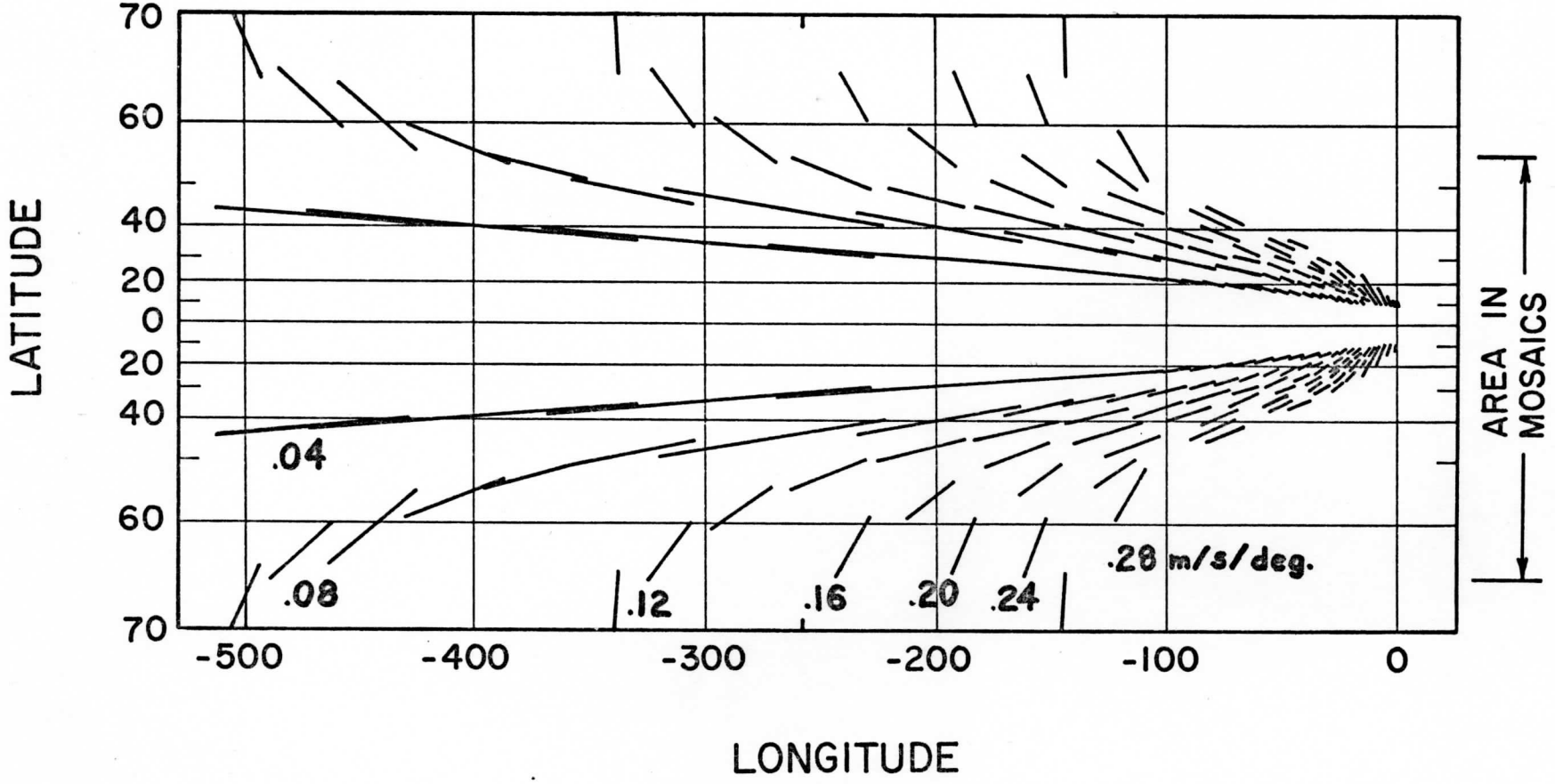

Figure 3. The seven streak families generated by differential rotation in a spherical shell are shown here. The velocity profiles used are defined in Figure 1. The longitude scale shows displacement from the point of origin (longitude zero) in a coordinate system moving with the mean equatorial flow of -92 m/s.

A poleward moving mass element would tend to distort, however. This effect can be approximated by considering two mass elements starting on the same meridian, but 100 km apart. Initially, a line connecting two such mass elements would be parallel to the meridian. As the effect of horizontal shear builds up, the line between the elements would both stretch and tilt. Figure 3 is a mercator plot of seven sets of such stretched and tilted lines corresponding to trajectory pairs for the meridional velocity gradients of 0.04, 0.08, 0.12, 0.16, 0.20, 0.24, and 0.28 m/s/deg as illustrated in Figure 1b.

The best analogy to what is illustrated in Figure 3 is the case of an observer in a boat floating down a stream. The observer throws a dye marker overboard and continues to watch the development of the resulting dye plume as he floats downstream with the mean flow. The spiral streak angle best fitting the streaks observed in the Mariner 10 images on day 39 corresponds to the 0.12 m/s/deg meridional velocity gradient in Figure 3. This compares nicely with our measured velocity gradients of 0.11 to 0.14 m/s/deg, so the streak model seems to be consistent with the data. Note, in addition, that the shape of the streaks in the model is not dependent on the magnitude of u, the zonal wind. The model is a function of $\partial u/\partial y$ and $\partial v/\partial y$ only. We cannot therefore directly predict divergence or infer vertical motion from the shape of the streaks, but because of the need to conserve angular momentum on a global scale, $\partial u/\partial y$ should be stable to 10-20%. We see no large storms or other dynamic features which could significantly perturb the mean zonal flow. As a result, the strong dependence of the model on $\partial v/\partial y$ makes the spiral streak angles extremely sensitive indicators of the magnitude of the meridional flow.

In the first movie made of the Venus flyby images (Danielson, 1975), one can see an oscillation or nutation of the bright polar ring. The period is about 4 days. A shift in latitude of the ring can also be seen in an early Mercator projection of the data (Murray, et. al., 1974, Figure 11). Belton, et. al. (1976) have generated an improved set of Mercator projections covering a full 7 day period and consisting of both high pass filtered and photometrically corrected versions of the data. We examined spiral streak angles in the high pass filtered mosaic to see if there existed a correlation of meridional velocity (inferred from the streak line tilt in the model) with the latitude shift of the polar band. Figure 4a is a copy of the Belton, et. al. mosaic. Figure 4b shows the streaks with the inferred value of the meridional velocity gradient needed to produce the observed tilt angle. The dashed line is the low latitude edge of the polar ring. A correlation is indeed present. The meridional velocities are higher when the polar ring is at higher latitudes. This appears to occur about every 4 1/2 days. One should, however, keep in mind how the projections are mosaiced. Figures 4a and 5 a are neither true space nor true time representations, but a mixture of the two. Shapes may be somewhat distorted or discontinuous at frame edges, although the mosaic taken as a whole gives the proper impression of what one would see using a "slit camera" aligned with the subspacecraft meridian.

Belton, et al. (1976) note that the darker regions of the photometrically corrected mosaic (Figure 5a) form the often observed dark "Y" feature, and that the coherence of this feature in time, and in the presence of the larger mid-latitude shear in our measured zonal wind profile (where higher latitudes have considerably higher angular velocity) argues for the association of the "Y" with a global scale wave.

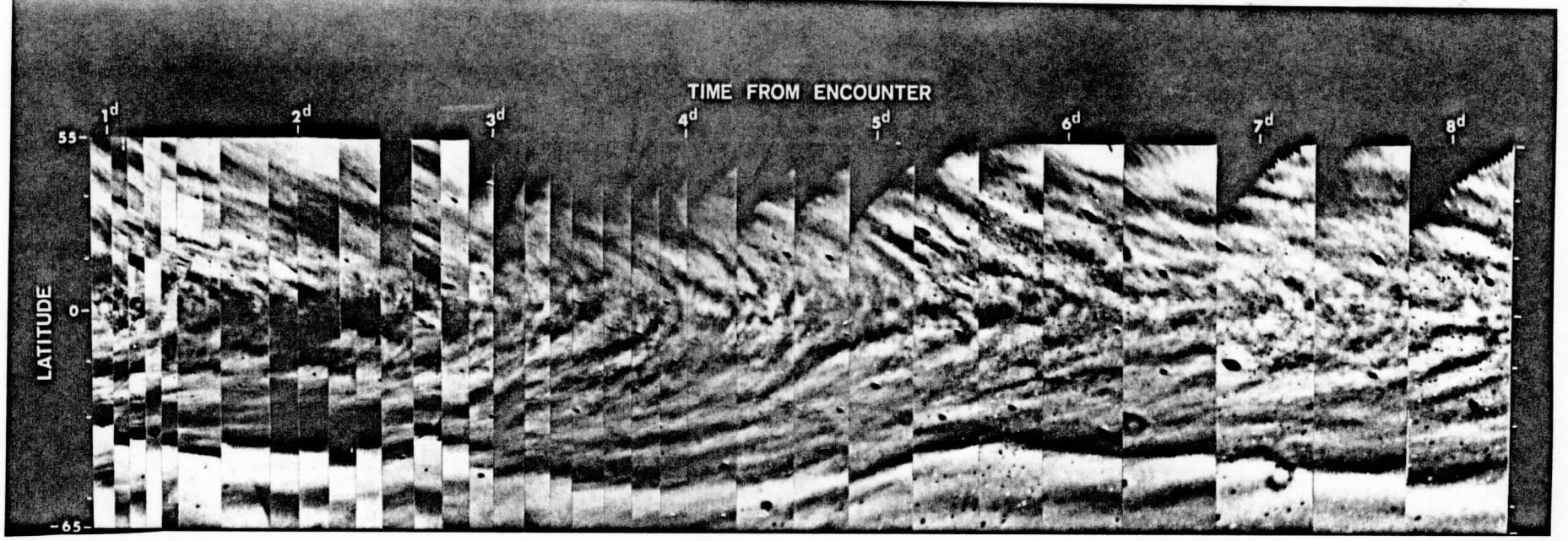

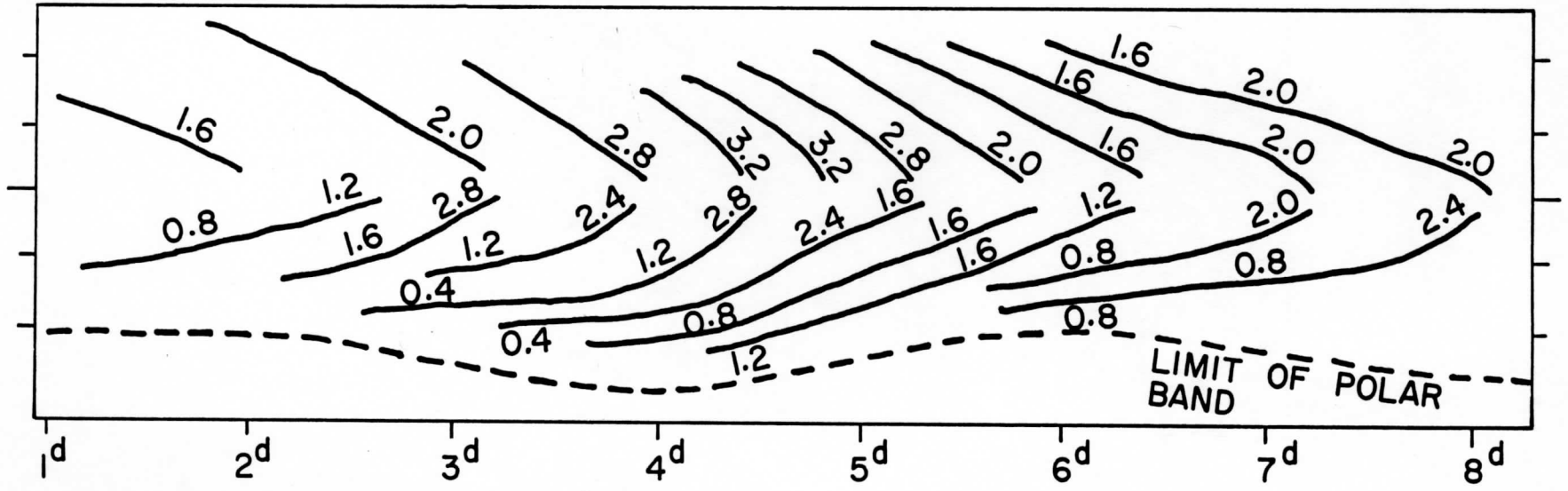

Figure 4. Mercator projection mosaic of high pass filtered pictures of Venus centered on the Mariner 10 spacecraft subpoint as a function of time. The vertical coordinate represents image data on a meridian passing through the subpoint, and is plotted as a function of days past Venus encounter along the horizontal axis. Figure 4b shows streak line curvature expressed in units of m/s/ten degrees as inferred from the shear model and Figure 4a.

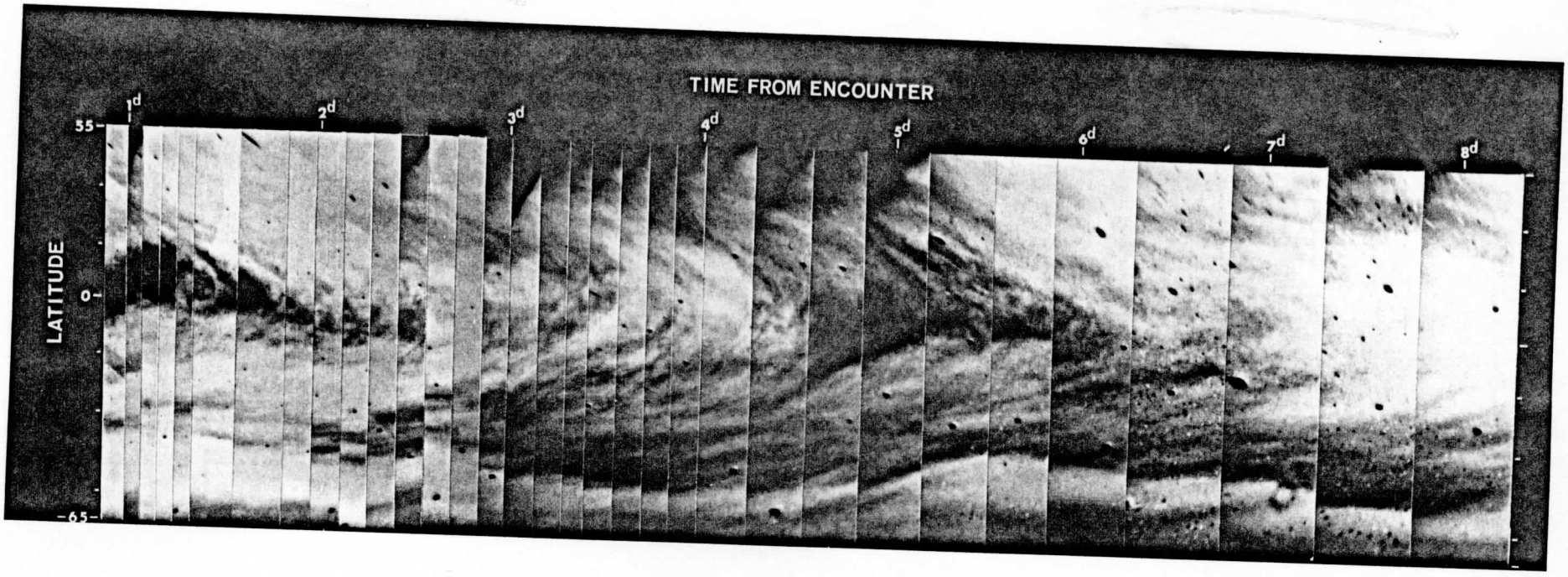

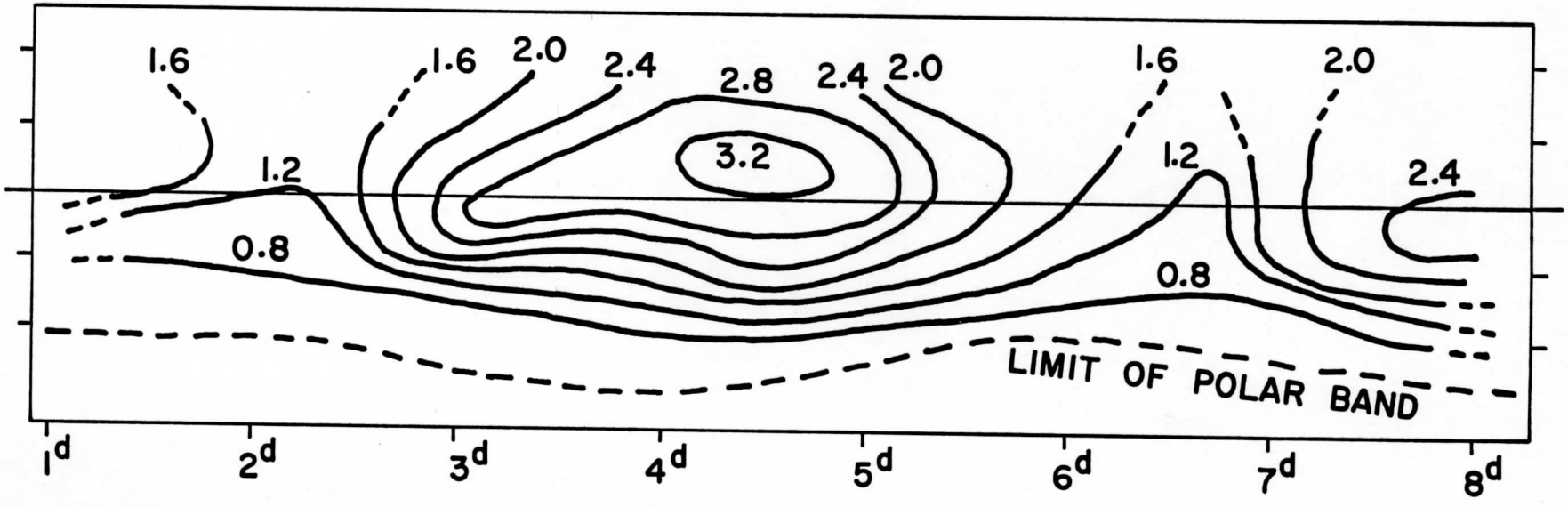

Figure 5. Same mosaic as Figure 4, except the images have been photometrically corrected. While Figure 4a is filtered to enhance small scale details in the clouds, Figure 5a preserves the albedo information. Figure 5b shows contours of the meridional velocity gradient as inferred by means of the model from the curvature of the streaks in Figure 4.

The meridional velocity gradient inferred from the spiral streak model also shows a correlation with the dark "Y" feature. This is most evident in Figure 5b where we have contoured the meridional velocity gradients inferred from the shape of the spiral streaks in Figure 4, and compare the contours with the photometrically corrected mercator mosaic (Figure 5a).

The brightest clouds in the equatorial regions occur when both the zonal and the meridional velocities are increasing, divergence is measured, and the polar ring moves toward higher latitudes. The darkest clouds at the equator form the leg or base of the "Y" feature, which narrows to a thin wisp near 2 days and again near 6 days after encounter. As the base of the "Y" is narrowing, the bright polar ring is moving toward the equator, and as the base of the "Y" disappears, the bright clouds begin to dominate the equatorial regions and velocities again begin to increase in both the u and v directions.

Note that there is a periodic 4 1/2 day undulation symmetric about the equator, with the dark leg of the "Y" appearing in the northern hemisphere, followed by the bright region between the arms of the "Y" appearing in the southern hemisphere. The contours in Figure 5b, however, show a systematic offset toward the northern hemisphere, indicating that the streak curvature is less there, and that the meridional flow is therefore stronger in the northern hemisphere than in the southern hemisphere.

VELOCITY FIELD ANALYSIS

With the streak model as developed, we can use the observed periodicity in the streaks to analyze the measured cloud motions. We have measured widespread zonal acceleration in low and mid latitudes on day 39 (Krauss, 1976a & b). Coupled with meridional flow toward the poles, this is direct evidence of divergence superimposed on the mean zonal flow. On day 40, we observe a divergent pattern early in the day, but it changes to an indeterminate pattern later in the day. The longitudinal gradient of the zonal velocity reverses sign while the meridional flow toward the poles continues to increase. The mean zonal velocity on day 40 is about 5 m/s higher than on day 39. Figures 6, 7, and 8 summarize the results of the velocity measurements made so far. We will be extending the measurements to earlier and later times in the future.

Now, the Mariner 10 flyby images show Venus as it usually appears in the great majority of ground based observations. It is reasonable to assume that this constitutes the nominal or "steady state" condition. That being the case, it would be unlikely for the trends we observe in Figures 6 and 7 from day 39 to day 40 to continue for any great length of time. Too much momentum would have to be transferred, and a substantial change would occur in the character of the global circulation. It is much more likely that we are observing oscillations or perturbations on the steady state, since these can be conservative and thus not seriously affect the mean flow. Indeed, from the 4 1/2 day periodicity evident in Figure 5b, such an interpretation of the trends in Figures 6, 7, and 8 appears to be a reasonable possibility.

One can, in fact, carry this interpretation one step further by using the rate of change of u and v in time, plus the 4 1/2 day period, to infer an amplitude for the oscillations. The dashed lines in Figures 6, 7, and 8

Figure 6. Mean value of zonal velocity measured at equator. Solid dots represent the separate 4 picture data sets, while crosses are averages for a given day. The dashed line is a 4 1/2 day period sine wave with an amplitude chosen to best fit the trend of the velocity measurements.

Figure 7. Meridional velocity gradient measured in the four data sets. Each data set is shown as a solid dot, and each day's average by a cross. The last point in day 40 is spuriously high because not enough points were measured at high latitudes and the least squares fit was influenced too much by measurement scatter. The average of all three data sets on day 40 is more meaningful. The sine curve amplitude is again defined by the slope of the data and an arbitrarily chosen 4 1/2 day period. Note that the phase is the same as in Figure 6.

Figure 8. The zonal velocity gradient shows a similar trend toward a 4 1/2 day cycle. Note that the velocity gradient here changes sign, indicating a tendency for the zonal wind to slow down. The "acceleration" shown here is 180° out of phase with the zonal velocity in Figure 6.

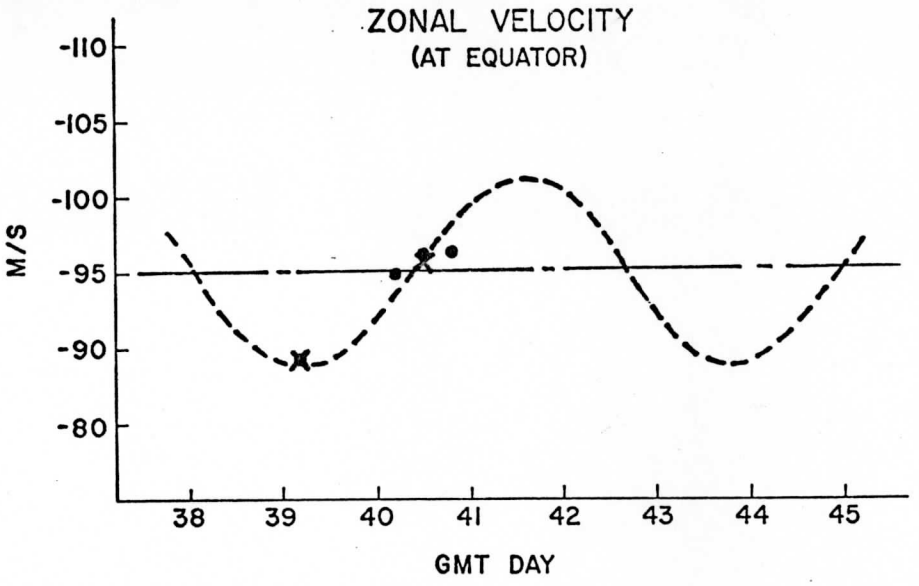
ZONAL VELOCITY
(AT EQUATOR)
-110
-105
-100
-95
-90
-80
M/S
38
39
40
41
42
43
44
45
GMT DAY

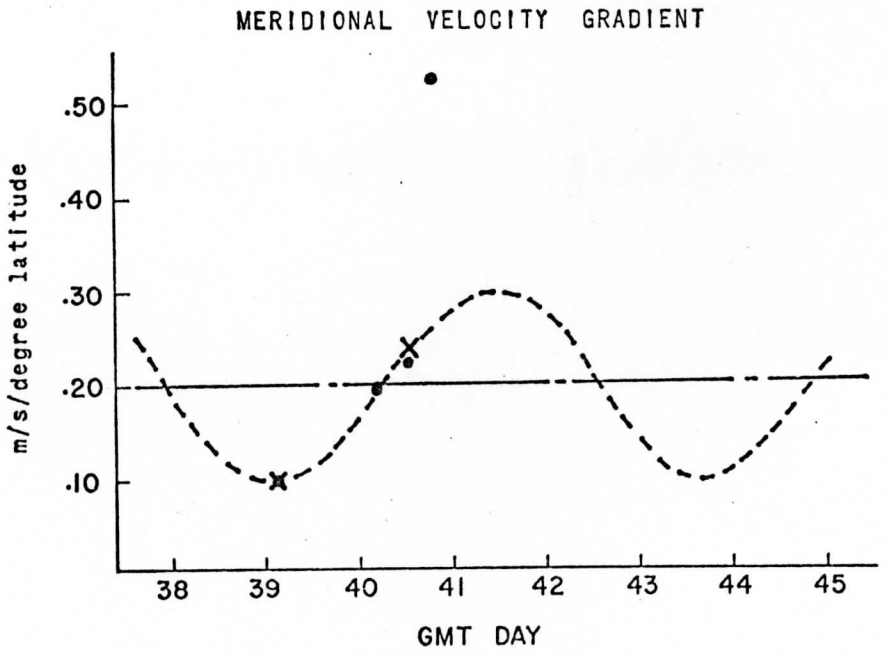
MERIDIONAL VELOCITY GRADIENT
.50
.40
.30
.20
.10
m/s/degree latitude
38
39
40
41
42
43
44
45
GMT DAY

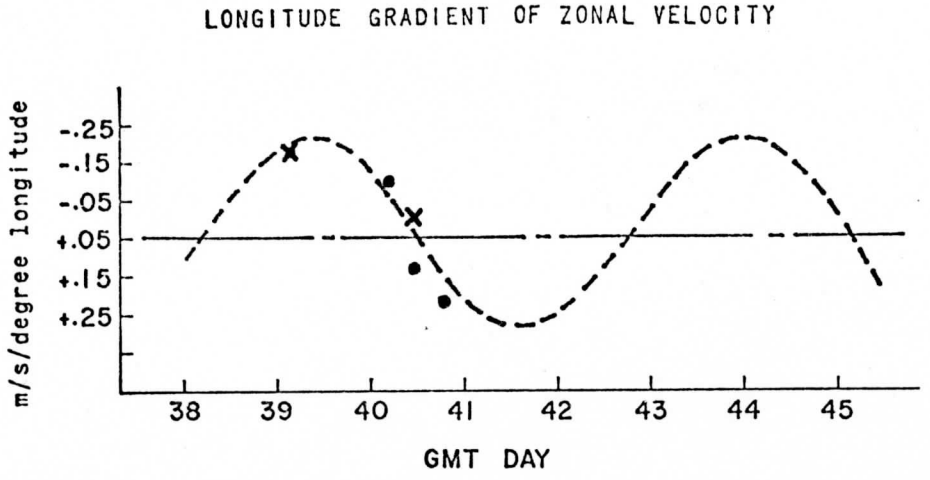
LONGITUDE GRADIENT OF ZONAL VELOCITY
-.25
-.15
-.05
+.05
+.15
+.25
m/s/degree longitude
38
39
40
41
42
43
44
45
GMT DAY

illustrate how the trends can be interpreted in terms of sinusoidal fluctuations with a 4 1/2 day period. Knowing the period from large scale albedo fluctuations and spiral streak curvature, and the slope of the sine curve from the actual velocity measurements, the amplitude of the oscillations can be easily inferred as well as the mean or equilibrium state.

The negative correlation of the zonal velocity (Figure 6) and the zonal velocity gradient (Figure 8) translates into an almost exact 180 degree phase difference. This is somewhat reminiscent of simple harmonic motion (the "restoring force" or velocity gradient is a maximum at maximum "displacement" or zonal velocity) and provides further support for the wave interpretation of the velocity fluctuations. Note too that the amplitude of the waves in Figures 6, 7, and 8 corresponds well with the magnitude of the eddy fluctuations determined on days 39 and 40 (Krauss, 1976b). While one cannot say that the eddy terms and the periodic fluctuations inferred from the streak model are one and the same, it is worthy of note that they are of the same size. The eddy terms, as measured, also tell us that there is some small amount of momentum transport toward the poles at the same time the mean velocities are fluctuating.

FURTHER SPECULATION

When Mike Belton first cut out the center portions of the disk of Venus out of a series of Mariner pictures and pasted them together on a sheet of paper (Murray, et. al., 1974, Figure 11), the entire MVM imaging team thought the result very profound, though at the time nobody could explain why. The importance of that pseudo-mercator projection is only now being appreciated. The correlation of the cloud albedo, spiral streak angles, polar ring motion, and the measured cloud velocities, all with an apparent 4 1/2 day period, is by far the most striking feature of our streak line analysis. It would certainly appear that large scale waves are affecting cloud formation and the velocity field. The evidence is preponderant, but nevertheless circumstantial, for no cause-effect relationship can be established as of yet. Indeed, one ought to be very careful of believing too strongly in a 4 1/2 day wave.

To make this more clear, and perhaps put things in better perspective, several points should be made. First, it must be kept in mind that the upper atmosphere of Venus rotates differentially. There is no "4-day rotation", although the term has become very commonly used and tends to affect how we think about the clouds. To substitute "4 1/2 day rotation" at this point would be equally misleading. Secondly, the hemispheric vortices are still the dominant dynamic structure of the general circulation. The wavelike phenomena we see in the changes of streak curvature, as well as the measured eddy components (Krauss, 1976b), are perturbations on the steady state, demonstrably over an order of magnitude less intense. Finally, only 8 days of Mariner 10 observation are a poor statistical sample. While the appearance of Venus in those 8 days is its most common, one must remember that spectroscopic evidence (Barker and Perry, 1975) gives periods of fluctuations of 6 and >9 days in addition to 4 1/2 days. The 4 1/2 day wave may merely be the most common fluctuation seen, or the most dominant, or perhaps only a superposition of several other waves with entirely different periods. The

fact that the "Y" feature occasionally disappears and then returns in ground based observations lends some credence to the superposition possibility.

Nevertheless, it is instructive to speculate further, for in so doing, we may be able to find a pattern into which the disparate pieces of the Venus puzzle will fit. Two additional pieces of evidence should be mentioned. First is the fact that we see vertical shear in some of the images, with the higher velocity clouds at the higher altitudes, obscuring lower features. This shear contributes substantially to the measurement scatter in the u-component. The second piece of evidence which will prove useful is that we see wavelike phenomena of different scale sizes at several different altitudes. What this implies is that there exists a rather tenuous balance of pressure, temperature and albedo at 60-70 km such that "something" influencing the optical properties of the atmosphere is significantly affected by local physical conditions. The observation of waves in addition to convection, differential motion, eddies, vertical shear, etc. leaves little doubt that the UV markings we are observing are embedded in a fluid flow field and are not something unknown masquerading as a familiar phenomenon. Consequently, though the atmospheric chemistry and cloud physics are different on Venus, the presence of familiar processes allows us to draw on our Earth-based dynamical experience. The general circulation of Venus must still obey the equations of motion.

A. The Mean General Circulation

The only explanation of the streaks consistent with the evidence is the hypothesis that the streaks are indicators of relative shear, i.e. cloud bands existing in a relatively thin spherical shell which is rotating differentially. On the basis of this hypothesis we can draw some further conclusions. The shape and curvature of the streaks does not locally change or show sinuous fluctuations of any kind. Whatever shears are operating, they appear to be reasonably uniform with longitude and change in a monotonic way with latitude. Thus, although we might hypothesize that the formation of the streak material may initially be due to interaction of the zonal flow with a sun-locked disturbance, and that the bow-like waves may be similarily generated, neither a persistent high pressure anomaly nor a solar thermal tide can be the predominant dynamic feature, because each would cause a change in curvature of the streaks when solar heating is turned off at night. Every 48 hours, the acceleration would change and the spiral streaks would show some wiggles. Any sun-locked effect can at most be a small perturbation on what must in general be a very uniform horizontal flow field. The Hadley cell, modified by the zonal flow is such a uniform flow field.

If a modified Hadley cell is the dominant dynamic feature then the convection cells are superficial. The shallow 200 km wide cells at low latitudes with 20:1 ratio of width to height are likely to be the result of solar heating, since they are visible where solar input is a maximum and do not appear near the morning terminator nor at latitudes above 30°. The divergence measured in the velocity field covers an even larger region, from equator to polar ring. One can interpret this as a generalized upwelling at low and mid latitudes with superimposed local heating in a layer about 10 km deep. There is no evidence of deep or very strong local convection. Meridional flow in both hemispheres is measured away from the equator, but is very slow. The

divergent region is not strong enough to overcome or significantly modulate velocities in the predominantly balanced zonal flow. We see only a small acceleration term in the zonal direction, equal to the meridional acceleration.

The zonal motion profile varies with latitude like a vortex. This conforms with the need for a Hadley cell to show convergence and sinking motion at the poles in addition to divergence at the equator. The motion field tends to conserve angular momentum except for a small loss attributable to friction. At 45° latitude we observe turbulent eddies approximately 200 km in diameter, strongly indicative of barotropic instability. The eddy curvature (see Murray, et. al., 1974, Figure 7) shows higher velocity on the poleward side, in the bright polar ring. The zonal velocity profile at 45° latitude obeys the approximate relation $\partial u/\partial y \tilde{\gtrsim} 2\Omega\sin\phi$, which is the theoretical threshhold for dynamic instabilities to form. We can thus infer that the bright polar band is a region of turbulent stirring and of higher eddy viscosity and is likely to be a transition zone to a region of less horizontal shear and more constant vorticity, because the atmosphere cannot support the laminar flow and conserve angular momentum at the same time. Beyond the 45° point we observe uniform angular velocity. Such an organization is exactly that of the inner portion of a vortex, which rotates at constant angular velocity as mass is drawn out of the horizontal plane and into vertical motion. It is hard to avoid concluding that the atmosphere of Venus similarly sinks at the poles.

Three pieces of evidence can support a sinking of the atmosphere of Venus at high latitudes. First, there is more CO_2 generally seen at the poles (L. D. G. Young, et. al., 1975), implying a lowering of the reflecting layer or cloud haze. Second, the poles are slightly colder in effective temperature most of the time, except when a "hot" spot ~5-10°K warmer than its surroundings appears (Murray, Wildey and Westphal, 1963). This hot spot could be the eye of the polar vortex, either made transparent by loss of clouds, or warmed by adiabatic compression. Third, radar observations (Sinclair, et. al., 1969) imply that, at the surface of Venus, the poles are probably a few degrees warmer than the equator. Such a reversal of the equator to pole temperature gradient is not possible under strict conditions of radiative balance, but is easily maintained if the atmosphere moves so that the polar regions could be warmed by advection or adiabatic sinking. A horizontal temperature gradient also guarantees that there will be atmospheric motion at the surface of Venus.

The general picture, so far described, is that of a simple Hadley cell modified by the zonal flow to resemble a hemispheric vortex. A single directly driven cell, with heat and momentum sources and sinks coinciding is impossible. On the Earth one needs the equivalent of a subtropical high to maintain geostrophic balance in the low level return flow, and this upsets the pressure gradients needed to perpetuate a pure Hadley circulation. The resulting compensating mechanism is a statistical three cell breakdown in the meridional structure of the general circulation (Lorenz, 1967). Since Venus seems to have a simple direct Hadley cell in its upper atmosphere, it is likely that compensation on Venus occurs in vertical cells which we cannot see. The vertical wind shear profiles from the Russian Venera probes (Kerzhanovich, et. al., 1972; Marov, et. al., 1973) and the turbulent layer seen by Mariner 10 (Howard, et. al., 1974; Woo, 1975) are possible glimpses of such structure.

Whatever else one can say about the vortex, it appears to be stable. The structure of the velocity profiles is much larger than our estimated errors and is well organized. Moreover, the motion field was independently derived from motion of small scale cloud features, yet is strongly correlated with the semi-permanent features such as the polar ring and the arms of the "Y" or spiral streak angles seen in earth based observations. The "Y" and reversed "C" always are oriented in the same direction (O'Leary, 1975). Consequently, the vortex is highly likely to be representative of the usual or mean state on Venus. The dynamical structure of the vortex is stable over at least short time periods, since its destruction would require redistribution of a large angular momentum. Over the long term, however, changes are likely. The bright polar rings, for example, occasionally disappear singly or in pairs (Dollfus, 1975). Venus thus appears to have a "change of climate" now and then in its upper atmosphere even though its axis is not significantly tilted.

B. Vertical Momentum Transport

If the vortex structure and modified Hadley cell are the usual conditions in the upper atmosphere on Venus, we must ask what drives the zonal winds. What maintains the zonal flow so uniformly in the face of frictional dissipation and cycles planetary angular momentum back up to the top of the atmosphere? Momentum should diffuse from regions of high velocity to regions of low velocity. To bring momentum upward at low latitudes from the slow moving surface into the 100 m/s flow requires a very efficient pump.

One such mechanism proposed was the "moving flame" model of Schubert and Whitehead (1969) and Schubert and Young (1970), and further developed by Gierasch (1970) and Malkus (1970). Periodic solar heating results in Reynolds stresses and tilted convection cells which move momentum upward in a vertical plane at constant latitude. The effect should be strongest at the equator where maximum heating occurs, and weaker acceleration should be visible at higher latitudes. In fact, we see no significant lessening of zonal acceleration at higher latitudes and the zonal velocities are higher there than at the equator. The spiral streaks are also too tilted at high latitudes to be directly related to a time lag due to solar heating. In addition, the mottled appearance of the subsolar convective zone shows no indication of large scale organized cells and associated cloud rolls or streets expected to be seen with a moving flame mechanism. Indeed, the only place where such periodicity is evident is in the streaks at the morning terminator after 48 hours of radiative cooling.

The existence of a thermal tide is also a possibility for transporting momentum upward, but suffers from two problems. First, the analysis of Ingersoll and Orton (1974) shows a two peak temperature fluctuation around the circumference of Venus with cold regions at the evening terminator and the morning terminator. This double peak could reflect the limited data analyzed (if, say, a single peak travelling around the planet were observed at several different phases). The point to emphasize here is that Ingersoll and Orton see no single stationary temperature maximum. A solar thermal tide would be consistently warm at the evening terminator, with one single wave around the planet. Secondly, the changing convergence and divergence as the atmosphere cools and sinks on the night side and warms and rises on the

day side might be consistent with the measured velocity profiles, but ought to give the same spiral streak curvature at all longitudes. Instead we see global scale longitudinally fluctuating curvature of the streaks coupled with a change in large scale albedo and a shift in latitude of the bright polar ring. The resulting picture is more that of a single wave travelling around the planet with maxima and minima both passing sequentially underneath the sun. Such a wave is also capable of transferring momentum upward in the presence of a mean steady state, and would exist as a perturbation on the vortex flow.

The spiral streak model can help to identify additional features of the motion field. For example, the streaks have north-south asymmetry. The meridional velocity gradient in the northern hemisphere (Figures 4b and 5b) is larger, and the acceleration contours are shifted off the equator. The meridional gradient is only about 1/3 as large at 45 degrees latitude as it is at the equator. Finally, we note that the meridional velocity gradient is likely to be a minimum at 2 days after encounter, while the mean meridional velocity gradient is probably closer to 0.20 m/s/deg (Figure 7). The highest meridional velocities ought to be measured at 4 1/2 days after Venus encounter. The brightest albedo features occur when the meridional velocity is increasing and we see divergence. The darkest feature "Y" occurs when the meridional velocity is decreasing and we see what is probably relative convergence.

Neglecting the question of what the UV clouds really are, we can digress a bit by considering the possible coupling of vertical motion to the wave features. What would we expect to see if rising motion generates bright UV clouds and sinking motion generates darker markings? We find a possible answer for why Young (1975) fails to see a correlation between shading and effective temperature. The bright clouds exist at temperatures of 250 ± 10°K. Depending on their relative altitude, the atmospheric parcels which have risen the farthest will be colder and brighter. Parcels which sink get dark and warm as bright cloud elements disappear from them. A bright region would not get much colder as it rises because there is a "lid" on convection in the stable upper layers. In general, the rising masses would tend to get brighter, colder, and more uniform in temperature as bright cloud elements are generated. The sinking atmospheric masses lose the lower clouds first so one gets to see lower and still warmer regions at a faster rate than the mean gas temperature of the whole mass would rise. Such sinking and partially transparent masses are darker, warmer, and less uniform in temperature with a tendency to show more scatter on the warm side, depending on cloud population as a function of altitude and area.

Such a theory of cloud contrast and formation is adaptable to correlation with CO_2 concentration as well. Large scale vertical motion both intensifies cloud formation by convection and intensifies destruction by subsidence so that one sees a tendency toward brighter clouds when the reflecting layer is rising and darker clouds when the reflecting layer is falling. At CO_2 maxima and minima one would see half bright and half dark and thus no correlation at all! At the poles, clouds have been stirred up and are thick, as well as being radiatively cooled. They could be sinking, but would not dissipate as fast as at the equator, so they would retain a high albedo.

C. Vertical Shear and Dynamic Balance

Pressure forces caused by horizontal temperature gradients can be quite large, even if the pressure differences are only a couple of millibars. There must be a balance condition for the fast zonal flow to keep it moving without deviating significantly from its path as a result of pressure differences induced by solar heating. Without this balance, for example, one would expect to see large jetlike features or streamlines deviating away from the subsolar region. The meridional flow would have to be considerably larger than it is measured to be.

On earth, the balance which keeps the westerlies westerlies and causes the jet stream to meander without moving far out of the temperate zone is called geostrophic balance. It is the equality between the pressure force generated by warmer air toward the equator and the horizontal component of the coriolis force. This balance guarantees that any air parcel moving zonally will tend to remain at constant latitude. If the parcel deviates too far to the north, the horizontal component of the coriolis force turns it back to the south. If it moves too far south, the coriolis force diminishes, but the pressure force pushes the parcel north.

A balanced flow such as this has another property. The equations of motion require that the wind at higher altitudes must move faster. The horizontal temperature gradient is larger at high altitudes on the average than at low altitudes, provided the gas is in vertical hydrostatic balance. This means that the velocity must be greater to balance the increased pressure force due to the larger horizontal temperature gradient at higher altitudes. Since geostrophic balance can only be achieved under conditions where there is a horizontal temperature gradient, the accompanying vertical wind shear is called the "thermal wind."

Venus rotates so slowly that the coriolis forces never amount to much and cannot offset the effect of solar heating. Leovy (1973) has suggested that the zonal flow might be maintained by the horizontal component of the centrifugal force instead. This is called cyclostrophic balance, and for the same reasons as above, we must also have a thermal wind present. . In other words, if the zonal wind on Venus is constrained by dynamic balances to move in the mean along lines of constant latitude, the simple requirement that the fluid also obey the hydrostatic equation necessitates the presence of a vertical wind shear.

It is instructive to look at the implications which Leovy derives. A 100 m/s zonal wind would require only a modest 3°K vertically averaged temperature bulge at the equator for the pressure gradient to balance the horizontal component of the centrifugal force. This could easily be maintained by solar heating. Simply stated, the zonal winds on Venus continue to move fast at higher altitudes because the equator is just a little warmer. The zonal rotation can be started in the right direction by a slow overturning of the atmosphere, initiated by solar heating. This motion then causes friction with the planetary surface and eventually brings a small amount of planetary angular momentum to the top of the atmosphere. Viscous losses and turbulent momentum transport would prevent this mechanism from working once the rotation of the upper atmosphere picked up speed, however. Leovy

finds it intuitively difficult to maintain an equatorial thermal bulge, even in the very uniform case with no longitudinal variations in solar heating. He suggest Kelvin waves propagating phase westward as a means of independently moving momentum flux upward against viscous and turbulent dissipation to maintain the cyclostrophic balance. Most of the momentum would then be dumped at an altitude where the phase velocity of the wave equals the speed of the upper level winds. Mass could not begin to move poleward until it was sufficiently warmed, and the pressure force became larger than the centrifugal force.

Now we can see changes in the meridional flow, periodic meridional movement of the polar ring, and a change in curvature of the spiral streaks. These are evidence for a meridional component in the 4 1/2 day wave. It follows that the large scale waves on Venus cannot be pure Kelvin waves, because Kelvin waves exhibit no meridional motion. The waves we see do form a potential source of momentum for the upper atmosphere, however, since they have the right size to coincide with our measured region of divergence and they have the right phase velocity to dump momentum in the altitudes where solar energy input is a maximum. That is, we see divergence and zonal acceleration in the same 60-70 km altitude slice. Consequently, it is possible, by maintaining a high zonal velocity near the equator, to keep the upper atmosphere where it will receive maximum solar input until the 3°K temperature bulge is achieved.

The slow meridional motion and vertical wind shear are strong indications that dynamic balance exists, and the planetary waves are a necessary part of maintaining the stability of the vortex by keeping the zonal velocity in balance with the solar heating. Presumably, the long term changes observed in the large scale UV markings on Venus (the disappearance of its polar caps, for instance) are situations where conditions have gotten unbalanced and need time to reestablish the nominal steady state.

SUMMARY

The fact that the spiral streaks on Venus are neither trajectories or jets nor completely wavelike in character has lead to an attempt to interpret them as indicators of relative mass motion in a differentially rotating shell. Using the measured velocity field in the upper atmosphere and assuming constant $dV/d\phi$ and no significant perturbations in the mean u or v at any given latitude, it is possible to reproduce the streak shape as seen in a pseudo-mercator projection. Once the connection between the velocity gradients and the streak curvature is established, one can use the streaks to infer large scale velocity field fluctuations from the Mariner 10 images. These velocity fluctuations are strongly correlated with the dark "Y" albedo feature and the latitude motion of the bright polar ring, and appear to have a 4 1/2 day cycle. This suggests a global scale wave phenomenon superimposed on the mean steady state. The velocity field measurements to date partially support this interpretation. They indicate trends which are consistent with a wave amplitude approximately 10% of the mean zonal flow. In addition a definite 90 degree phase relationship exists between velocity and "acceleration," i.e. between zonal velocity and the zonal velocity gradient. Eddy components of the order of magnitude of 10% have also been measured.

The zonal winds on Venus are organized in a vortex structure with an equatorial velocity of -95 m/s, a slight meridional flow with a mean gradient of 0.22 m/s/deg away from the equator, and a tendency to conserve angular momentum while moving to higher latitudes. At 45° latitude, coinciding with the onset of dynamic instability predicted from the measured velocity profile, we observe turbulent eddies and transition to a more viscid regime of solid rotation, corresponding to the central region of a vortex where motion in the vertical becomes a dominant characteristic. This sinking at the poles is supported by Earth based observations of occasional polar hot spots in the effective temperature of the upper atmosphere, increased CO_2 absorption above the polar reflecting layer, and hot poles at the surface of Venus which could be from adiabatic warming due to a sinking atmosphere.

The vortex appears to be a reasonably consistent feature on Venus because the high velocity zonal winds and the shape of the often observed "Y" features are commonly found in Earth based observations of Venus and are closely related to the motion field we measure. Any change to a different circulation regime would require redistributing large quantities of angular momentum and establishing a different kind of dynamic balance.

The large scale dynamic balance appears to be cyclostrophic. We observe a vertical wind shear of 10-15 m/s, with the higher altitude clouds moving faster than the low altitude clouds which form the majority of our measurements in the 60-70 km altitude layer. The -95 m/s mean equatorial velocity is very close to the phase velocity of the 4 1/2 day wave. This wave phenomenon produces observed variation in planetary albedo, and is correlated with both the meridional motion of the bright polar ring and with changes in curvature of the spiral streaks. Such a wave, propagating phase westward, could bring angular momentum up from below to support the zonal winds.

The momentum supplying wave, being correlated with a small change in planetary albedo, can be driven by the sun. Convective cells in the subsolar region are evidence of energy input at the right altitude. The only requirement is that the amplitude of the wave oscillations not be large enough to disrupt the zonal or meridional flow in the vortex, which in the mean must provide the necessary equator to pole energy transport to maintain global radiative equilibrium. If we believe the streak model, which seems so nicely correlated with everything else, the mean meridional velocity gradient is 0.20 m/s/deg and the amplitude of the wave is 0.10 m/s/deg. The strong vertical wind shear and turbulence observed near the equator at 45-50 km altitude by the Venera probes and Mariner radio occultation may form a lower bound for such planetary scale waves in the vertical.

The combination of an upper level vortex, cyclostrophic balance, and a global wave maintaining the zonal momentum supply in equilibrium with solar heating provides a consistent explanation for the stability of the upper atmosphere circulation pattern on Venus. The wave coupled cloud forms, subsolar convection intensity, and the associated albedo changes provide a means to perturb the mean flow (and thus pump in more or less solar energy as needed to drive the global wave) and also provide an adequate supply of feedback mechanisms to stabilize the vortex over periods of days or weeks and maintain the global energy balance. Long term changes, such as the disappearance of the bright polar cloud caps, may relate to more severe dynamic imbalances. Determining the interaction of the varied mechanisms

requires a longer time base study than the 8-day Mariner 10 flyby data provides. It should be possible to measure the relative strengths of the rich array of visible phenomena, however, and thereby determine which physical processes are likely to be important pieces of the dynamic puzzle of Venus.

ACKNOWLEDGEMENTS

The author wishes to thank Sanjay Limaye for numerous informative and educational discussions and Linda Kluck for typing of the final manuscript.

This research was supported by NASA Grant #NGR-50-002-189.

BIBLIOGRAPHY

Barker, E. S. and Perry, M. A.; 1975: "Semi-Periodic Variations in CO_2 Abundance on Venus," Icarus, 25, 282-295.

Belton, Michael J. S.; Smith, Gerald R.; Elliott, Denis A.; Klaasen, Kenneth; and Danielson, G. Edward; 1976: "Space-Time Relationships in the UV Markings on Venus," J. Atmos. Sci. (to be published).

Danielson, Edward; 1975: "Mariner 10 Imaging System," The Atmosphere of Venus, NASA SP-382, 40-41

Dollfus, Audouin; 1975: "Venus: Evolution of the Upper Atmospheric Clouds," J. Atmos. Sci., 32, 1060-1070.

Gierasch, Peter J.; 1970: "The Four-day Rotation in the Stratosphere of Venus: A Study in Radiative Driving," Icarus, 13, 25-33.

Howard, H. T., et. al.; 1974: "Venus: Mass, Gravity Field, Atmosphere, and Ionosphere as Measured by the Mariner 10 Dual Frequency Radio System," Science, 183, 1297-1301.

Ingersoll, A. P. and Orton, G. S.; 1974: "Lateral Inhomogeneities in the Venus Atmosphere: Analysis of Thermal Infrared Maps," Icarus, 21, 121-126.

Krauss, Robert J.; 1976a: "UV Cloud Motions on Venus from Mariner 10 Images," SSEC Annual Report for 1975 on JPL Contract 953034 and NASA Grant NGR50-002-189.

Krauss, Robert J.; 1976b: "New Measurements of UV Cloud Motions on Venus," SSEC Annual Report for 1975 on JPL Contract 953034 and NASA Grant NGR50-002-189.

Leovy, Conway B.; 1973: "Rotation of the Upper Atmosphere of Venus," J. Atmos. Sci., 30, 1218-1220.

Lorenz, Edward N.,; 1967: "The Nature and Theory of the General Circulation of the Atmosphere," World Meteorological Organization.

Malkus, Willem V. R.; 1970: "Hadley-Halley Circulation on Venus," J. Atmos. Sci., 27, 529-535.

Marov, M. Ya; Avduevsky, V. S.; Kerzhanovich, V. V.; Rozhdestuensky, M. K.; Borodin, N. F.; Ryabov, O. L.: 1973: "Venera 8: Measurements of Temperature, Pressure and Wind Velocity on the Illuminated Side of Venus," J. Atmos. Sci., 30, 1210-1214.

Murray, Bruce C.; Belton, Michael J. S.; Davies, Merton E.; Gault, Donald; Hopke, Bruce; O'Leary, Brian; Strom, Robert G.; Suomi, Verner; and Trask, Newell; 1974: "Venus: Atmospheric Motion and Structure from Mariner 10 Pictures," Science, 183, 1307-1315

Murray, Bruce C.; Wildey, Robert L.; and Westphal, James A.; 1963: "Venus: A Map of Its Brightness Temperature," Science, 141, 391-392.

O'Leary, Brian; 1975: "Comment on Mariner 10 and Ground Based UV Observations," The Atmosphere of Venus, NASA SP-382, 63-68.

Schubert, G. and Whitehead, J. A.; 1969: "Moving Flame Experiments with Liquid Mercury: Possible Implications for the Venus Atmosphere," Science, 163, 71-72.

Schubert, Gerald and Young, Richard E.; 1970: "The 4-Day Venus Circulation Driven by Periodic Thermal Forcing," J. Atmos. Sci., 27, 523-528.

Sinclair, A. C. E.; Basart, J. P.: Buhl, D.; and Gale, W. A.; 1972: "Precision Interferometric Observations of Venus at 11.1cm Wavelength," Astrophys. J., 175, 555-572.

Suomi, Verner; 1975: "Cloud Motions on Venus," The Atmosphere of Venus, NASA SP-382, 42-58.

Woo, Richard; 1975: "Observations of Turbulence in the Atmosphere of Venus Using Mariner 10 Radio Occultation Measurements," J. Atmos. Sci., 32, 1084-1090.

Young, Andrew T.; 1975: "The Clouds of Venus," J. Atmos. Sci., 32, 1125-1132.

Young, L. G.; Young, A. T.; Young, A. W.; and Bergstrahl, J. T.; 1973: "The Planet Venus: A New Periodic Spectrum Variable," Astrophys. J., 181, L5-L8.

APPENDIX C

Venus: Global scale inertial oscillations. S. S. Limaye, Dept. of Meteorology, U. of Wis., Madison.- Scale analysis of equations of motion for a slowly rotating planet such as Venus shows that to a first order approximation the meridional profile of zonal speed resembles that obtained under conservation of absolute angular momentum and that the pressure gradient force is balanced by the horizontal component of centripetal force as also suggested by Leovy (1973, J. Atmos. Sci., 30, 1218-1220). If this is the case then provided the perturbation pressure components are small or are axisymmetric the frequency of inertial oscillations in a uniform horizontal basic flow is given by the expression: $n^2 = 2U^2 \tan^2 \phi/a^2 + 3fU \tan \phi/a + f^2$. The resulting perturbation kinetic energy is not constant with time but varies at twice the frequency of inertial oscillations. Sample calculations of inertial oscillation trajectories show global scale coverage in a matter of days. It appears that oscillations of this kind cannot be ruled out in the stratosphere of Venus where the UV markings delineate the atmospheric flow. The subsolar high pressure region could be the source of velocity perturbations. Such oscillations may be apparent in the measurements of motions of the UV features obtained by Suomi (1975, NASA SP 382).

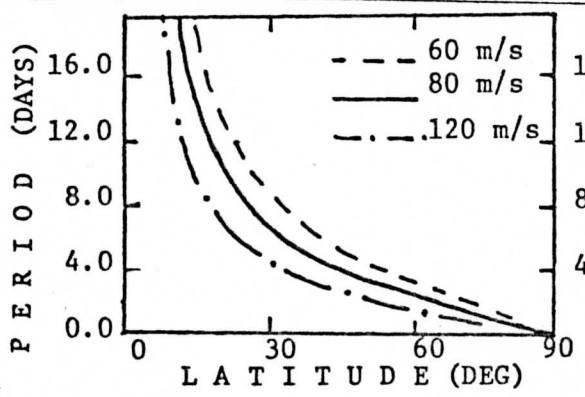

INERTIAL OSCILLATION PERIODS FOR VARIOUS UNIFORM MEAN ZONAL FLOWS FOR VENUS

APPENDIX D

Reprinted from JOURNAL OF THE ATMOSPHERIC SCIENCES, Vol. 34, No. 1, January 1977
American Meteorological Society
Printed in U. S. A.

A Normalized View of Venus[1]

SANJAY LIMAYE AND VERNER SUOMI

Space Science and Engineering Center, University of Wisconsin, Madison 53705

(Manuscript received 16 June 1976, in revised form 5 October 1976)

ABSTRACT

It is now known that Venus has a fairly thick and massive atmosphere, the 10 mb level occurring at a height of about 80 km above the surface. Mariner 10 television observations agree with an isotropic scattering model with single scattering albedo of about 0.92 in the untralviolet region of the spectrum. Based on this knowledge, a few Mariner 10 images have been "normalized" to a standard scattering geometry using the exact solution by Chandrasekhar involving his H functions.

The most striking feature of the normalized images is the bright polar ring or cap beyond about 50° latitude circle and a narrower brightness frequency distribution. The brightness variation along a meridian shows substantial axial symmetry on a large scale, and small-scale brightness variations over the planet are no more than about 10%. Inferences regarding the polar cloud tops in light of available evidence are discussed.

The variation of mean brightness and of the ratio of mean square deviation of brightness to average brightness is comparable to the performance limits of the vidicon camera for the image sequence lasting about a day so that the variation in distribution of dark and bright features over the planet and the UV albedo of the planet over about a day is small.

1. Introduction

This paper deals with "normalization" of several Mariner 10 ultraviolet images of Venus based on the assumption of diffuse reflection by the cloudy atmosphere such that every point on the planet is viewed in the image with the same scattering geometry. This facilitates a comparison of the absolute brightness of the UV features in various regions of the sunlit planet. The terrestrial experience is that in a normalized image the general rule of thumb that brighter clouds are optically thicker can be quantified (Martin *et al.*, 1975). The question of the UV contrasts in the atmosphere of Venus is still unsettled and it is not possible to postulate a general yardstick between the brightness of UV features and their optical and/or geometric thickness. Nevertheless, the sun and viewing angle normalized images show up some interesting characteristics.

It was pointed out by Huggins (1867) that optically thick planetary atmospheres would behave roughly like Lambertian reflectors. This was confirmed by observations of Mars from Mariner 9 (Leovy *et al.*, 1972) even though the Martian atmosphere is thin compared to that of Venus.

Horak (1950) reported that the visual and photographic curves for Venus can be represented by known laws of diffuse reflection for phase angles $<130°$ with isotropic scattering and a single scattering albedo $\tilde{\omega}_0=0.950$. It is interesting to note that the limb darkening in yellow light can also be represented fairly well by isotropic scattering again with $\tilde{\omega}_0=0.950$ and that the polarization of the atmosphere of Venus is not due to Rayleigh scattering (Horak, 1950).

Hapke (1976) has found similar results from observations of the UV images from Mariner 10. In particular, a single scattering albedo $\tilde{\omega}_0$ between 0.91 and 0.93 with isotropic scattering agrees very well with the observations, better than results from Mie scattering or Rayleigh scattering. In order to absolutely "normalize" the Venus images one would wish to use a scheme which would include effects of Rayleigh scattering of the atmosphere and of Mie scattering of the aerosols and clouds plus any polarization effects which we now know to exist [see Coffeen and Hansen (1974) for a review of polarimetric studies]. Such an approach would require an enormous computational task as well as require specific information on scattering particles. Fortunately, the relative variations in brightness of the Venus images can be simulated (except of course the UV features) using a simple isotropic scattering approximation, and because of the simplicity of the solution, the approach used seems justified.

Using a mean single scattering albedo in the law of diffuse reflection, it is possible to normalize a Mariner 10 Venus image to a standard sun-planet-camera geometry for every point on the planet so that the

[1] Presented at the Division of Planetary Science Meeting of the American Astronomical Society, Austin, Tex., 31 March–4 April 1976.

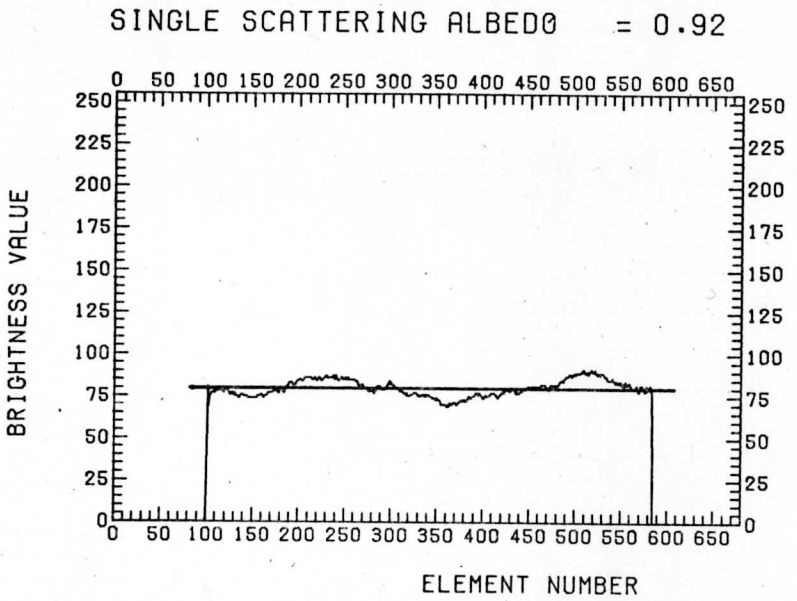

FIG. 1. Typical brightness variation along a scan line, through both the subsolar point and the subspacecraft point on the planet in a normalized image. The solid line shows the mean H-function solution for $\tilde{\omega}_0=0.92$.

brightness variations in a normalized image represent actual physical characteristics of the features alone and are not due to different solar and spacecraft (camera) zenith angles.

2. Image normalization

a. Brightness variations due to changing scattering geometry

Fig. 1 shows the intensity along a particular image scan line passing through both the subsolar and the subspacecraft point in the normalized version of a UV image (FDS #64897). The solid line represents the mean H-function solution for $\tilde{\omega}_0=0.92$, based on Hapke's (1975) results that isotropic scattering models with $\tilde{\omega}_0$ between 0.91 and 0.93 match with observed intensities. The departures from the mean photometric curve are the Venusian light and dark features. The images analyzed were corrected for geometric distortion as well as for photometric deviations at the Image Processing Laboratory (IPL) of the Jet Propulsion Laboratory.

Mariner 10 images of Venus show a large number of atmospheric features in the ultraviolet, and the observed contrast is generally fairly small. In particular, one sees a few recurrent bow-like features which seem to move at approximately the same speed as other features without drastically changing their shape or size (Murray *et al.*, 1974).

In other regions of the planet "cloud clusters" or large bright patchy features move from the morning terminator side toward the subsolar region rapidly changing their shape and brightness. As seen in the "raw" sequence in Fig. 3 (left), there are certain features which show a marked change in their overall brightness as they move across the planet. Since the solar and camera zenith angles vary substantially for a certain feature as it moves across the planet disc, it is not immediately clear whether the observed changes in the overall brightness of a feature are real or whether they are simply due to a change in illumination and viewing angles. The normalization of a sequence of Mariner 10 Venus image would ensure that any changes in the brightness of a feature as it moved across the planet would be due to actual physical changes in the feature and not be due to changing scattering geometry. Thus, standardizing every point on the planet to the same sun-camera geometry enables us to gain information about the properties of the features themselves.

b. Normalization procedure

Chandrasekhar (1950) has obtained the exact solution for the case of diffuse reflection from a plane parallel atmosphere as

$$I(0,\mu)=\frac{\tilde{\omega}_0 F}{4\pi}\left(\frac{\mu_0}{\mu_0+\mu}\right)H(\mu)H(\mu_0), \qquad (1)$$

where I is the emergent intensity, πF is the flux incident on the planet, $\mu_0=\cos\zeta$ is the cosine of the solar zenith angle, and $\mu=\cos\eta$ is the cosine of camera zenith angle. The isotropic scattering phase function $P(\cos\theta)=\tilde{\omega}_0$ has been used, wherein $\tilde{\omega}_0$ is the single scattering albedo. $H(\mu)$ and $H(\mu_0)$ are Chandrasekhar H-functions, and tabulated values are available (Chandrasekhar, 1950). Fig. 2 shows the values of

$H(\mu)$ for various values of the single scattering albedo $\tilde{\omega}_0$.

For normalizing an image, we introduce an arbitrary scaling constant $X(\lambda,\phi)$ to describe the light and dark features seen on the planet in Eq. (1):

$$I_{\text{OBS}}=\frac{\tilde{\omega}_0 F}{4\pi}\left[\left(\frac{\mu_0}{\mu_0+\mu}\right)H(\mu)H(\mu_0)\right]X(\lambda,\phi).$$

Thus $(F/4\pi)X(\lambda,\phi)$ is the normalized brightness for the point (λ,ϕ) on the planet, given by

$$I^*=\frac{F}{4\pi}X(\lambda,\phi)=I_{\text{OBS}}\frac{(\mu_0+\mu)}{\tilde{\omega}_0\mu_0 H(\mu)H(\mu_0)}.$$

One then needs to know the single scattering albedo $\tilde{\omega}_0$ and the two zenith angles ζ and η for the sun and spacecraft in order to obtain the normalized brightness for every point.

To be able to compute $\mu_0=\cos\zeta$ and $\mu=\cos\eta$ the image has to be navigated first [i.e., to obtain a transform between the image plane coordinates of a point $P(l,e)$ where l is the scan line number and e the sample element number in that scan line] to the absolute position $P(\lambda,\phi)$ in latitude and longitude on the planet:

$$T(l,e,\lambda,\phi)P(l,e)=P(\lambda,\phi).$$

The coordinate transformation function $T(l,e,\lambda,\phi)$ can be obtained from a knowledge of the spacecraft orbit parameters and the location of the sub-solar point and the sub-spacecraft point with the crucial constraint that the sub-solar point and the sub-spacecraft point lie on the same image scan line. A more detailed description of image navigation is given by Phillips and Limaye (1976).

The H-functions for $\tilde{\omega}_0=0.92$ [a value between the limits of 0.91 and 0.93 suggested by Hapke (1976). However, the exact value of $\tilde{\omega}_0$ is not too crucial as we are interested in relative intensity variations and not absolute values. In fact, qualitatively the same normalized image is obtained if normalization is done on an even simpler diffuse reflection law: such as Lamberts law] for the zenith angles were computed by a 4-point Lagrangian interpolation scheme from the tabulated values given by Chandrasekhar (1950).

3. Analysis of normalized images

The unnormalized and normalized versions of the 12-image sequence on Julian Day 40 (1974) are shown in Fig. 3 in the left and right columns, respectively. The unnormalized versions were decalibrated using the program FICOR at IPL, so that the digital brightness numbers are related linearly to the actual intensity at least at brightness number $\gtrsim 10$ on a 0 to 255 scale. During the normalization of the images it was ensured that the dynamic range of all the images was between 0 and 255 and that there was no saturation. Thus a comparison of the brightness of a feature in successive frames is possible and is limited only by the absolute accuracy limit of the vidicon. The brightness changes observed in the normalized sequence are thus indicative of actual changes in the scattering characteristics of the features in terms of their shape, size and scatterers as long as they are greater than the accuracy limits of the vidicon.

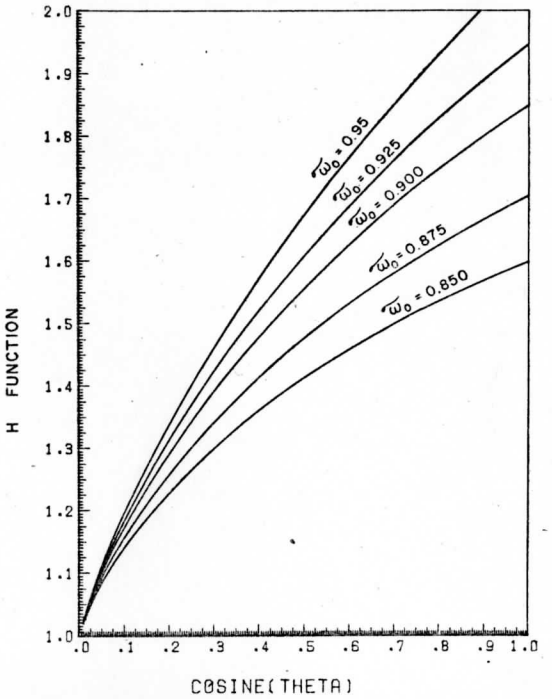

FIG. 2. Chandrasekhar H-function values for $\tilde{\omega}_0=0.95$, 0.925, 0.9, 0.875 and 850 as a function of cosine of angle (from Chandrasekhar, 1950).

Within a single frame the relative photometric accuracy of the vidicons is believed to be about $\pm 3\%$ and the absolute accuracy is believed to be about $\pm 10\%$ (Hapke *et al.*, 1975).

Fig. 4 shows a comparison of brightness frequency histograms for the original and normalized versions of a typical Mariner 10 UV image. The normalized version shows a bi-modal distribution, where the lower peak corresponding to higher brightness values is due to brighter polar region and the median polar region brightness is about 50% higher than the equatorial value.

a. Mean brightness and rms deviation

The mean brightness of the visible disc in both the raw and the normalized versions show a slow monotonic decrease with the exception of an image at about 12.3 hours, where the anomalously lower brightness is due presumably to the performance characteristics of the vidicon.

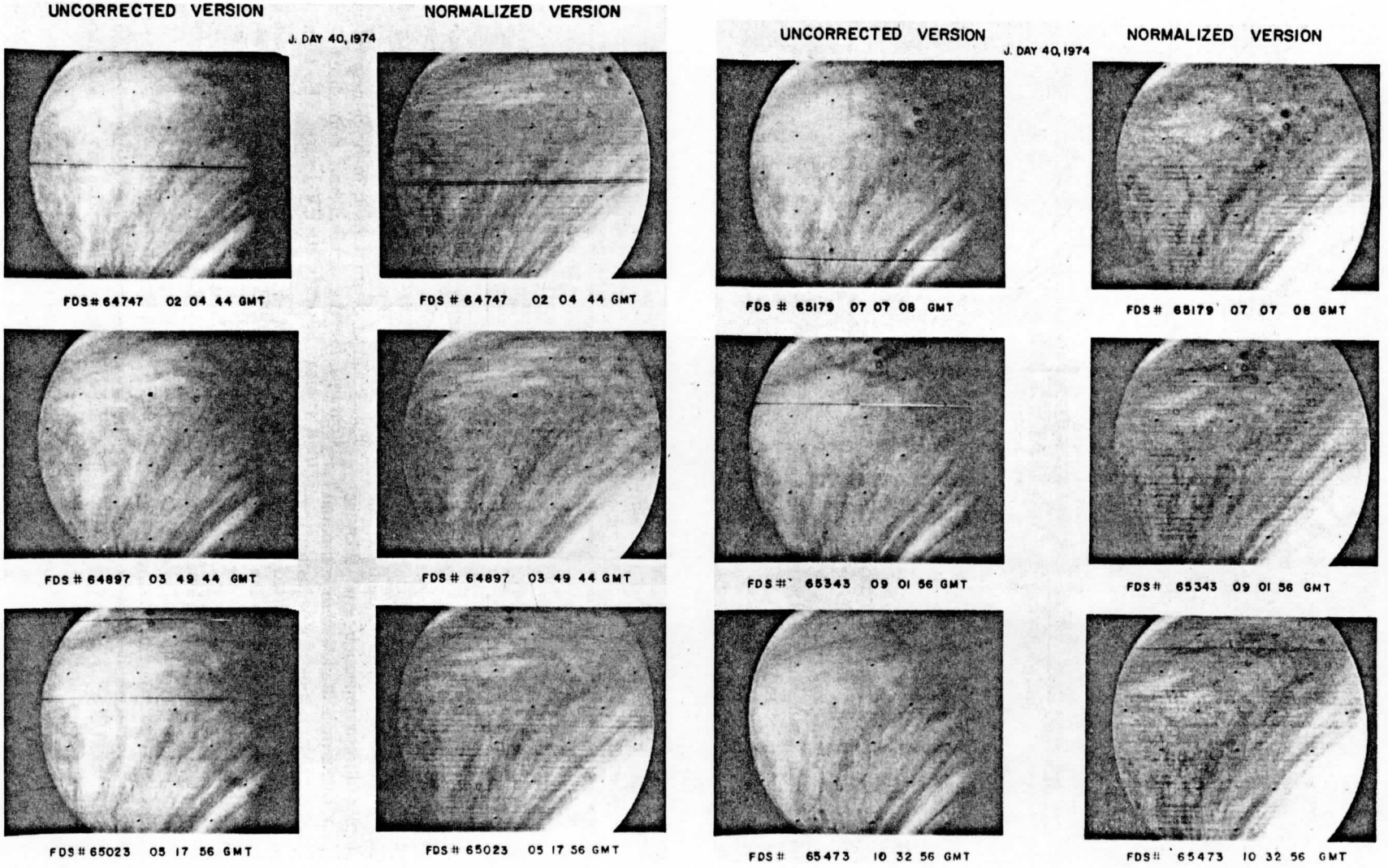

FIG. 3. A sequence of unnormalized Mariner 10 UV images of Venus (left) and the corresponding normalized versions (right). The last image is taken from Camera B (FDS #66380) while the rest of the images are from Camera A.

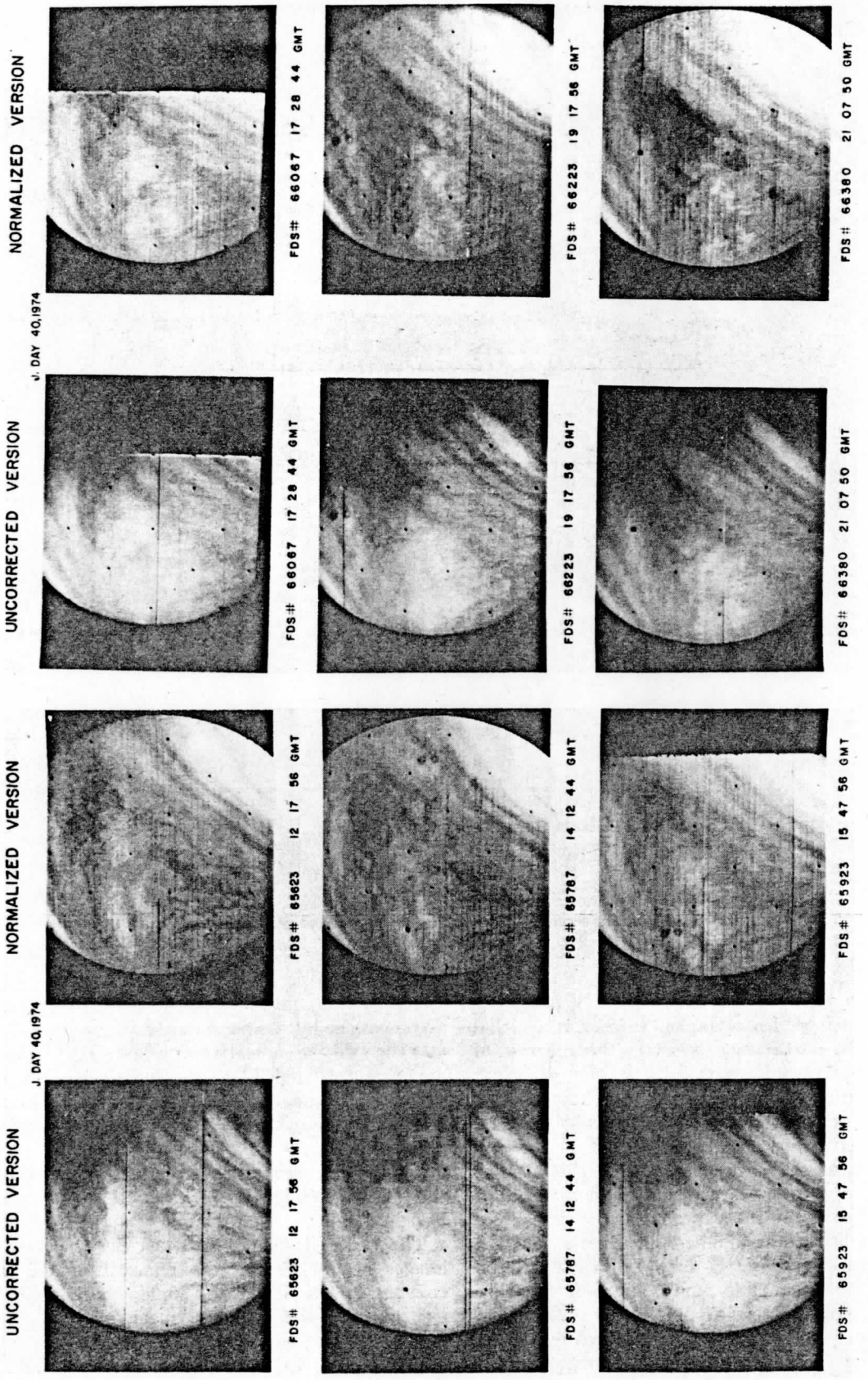

FIG. 3. (*continued*).

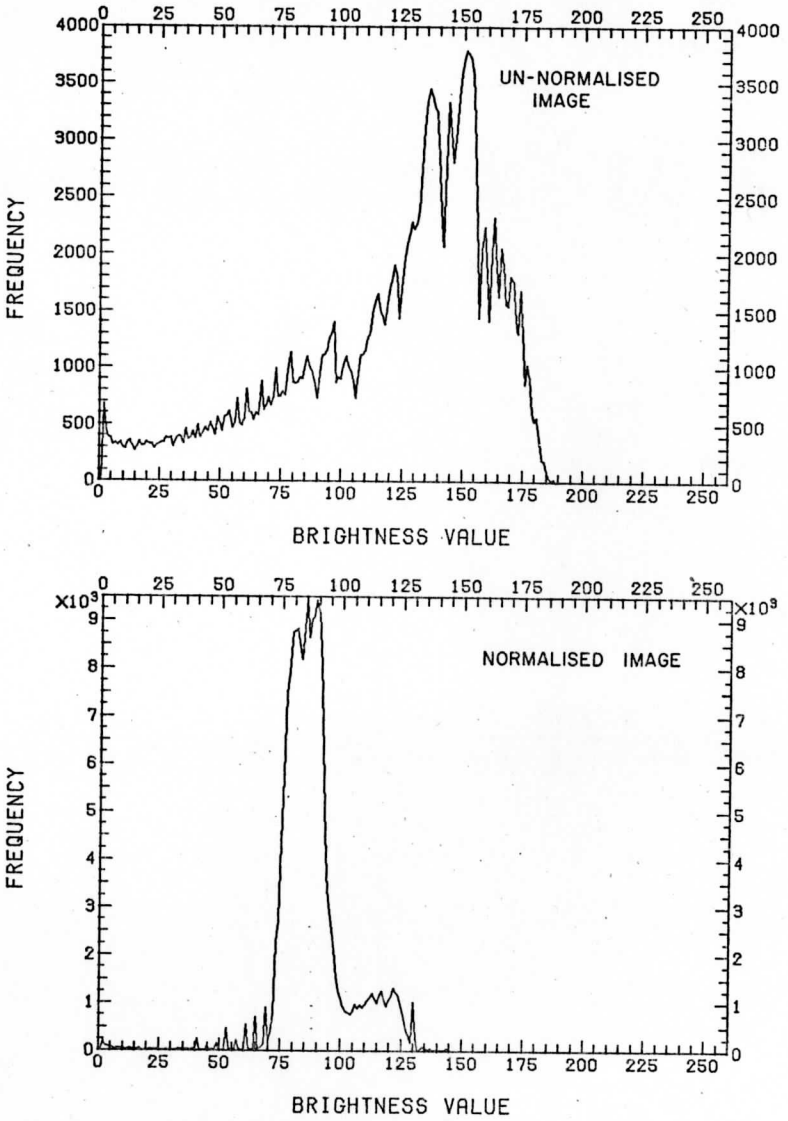

FIG. 4. Brightness digital number histograms for an unnormalized image and its normalized version. The second smaller peak in the normalized version is due to the enhanced brightness in the polar region.

It is known that the contrast in the UV images of Venus is scale-dependent (Hapke, 1975). On a global scale when the phase angle is small, the contrast of the whole disc depends on the distribution of bright and dark features which are reported to move across the disc at speeds between 80 and 130 m s^{-1} (Suomi, 1974). Any large spatial dependence of bright and dark features in the upper atmosphere should thus show up in a time series of pictures monitored for contrast. Fig. 5 shows the variation in contrast c, the ratio of rms brightness number deviation σ and the mean brightness number $\bar{B}$ for 11 UV images on Julian Day 40. The solar zenith angle at the subspacecraft point decreased from 29.12° in the beginning of the sequence to 28.16° at the end of the sequence. Two of the images were partial images.

The monotonic decrease in mean brightness is accompanied by a slow increase in contrast (Fig. 6), and the two are indicative of a large UV dark feature moving into the visible hemisphere from the night side over the duration of the sequence (~18 h).

Since the variation in the constrast in raw images is not more than 1% over the sequence, the number of light and dark features over the visible planet and the UV albedo over this 18 h period can be considered to be constant.

The reduced overall contrast in the normalized images occurs due to the removal of the gradual changes in the scattering angle over the planet as evidenced by the constant "mean" brightness in the normalized version (Fig. 1) [i.e., the equivalent variation given by Eq. (1) in the unnormalized image].

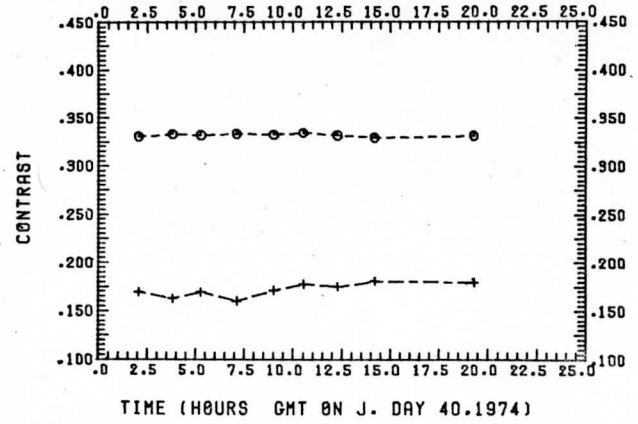

FIG. 5. Variations of the average brightness digital number for images in the sequence. Upper curve is for the unnormalized version and lower curve for the normalized version. [Partial disk frame data and Camera B data for FDS #66380 have not been shown.]

The normalization procedure reduces the contrast for values of normalization factor <1, i.e., for low sun and spacecraft zenith angles, and enhances it for larger sun and spacecraft zenith angles when the normalization factor is greater than unity.

b. The bright polar region

The meridional variation of uncorrected and normalized brightness along meridians through the subsolar and the subspacecraft points are shown in Figs. 7a and 7b, respectively. The two normalized profiles show virtually identical large-scale brightness variations, and the small-scale variations, which are the signatures of the UV features, are less than about 10%, thus indicating the small longitudinal dependence of brightness. The normalized profiles show a much lower brightness in the equatorial region than in the polar region.

The edge of the southern bright polar cloud or ring on Day 40 is around about 52° latitude. An indication of a similar bright polar cloud in the Northern Hemisphere at about the same latitude can be seen. Unfortunately, the flyby trajectory of Mariner 10 was unsuitable for imaging the north polar region. Dolfuss (1974) has examined earth-based photographs of Venus over a long period and reports a variability in the appearance of the polar clouds. They seem to appear and disappear periodically, and all four cases [(i) both the polar cloud, (ii) northern polar cloud only, (iii) southern polar cloud only and (iv) no polar cloud] have been observed. The equatorward periphery of the bright polar band in the Northern Hemisphere is at about 45°N latitude.

c. Conditions that may cause enhanced polar (UV) brightness

The increase in brightness of UV in polar latitudes can be clearly seen in Fig. 7 which is a plot of brightness along a meridian. The higher brightness of polar clouds is indicative of different scattering conditions. To the authors' knowledge at present there is no ground-based observational evidence regarding different properties or structure of polar clouds and this enhanced brightness is a puzzle. It would be difficult to attribute the difference in scattering to different cloud constituents in polar latitudes where atmospheric circulation would create strong mixing.

The available observations do facilitate speculation upon several situations which could cause enhanced polar brightness:

1) Due to the small inclination angle of the rotation axis of Venus with its orbital plane one would expect a poleward decrease of temperature on isobaric surfaces and hence lower cloud-top temperatures in polar bands. It is possible then that perhaps the phase of the scatterers in polar clouds is different from equatorial clouds due to lower temperatures. A different phase of the scatterers would be expected to have different scattering properties and thus could cause the enhanced brightness. Unfortunately, all available temperature measurements at cloud tops have been in low latitudes. The ground-based thermal measurements of the disk of Venus cannot be unambiguously reduced to obtain cloud top temperatures for lack of knowledge of cloud emissivity.

2) It is possible that the polar clouds could be lower in altitude as several earlier observations also suggest (see, e.g., Moroz, 1971; Barker and Perry, 1975; Link, 1969) and the enhanced brightness could be due to increased UV scattering above the cloud tops. In this case the cloud structure will be reflected in thermal maps, polarization measurements, carbon dioxide abundance above clouds, etc., and some of these are discussed next.

Calculations by Ingersoll and Orton (1974) of the sun-associated component of the brightness tem-

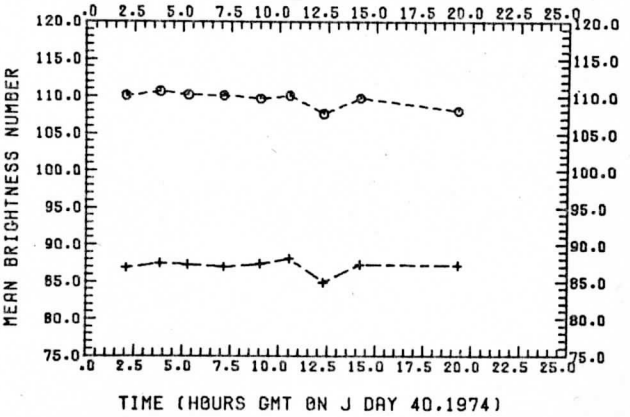

FIG. 6. Variation of the ratio of the standard deviation of the brightness digital number $\bar{B}$: upper curve, unnormalized version; lower curve, normalized version. [Partial disk frame data and Camera B data for FDS #66380 have not been shown.]

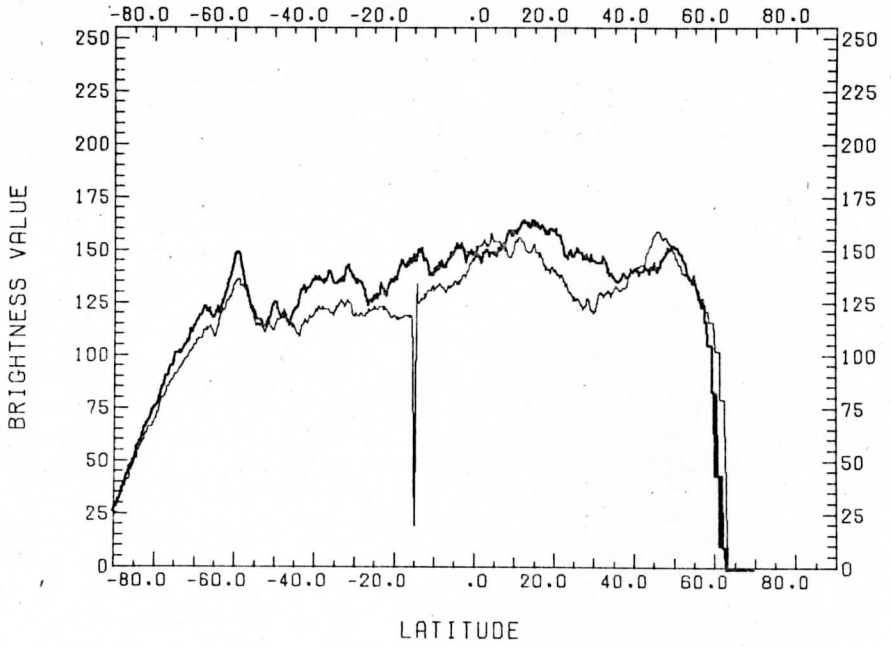

FIG. 7a. Variation of brightness in the original image (FDS #64897) along meridians passing through the subsolar and subspacecraft points. The two are virtually identical and show the axial symmetry of large-scale brightness variations. (Thick line through subsolar point, thin line through subspacecraft point.)

perature indicate that at least on the night side at about 50° latitude the temperature is approximately 7 K lower than at the equator. This might be the case on the dayside also. It is likely that this brightness temperature corresponds to the "cloud top" temperatures and that such cloud tops are seen as UV features in the UV images. As the above authors point out, it is difficult to resolve the observed brightness temperature variations into horizontal and vertical components from available data. It is known that at least in the lower latitudes, the atmosphere is very stable with a subadiabatic

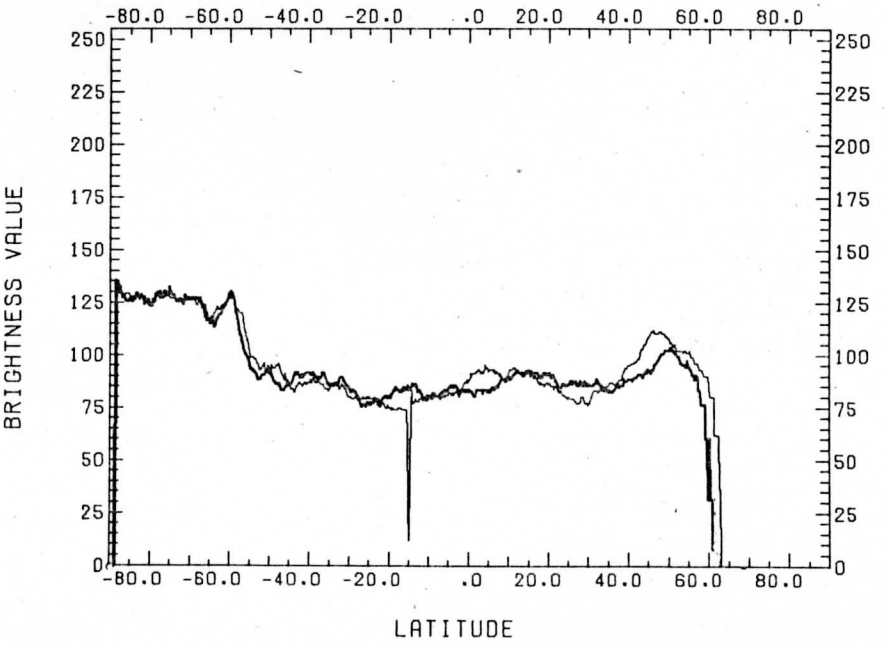

FIG. 7b. As in Fig. 7a except for the normalized version. The polar regions show enhanced brightness and a rather sharp transition zone.

lapse rate of 4–5 K km^{-1} (Howard *et al.*, 1974). Assuming similar lapse conditions at higher latitudes the lower cloud tops in polar regions could have a lower brightness temperature if the temperature decreases on a level surface towards the poles sufficiently.

It is possible then that this polar region of enhanced brightness has lower "cloud tops" than its equatorial counterpart with a somewhat lower brightness temperature. If this is the case, then there is likely to be more Venus air mass (mostly carbon dioxide gas) above the polar clouds than over the rest of the planet and spectroscopic observations of CO_2 line strengths with sufficient spatial resolution should be able to detect it.

From ground-based spectroscopic measurements Young *et al.* (1973) find that while the correlation between the CO_2 abundance over the cloud tops and light UV markings is not obvious, there is an indication that there is more carbon dioxide above the brighter areas. If this is true, this lends support to the hypothesis that the cloud tops in the polar regions are lower than in the equatorial regions, and the brightness temperature in those regions is lower due to a north-south horizontal temperature gradient large enough to offset the higher cloud top temperatures.

If the polar clouds have tops lower in altitude, then the cloud-top pressure regions are thus likely to be higher and hence the equivalent bandwidth of CO_2 lines must be larger near the south pole than at the equator. Moroz (1971) reports this exact finding: the 1.6 μm band observations indicate that the pressure there is considerably higher than at a similar level for the equatorial regions and argues that the polar cloud tops may be 4–7 km lower than in the equatorial region. There is other evidence available.

More recent observations of Barker and Perry (1975) of the CO_2 line strengths indicate that the south polar CO_2 abundance (presumably above the "visible" cloud tops) is about 8% greater than that over the equatorial region. Some of their reported observations taken through the 100-inch telescope at McDonald observatory coincided with the Venus encounter of Mariner 10 (Julian Days 38–40, 1974). It is quite likely that this difference in relative abundance of CO_2 is actually higher than the observed value since the spatial resolution of ground based observations even near inferior conjunction is quite small, and thus observations of Barker and Perry (1975) are mean values over a large area.

There is one important consequence of horizontal inhomogeneity of clouds. For a given phase angle the observed linear polarization above the polar regions with lower cloud tops would be expected to be higher if the atmosphere above the clouds is clear (see Coffeen and Hansen, 1974). Observations of Coffeen and Gehrels (1969) indicate that the positive polarization increases rapidly toward the poles in agreement with the hypothesis of lower polar cloud tops. An excess "clearing" above the clouds can indeed be produced in the polar regions of Venus where large-scale sinking motion is likely to be present.

Finally, it is possible to place an upper limit on the possible altitude difference between the equatorial and polar cloud tops if one assumes a certain meridional temperature variation. For example, it can be shown that for a cosine decrease of temperature with latitude, the maximum equator-to-pole temperature contrast that can be maintained through global radiative balance is about 70 K. For an average lapse rate of about 5 K km^{-1} above 65 km altitude everywhere, and noting that the surface polar temperature seems to be at least as high as, if not higher than, the equatorial temperature from microwave measurements (Sinclair *et al.*, 1972), the polar cloud tops can therefore only be a maximum of about 14 km lower than the equatorial cloud tops. However, the actual temperature difference is probably much smaller as well as the cloud top altitude difference.

3) The polar clouds could be optically thicker in UV and extend deeper in the atmosphere. This is similar to the terrestrial case where the optically thicker cloud appears brighter. The polar cloud tops could still be lower in altitude than equatorial clouds and much of the discussion in the second case would apply.

This discussion has not exhausted all the possibilities which could lead to enhanced polar brightness. It is possible that all three mechanisms discussed here contribute to the enhanced brightness.

The dynamic conditions that could cause polar clouds are briefly presented next.

d. Transition zone

At this point it is interesting to note that the zonal component of the motion of UV features as revealed by Mariner 10 images shows a maximum somewhere between 45° and 50° latitude in the Southern Hemisphere (Suomi, 1974). Poleward of that the zonal component is smaller and must vanish at the pole. The meridional shear of such a profile is quite large beyond the latitude of maximum zonal wind and according to the Rayleigh criterion this is the favored zone for onset of barotropic instability. The exact latitude for the instability is given by the necessary and sufficient condition that the absolute vorticity vanish. The equatorial edge of the polar clouds in the normalized image sequence is around about 52° latitude circle, i.e., close to the latitude of maximum

zonal component of motion of UV features. It is tempting to suggest that the polar clouds are related to a dynamic instability—perhaps barotropic.

In this transition zone around about 50° latitude (which contains the latitude of maximum zonal motion of UV features and on the poleward side of which the cloud tops appear to be at a lower altitude than on the equatorial side) the situation is similar to the terrestrial atmosphere in the vicinity of a front. Admittedly a front (for example, a polar front on Earth) is a baroclinic zone; on Venus, however, the maximum temperature differences are quite small so that in effect a small temperature contrast of a few degrees may have effects similar to a state of baroclinicity. In the case of Venus there is evidence to believe that (i) a zonal wind maximum exists, (ii) cloud tops at different altitudes are found on either side of the zone of maximum zonal wind, (iii) large horizontal shear in atmospheric flow exists in the vicinity of the maximum wind region, and (iv) high vertical wind shear is likely in the vicinity of periphery of polar clouds.

The upper atmospheric dynamics and the large scale polar-equatorial brightness difference appear to be very closely related. This transition zone in the upper atmosphere of Venus at the level of cloud tops exhibits properties of a frontal zone. It is important, therefore, to determine the meridional temperature gradient and the wind shear across this zone from future observations such as those from the Pioneer Venus Multiprobe Mission, which may shed new light on the polar clouds and the transition zone.

4. Summary and recommendations

A sequence of Mariner 10 Venus images have been normalized according to an exact solution obtained by Chandrasekhar (1950) for the problem of diffuse reflection from a semi-infinite plane parallel atmosphere. The isotropic scattering phase function with single scattering albedo of 0.92 based on Hapke's results (1975) was used for normalization. A sequence of images normalized in this fashion helps identify physical changes in the UV features seen in the image sequence by isolating them from effects of varying scattering geometry.

The south polar region stands out as the brightest part of the image with little contrast. The subsolar region is relatively dark. The high brightness of the polar cap is suggestive of significant different atmospheric conditions.

The mean brightness of the planet over the unnormalized sequence of images studies shows a slow monotonic decrease except for one image which is anomalously dimmer. The variation is within the performance limit ($\sim\pm 4\%$) of the vidicon and thus within those limits the UV albedo of Venus is constant. The contrast, defined as the ratio of the rms deviation from the mean brightness and the mean brightness, increases gradually in the unnormalized over the sequence and is associated with the movement of a large UV dark feature into the visible hemisphere from the nightside.

It is strongly recommended that at least one of the atmospheric probes from the next Pioneer mission to Venus be launched so as to probe the atmosphere in the polar cap region. Temperature profiles obtained through radio occultations from the Venus orbiter would give valuable information about the three-dimensional thermal contrasts in the atmosphere.

Maps of carbon dioxide abundances with the high enough spatial resolution might prove to be valuable in understanding the UV contrasts on Venus, in particular the pole-equator differences. Thermal infrared maps will also be useful in finding an answer to this riddle. Polarimetric studies with a view to look for regional and temporal variations such as are proposed to be made from Pioneer Venus Orbiter mission would provide additional data on the structure of cloud tops on Venus.

Acknowledgments. The authors express thanks to the people at the Image Processing Laboratory at JPL, Pasadena, Calif., for providing photometrically and geometrically corrected pictures. We are thankful to Mr. Fred Mosher and to Mr. Robert Krauss for the discussions and to Drs. Bruce Hapke and Michael Belton for their critical comments. We appreciate the programming help of Messrs. Eric Phillips and Ralph Dedecker.

We also appreciate the helpful comments of the referees on the present paper.

This research was supported by NASA Grant NGR-50-002-189.

REFERENCES

Barker, E. D., and M. A. Perry, 1975: Semiperiodic variations in CO_2 abundance on Venus. *Icarus*, **25**, 282–295.

Chandrasekhar, S., 1950: *Radiative Transfer Theory*. Clarendon Press, 381 pp.

Coffen, D. L., and T. Gehrels, 1969: Wavelength dependence of polarization. XV. Observations of Venus. *Astronom. J.*, **74**, 433–445.

——, and J. E. Hansen, 1974: Polarization studies of planetary atmospheres. *Planets, Stars and Nebulae Studies with Photopolarimetry*, T. Gehrels, Ed., University of Arizona Press, 1133 pp.

Dolfuss, A., 1975: Venus: Evolution of the upper atmospheric clouds. *J. Atmos. Sci.*, **32**, 1060–1070.

Hapke, B., 1976: Photometry of Venus from Mariner 10. *J. Atmos. Sci.*, **33**, 1803–1815.

——, G. E. Danielson, K. Klaasen and L. Wilson, 1975: Photometric observations of Mercury from Mariner 10. *J. Geophys. Res.*, **80**, 2431–2443.

Horak, H. G., 1950: Diffuse reflection by planetary atmospheres. *Astrophys. J.*, **112**, 445–463.

Howard, H. T., C. L. Tyler, G. Fjeldbo, A. J. Kliore, G. S. Levy, D. L. Brunn, R. Dickinson, R. E. Edelson, W. L.

Martin, R. B. Postal, B. Seidel, T. T. Sesplauleis, D. L. Shirley, C. T. Stelzried, D. N. Sweetnam, Z. I. Zygielbaum, P. B. Esposito, J. D. Anderson, I. I. Shapiro and R. D. Reasenberg, 1974: Venus: Mass, gravity field, atmosphere, and ionosphere as measured by the Mariner 10 dual frequency radio system. *Science*, **183**, 1297–1306.

Huggins, W., 1867: On the spectrum of Mars, with some remarks on the colour of that planet. *Mon. Not. Roy. Astron. Soc.*, **27**, 178–181.

Ingersoll, A. P., and G. S. Orton, 1974: Lateral inhomogeneities in the Venus atmosphere: Analysis of thermal infrared maps. *Icarus*, **21**, 121–128.

Leovy, C. B., G. A. Briggs, A. T. Young, B. A. Smith, J. B. Pollack, E. N. Shipley and R. L. Wildey, 1972: The Martian atmosphere: Mariner 9 television experiment progress report. *Icarus*, **17**, 373–393.

Link, F., 1969: *Eclipse Phenomenon in Astronomy*. Springer-Verlag, 271 pp.

Martin, D. W., J. Stout and D. N. Sikdar, 1975: GATE area rainfall estimation from satellite images. (See Appendix B of F. Mosher: Brightness normalization of satellite images.) Report, NOAA Grant 04-5-158-47, Space Science and Engineering Center, University of Wisconsin, Madison.

Moroz, V. I., 1971: Polar tropopause on Venus. *Soviet Astronomy-AJ*, **15**, 448–453.

Murray, B. C., M. J. S. Belton, G. E. Danielson, M. E. Davies, D. Gault, B. Hapke, B. O'Leary, R. G. Strom, V. Suomi and N. Trask, 1974: Venus atmospheric motion and structure from Mariner 10 pictures. *Science*, **183**, 1307–1315.

Phillips, D., and S. S. Limaye, 1976: Navigation of Mariner 10 images of Venus. Space Science and Engineering Center, University of Wisconsin, Madison.

Sinclair, A. E. C., J. P. Basart, D. Buhl and W. A. Gale, 1972: Precision interferometric observations of Venus at 11.1 cm wavelength. *Astrophys. J.*, **175**, 555–572.

Suomi, V. E., 1974: Mariner 10 observations of cloud motions. Presented at the Conference on the Atmosphere of Venus, Goddard Institute of Space Studies, 15–17 October 1974. [Also NASA-Report SP-382 (1975).]

Young, L. G., A. T. Young, J. W. Young and J. T. Bergstralh, 1973: The planet Venus: A new periodic spectrum variable. *Astrophys. J.*, **181**, 15–18.

APPENDIX E

VENUS: FURTHER EVIDENCE OF VORTEX CIRCULATION

Verner E. Suomi and Sanjay S. Limaye

Space Science and Engineering Center

University of Wisconsin-Madison

Madison, Wisconsin

17 March 1977

(Submitted to Science)

ABSTRACT

A space-time composite of polar stereographic UV images of Venus from Mariner 10 shows a remarkable circum-polar vortex. The vortex is characterized by a cloud which appears like dense terrestrial stratus having a 50% higher albedo. Spiral streaks converge into it from low latitudes, akin to the spiral bands of a hurricane. The bright visible polar cloud is not axisymmetric but has roughly an elliptical shape.

The bright polar cloud probably has different dynamic origins than the rest of the cloud cover.

Soon after Mariner 10 encounter with Venus, the MVM-73 imaging team (1) presented a preliminary view of the atmospheric circulation on Venus as revealed by the UV markings. In particular Murray et al. had following comments about the polar region: "... our preliminary impression is that the pole of atmospheric rotation is on the terminator. There is an indication of vortex structure in the streaks emanating from the poleward side of the edge of the polar region. Indeed, the entire polar region may be a vortex fed by meridional flow from the equatorial regions ..." Subsequently Suomi (2) and Suomi et al. (3) have presented results based on systematic tracking of UV features in a number of Mariner 10 UV frames taken during a small time interval compared to the total Venus encounter duration of Mariner 10. These results were obtained by precisely navigating individual frames and tracking UV features by digital as well as visual correlation techniques.

In general the measurements of movements of UV features showed a fair amount of scatter in the motions which tend to conserve absolute angular momentum in low and mid latitudes and which tend toward solid rotation at high latitudes of the planet, in the upper atmosphere. The unfavorable geometry and lack of sufficient texture made it difficult to obtain measurements of motion of UV features within the polar ring cloud.

We have continued the analysis of Mariner 10 images to cover almost the entire Venus encounter period -- about seven days. For the purpose of making measurements of motion of UV features the time interval between the images was chosen to be commensurate with the spatial resolution at the sub-spacecraft point. Figure 1 shows the relationship between the Flight

Data System (FDS) numbers which identify a specific image, the distance of the spacecraft from the planet center and resolution of the vidicon image at the sub-spacecraft point in the cross-line direction. The de-grading spatial resolution due to the fly-by nature of the trajectory makes it difficult to obtain a homogeneous set of measurements of motion of UV features on the same spatial and temporal scale. Thus analysis of such measurements to ascertain the nature of the stratospheric circulation of Venus in terms of scale dependence and temporal variations must take into consideration the inhomogeneity of the data. In order to make analysis of such measurements somewhat easier, a different approach was sought to first confirm the qualitative nature of the vortex circulation that was suspected. The new approach has produced striking evidence of a global circumpolar vortex in the stratosphere of Venus that we wish to report here.

First, all of 22 frames spanning 6.85 days were normalized to a standard scattering geometry. The normalization was performed in order to see an image in the remapped version devoid of any shading due to scattering geometry variation over the planet. The images were 'normalized' to a standard sun-planet-observer geometry as described by Limaye and Suomi (4). Second, the images were remapped into a polar stereographic projection so as to give a better view of the high latitude regions of Venus since the fly-by trajectory of spacecraft past Venus on to Mercury offered only a highly foreshortened view of the south polar region of Venus. Third, several polar stereographic projections and normalized images were made into a composite for the whole polar region.

The polar projection has the advantage that it is easier to discern motion patterns in the high latitudes than in the original oblique perspec-

tive view obtained from Mariner 10 cameras. Clearly, the information content of normalized polar stereographic projections is not different from the initial unprocessed oblique perspective view -- it is only the ease of interpretation which vastly differs in the two cases, due to the particular nature of circulation on Venus.

The sequence which covered almost the entire Venus encounter (2117 GMT on day 037 of 1974 to 1976 GMT on day 044 of 1974) began with one of the highest resolution images that could be navigated without mosaicing (FDS #61182) and ended with one of the last images taken from Mariner 10. The phase angle of the planet relative to Mariner 10 spacecraft varied from ~30 degrees to ~24 degrees at the end of the sequence. Images taken in the first half of the sequence (FDS #61182-66380) were FICORed, GEOMed and Scaled at Image Processing Laboratory (IPL) at the Jet Propulsion Laboratory (JPL), Pasadena, California. Images starting with FDS #66956 (03 53 19 GMT on day 041) were corrected only for shot noise. Because the planet covered only a rather small fraction of the vidicon photo cathode area in the original image, deviations in the photo cathode sensitivity would not be very large, and thus the results described by Limaye and Suomi (4) showing a high contrast between polar and equatorial clouds would appear to be true for the entire sequence spanning 7 days.

The analysis of normalized polar-stereographic sequence by time lapse display on Man-computer Interactive Data Access System (McIDAS, 5) thus far has revealed several features about the stratospheric circulation on Venus through the motion of the UV markings. Figure 2 shows a typical view of high latitudes. The ability to follow features as they move about the south pole is hampered by lack of image detail in high latitudes. However, as far

as we can discern, changes in the shape of UV features are not too large to perceive motion. The resolution at subspacecraft point (-18.4°W) of this particular image was about 12 km per pixel. The spiral streaks that Belton et al. (6) indicated in their analysis can be clearly seen to extend practically all the way to the south pole.

In fact, evidence for the high latitude extensions of the spiral streaks is also seen in Figure 3 which is a much higher resolution mosaic than the one that appeared in Science, Volume 183, No. 4131. Noteworthy in this figure is the more stratiform cloud structure near the pole compared with lower latitudes and the "hooks" and "whorls" described previously by the imaging team (1) which are suggestive of intense dynamical activity at the boundary of the polar cloud. This mosaic was assembled by U.S. Geological Survey Personnel at the Jet Propulsion Laboratory, NASA, Pasadena, California.

Figure 4 shows a portion of the sequence from FDS #63601 (Day 039 12:42:03) to FDS #66380 (Day 041 21:07:50 GMT). The persistence of large scale features can be seen clearly even in high latitudes.

In particular our new findings from analysis of this sequence are:

(i) The polar cloud is about 50% brighter than the cloud cover over the rest of the visible southern hemisphere in UV throughout the seven days.

(ii) This polar cloud is not axisymmetric as reported by Belton et al. (6). However, the gross shape of the visible polar cloud is an ellipse, which by its asymmetry causes an illusion of meridional displacements when viewed in an unmapped image sequence. We are unable to discern substantial changes in the area of the polar

cloud in the images studied, and the ellipse is suggestive of wavelike motions at this latitude having planetary wave number two.

(iii) This projection allowed us to see more clearly the motions of features within the polar cloud even though much less detail is present there than in equatorial or mid-latitude regions of the planet. Features found at latitudes as high as 60 to 65 degrees still show a dominant solid like zonal motion.

(iv) UV features in these views definitely show differential rotation in mid to low latitudes as indicated by Suomi (2) and Suomi et al. (3). This is easily confirmed through a simple exercise of constructing a composite hemispheric view. Given the constraint that only a rotation is required about the pole, continuity of observed UV features across the boundaries can only be preserved if the longitudinal displacement between picture time intervals actually corresponded to the zonal motion for that latitude. Figure 5 shows one example of match coordinates computed according to a model fit to observe zonal speeds. The space time composite thus constructed is shown on the cover and in Figure 6 of this issue. The similarity between such a composite view and a satellite view of a tropical cyclone is very striking. Indeed, both are examples of cyclostrophic motion where the pressure gradient is balanced by the horizontal component of the centripetal acceleration as suggested for Venus by Leovy (7) and by textbooks for hurricanes, although of course on vastly different scales.

(v) Figure 7, despite the very unfavorable viewing geometry, also suggests a vortex on the opposite pole. this is a single image showing the northern hemisphere in a polar stereographic projection. The image was normalized to a standard scattering geometry as described previously. A time lapse display of several such frames suggests a circulation similar to that seen in the southern hemisphere sequence.

Indeed, the polar cloud in both the hemispheres and the spiral streaks emanating from low latitudes are compelling suggestions that at least during the 7 days of the Mariner 10 flyby in 1974 the stratospheric circulation was composed of two giant vortices more or less centered on each pole with meridional inflow from low latitudes toward each pole. The vortex seen in the composite view of Venus would be characterized by a region of mass sink in the polar regions in the upper atmosphere and a mass source in the low latitudes -- essentially a hemispheric Hadley circulation cell strongly organized by the vortical zonal flow. A meridional flow is implied with such a circulation.

(vi) The scatter seen in the measured zonal and meridional speeds of the ultraviolet features is realistic and not due to navigational

errors. A possible explanation for this scatter is existence of oscillations due to inertia superposed on a steady zonal flow (8). Rough calculations show that the resultant trajectories spiral in toward high latitudes. A confirmation of such oscillations will require further analysis. It can be shown that the classical Rayleigh criterion for barotropic instability is applicable even to the case of a slowly rotating plant such as Venus, where the coriolis termsin the equations of motion are quite small and centripetal accelerations dominate. The criterion is that the vertical components of absolute vorticity must change sign somewhere within the zonal current. This necessary condition for instability may be met in low latitudes if the perturbations on the model flow are small.

Some Implications and Conjectures:

a) Stratospheric Circulation

The similarities between the polar stereographic composite view and a vortex such as a hurricane tempt us to speculate about the circulation in the stratosphere of Venus. The inflow at the top of the Venus vortex corresponds to the inflow at the surface of a typical hurricane. If the analogy is valid, then the outflow at the top of a hurricane should have a corresponding outflow region in the Venus vortex at some lower layer, possibly close to the surface. An inflow region in the upper levels of the atmosphere can easily exist on Venus. The stratosphere (portions of the atmosphere above 38 km) is known to be very stable and stratified (at least in low latitudes). The bulk of the solar energy which maintains the circulation appears to be deposited in this layer (9). There is thus a possibility that

that an upper boundary layer exists on Venus as suggested by Goody and Robinson (10) but with the return circulation at the poles rather than at the anti-solar point.

We have, at present, no evidence that large amounts of latent heat are released in the Venus atmosphere, hence there is a major difference between the circulation on Venus and that of a tropical cyclone: The tropical cyclone is maintained dominantly by latent heat release in the atmosphere; the circum-polar vortex in the stratosphere of Venus is maintained through conversion of solar energy into sensible heat.

Another aspect of energy conversion should be mentioned, here; namely the kinetic energy. In view of the fact that the lower atmosphere may be adiabatic a thermally direct circulation can transfer heat downward only through conversion of kinetic energy into internal energy along with conversion of geopotential energy into internal energy. Certainly, there is evidence that the winds in the upper levels of the atmosphere are faster. In the upper atmosphere the flow is faster in low and mid latitudes than in high latitudes. The total energy per unit volume is thus higher in low and mid latitudes by virtue of faster zonal speeds. It is perhaps easier to think of a "kinetic potential temperature" for the case of Venus atmosphere since the range of possible speeds is so significant. The faster the motion, the "higher the kinetic potential temperature." So far, this aspect of circulation has not been widely considered and may be helpful in studies of the Venus atmospheric circulation.

b) The Bright Polar Cloud

It is tempting to ask what are the possible consequences of such a circulation. We do not resist the temptation and ask some simple questions by means of simple sketches.

(1) Is the polar cap cloud a "different" cloud? As the sketch in Figure 8a shows we limit this cloud to the same general level. We have found this cloud to have almost 50% higher UV albedo than the equator and clouds. Is this brightness increase due to some phase change? Polarization studies by Coffeen et al. (11) and Dolfuss (12) do indeed show different characteristics in the polar region. On the other hand spectral studies by Barker and Perry (13) show more CO_2 atmosphere over the polar regions and more IR flux near the pole, both hardly likely if the cloud is at the same level unless the UV brighter cloud is more transparent in the IR than the "other" clouds.

(2) Is it a thicker cloud as shown in Figure 8b? A thicker cloud of the same material would be brighter; clouds have different polarization, and indeed could appear to have more CO_2 "above" it from additional multiple scattering. However, it would be difficult to assume greater IR transparency as a thick cloud at much lower levels. Continuity requirements of the suggested meridional flow would require a process other than condensation to produce a thicker cloud in a region of general descending motion.

(3) Is there a possibility that there is no high cloud at all? Having no high cloud at all where the planet has the highest albedo in UV almost requires a sleight of hand. However, we have had suggestions for an ubiquitous cloud cover at lower levels previously (14). This lower cloud layer has been verified to exist in low latitudes by three Soviet entry probes thus far. Indeed, the X-band occultation experiment on Mariner 10 showed strong absorption at the upper levels

of the ubiquitous cloud. Thus, if we had a very turbid atmosphere in the low latitudes where convection and vertical mixing of aerosols is strong, and a clearer atmosphere in polar regions where convection is suppressed, the "seeing" down to the lower clouds could be better in the polar regions if the aerosols were a strong UV absorber. The polar regions could thus conceivably show a higher albedo despite the missing cloud layer. Sinking within the vortex "eye" could prevent an upsurge of the turbid gas and/or cause evaporation of any condensibles in the atmosphere. A deep clear region above the polar cloud would also result in: (i) a different amount of polarization of reflected UV light, mainly due to increased Rayleigh scattering by gas molecules; (ii) a greater amount of carbon dioxide, the predominant constituent of the Venus atmosphere above the polar cloud since the cloud-top is now lower; and (iii) an increased IR flux emanating from the lower and most probably warmer cloud layer. Available observations do in fact verify these expectations. Coffeen et al. (11) and Dollfuss (12) have measured a greater UV polarization over the polar regions. Barker and Perry (13) had reported observing about 8 percent more carbon dioxide in the polar regions from ground based observations, and the warm anomaly has been seen in telescopic observations of Murray et al. taken in 1962 (15) and those of Diner and Westphal during the 1974 inferior conjunction (16). The prevailing evidence would thus tend to favor the last model presented.

These are but three conjectures on what could cause the enhanced albedo in the polar regions of the planet in UV light. No doubt, other cloud structures are possible. One thing appears clear, however; the structure of the atmosphere, both in terms of clouds and circulation, is very different in high and polar latitudes. The measured motions in the high latitudes are indicative of an increasing tendency toward solid-body rotation of the atmosphere -- a different regime from the one observed in low latitudes. A different regime of circulation is also evidenced by the appearance of "whorls" and "hooks" on the edge of the "polar cloud" or hole as seen in the high resolution mosaic (Figure 3). The features may be indicative of large lateral shears which are lacking in low latitudes. The polar cloud, as seen in Figure 3, is remarkable by the absence of any small scale texture. There is no indication of any convective activity, a common feature of low latitudes. In fact, the appearance of the polar cloud in the high resolution mosaic is similar to that of a deck of dense stratus -- a cloud that usually forms in the presence of a large scale descent.

The possibility of different or deeper cloud, no high cloud at all over the polar regions of the planet, or neither of the above certainly suggests that we should strive to target one of the three small probes on the Pioneer Venus Multiprove Mission planned for encounter with Venus in December 1978 into this region. These probes are equipped to measure the presence of clouds (the nephelometer experiment), temperature as a function of pressure (the atmospheric structure experiment), net radiation (the net flux radiometer experiment), and most important, the horizontal and vertical wind structure (the Doppler Long Base Interferometry Experiment). If an entry probe into this region did detect a different cloud structure, a clearer region, or

different circulation, it could have a profound effect on our notions about the general circulation on Venus.

There are many questions yet to be answered and asked about the atmosphere of Venus. Pioneer Venus Multiprobe and Orbiter Missions planned for 1978 should provide answers to some of these questions and raise new ones. The relative longevity of the Orbiter Mission will certainly be able to amplify the observations of atmospheric circulation. Until then, caution needs to be exercised on speculation on the exact nature of the Venus circulation.

The observations during Mariner 10 flyby lasted only eight days, and we must not draw too general conclusions from this very limited data set; particularly since ground based observations show the bright cloud to appear and disappear occasionally in the polar regions (17). The cause of such long term instabilities is still a mystery. Nevertheless, polar cloud or no polar cloud, the atmospheric circulation in polar and high latitudes is different and important for a deeper understanding of the Venus atmosphere and its circulation, and those regions deserve further observational and theoretical investigations.

17 March 1977

Verner Edward Suomi
Sanjay Shridhar Limaye

Space Science & Engineering Center
University of Wisconsin
1225 West Dayton Street
Madison, Wisconsin 53706

REFERENCES

1. B.C. Murray, M.J.S. Belton, G.E. Danielson, M.E. Davis, D. Gault, B. Hapke B. O'Leary, R.G. Strom, V. Suomi, N. Trask, Science, 183, 1307-1315 (1974).

2. V. Suomi in The Atmosphere of Venus, T. Hansen, Ed., NASA SP-382 (1974).

3. V.E. Suomi, S.S. Limaye, R.J. Krauss, Bull. Am. Astron. Soc., 9, 486 (1976).

4. S.S. Limaye and V.E. Suomi,J. Atmos. Sci.,34,206-215 (1977).

5. E. Smith, IEEE Trans. on Geosci. Elect. (GE-13), 123-145 (1977); also V.E. Suomi and G. Chatters in the same issue 137-145.

6. M.J.S. Belton, G.R. Smith, G. Schubert, A.D. DelGenio , J. Atmos. Sci., 33, 1394-1417.

7. C.B. Leovy, J. Atmos. Sci., 31, 1218-1221 (1973).

8. S.S. Limaye, Paper presented at the DPS Meeting, Honolulu, Hawaii, January 18-22, 1977.

9. A.A. Lacis, J. Atmos. Sci., 32, 1107-1124 (1975).

10. R.M. Goody and A.R. Robinson, Astrophys. J., 146, 339-353 (1966).

11. D.L. Coffeen and T. Gehrels, Astron. J., 74, 433-445 (1966).

12. A. Dollfuss, Ph.D. Thesis, University of Paris (also NASA TT F-188).

13. E.D. Barker and M.A. Perry, Icarus, 25, 282-295 (1975).

14. Probably the first suggestions of an ubiquitous cloud in the lower atmosphere came from Ross in 1928.

15. B.C. Murray, R.L. Wildey and J.A. Westphal, Science 140, 391; also J. Geophys. Res., 68, 4813-4818 (1963).

16. D. Diner and J.A. Westphal, Icarus, 27, 191-195 (1976).

17. A. Dollfuss, J. Atmos. Sci., 32, 1060-1070 (1975).

18. The research described in this paper is part of the work done by the junior author towards his Ph.D. at the Department of Meteorology, University of Wisconsin, Madison. We thank the Mariner Venus Mercury Imaging Team, Dr. Bruce Murray, Chairman, Mr. G. E. Danielson and the staff of Image Processing Laboratory, JPL, and Mr. R. J. Krauss and Dr. R. Daly of University of Wisconsin. This research was supported by NASA Grant NGR-50-002-189. A 16 mm color movie with sound "Exploration of Venus: Mariner 10 Looks at Stratospheric Circulation" has been produced that depicts the motions described in this paper.

LIST OF FIGURES

Figure 1. Relationship between range of the spacecraft from Venus, time and the along-scan image resolution per sampling element at the sub-spacecraft size. The approximate number of scan lines comprising the whole disc is shown on the scale on the right.

Figure 2. A view of the high latitudes of Venus in a contrast stretched normalized version of a polar stereographic projection of a Mariner 10 UV image. Note the different texture of the bright polar cloud and the lack of any evidence of any convective activity therein.

Figure 3. A high resolution mosaic of Mariner 10 UV images prepared at the Jet Propulsion Laboratory, Pasadena, California.

Figure 4. A portion of the polar stereographic image sequence prepared is shown here. The south pole is located at line 200 and element 200 in these normalized versions. The photographs were produced at the Image Processing Laboratory, JPL, Pasadena, California, from digital tapes produced at the Space Science and Engineering Center, University of Wisconsin- Madison. The images have been contrast stretched somewhat to enhance detail.

Figure 5. Match point longitudes (left) predicted from a model of zonal speed profile (right) for a particular time interval between two images. The meridional displacement of the UV features is small and ignored in the calculation.

Figure 6. A space-time composite prepared from several remapped images according to computed match longitudes as indicated in Figure 5. The vortex-type organization of the UV features is unmistakable. The center of the vortex is at the south pole as far as can be discerned and is in the center of the image. This composite provides a time-lapse view of the southern hemisphere of Venus in a polar stereographic projection. Thus the outer edge of the image is the planet equator and latitude parallels are a series of concentric circles within. One image was unavailable in photometrically rectified version and appears differently, at the bottom of the picture. There is a time boundary immediately to the left of this image which was shuttered at 10:17:57 GMT on day 38 of 1974. Clockwise from this image the images are taken at 038-15:32:57, 039-08:58:03, 039-16:13:26, 040-01:43:14, 040-10:32:56, 040-21:07:50 and 041-17:14:49. Southern half of the dark Y-feature is seen in the image in the southeast quadrant. The motion of the features is in anti-clockwise direction.

Figure 7. A single frame showing the northern hemisphere in a polar stereographic projection. The location of the north pole is marked by the cross in this normalized (see text for details) version. The view afforded is identical to the southern hemisphere and indicates a vortex organization in the northern hemisphere also.

Figure 8. Sketches of possible cloud structure that could lead to the strong albedo contrast in high latitudes. See text for details.

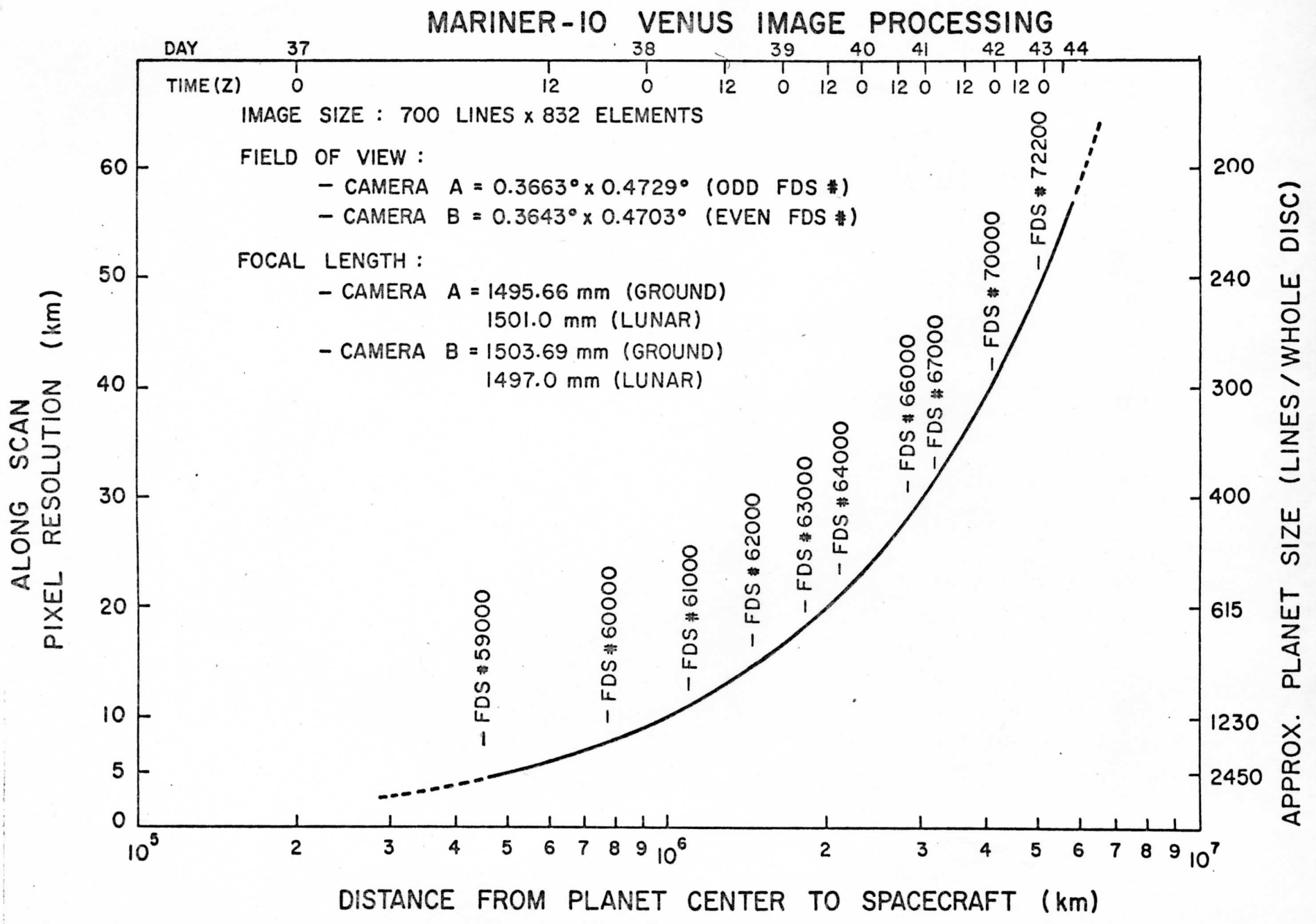
MARINER-10 VENUS IMAGE PROCESSING
DAY 37 38 39 40 41 42 43 44
TIME(Z) 0 12 0 12 0 12 0 12 0 12 0 12 0 12 0
IMAGE SIZE : 700 LINES x 832 ELEMENTS
FIELD OF VIEW :
– CAMERA A = 0.3663° x 0.4729° (ODD FDS #)
– CAMERA B = 0.3643° x 0.4703° (EVEN FDS #)
FOCAL LENGTH :
– CAMERA A = 1495.66 mm (GROUND)
1501.0 mm (LUNAR)
– CAMERA B = 1503.69 mm (GROUND)
1497.0 mm (LUNAR)
– FDS # 59000
– FDS # 60000
– FDS # 61000
– FDS # 62000
– FDS # 63000
– FDS # 64000
– FDS # 66000
– FDS # 67000
– FDS # 70000
– FDS # 72200
ALONG SCAN PIXEL RESOLUTION (km)
60 50 40 30 20 10 5 0
200 240 300 400 615 1230 2450
APPROX. PLANET SIZE (LINES / WHOLE DISC)
10^5 2 3 4 5 6 7 8 9 10^6 2 3 4 5 6 7 8 9 10^7
DISTANCE FROM PLANET CENTER TO SPACECRAFT (km)

Figure 1

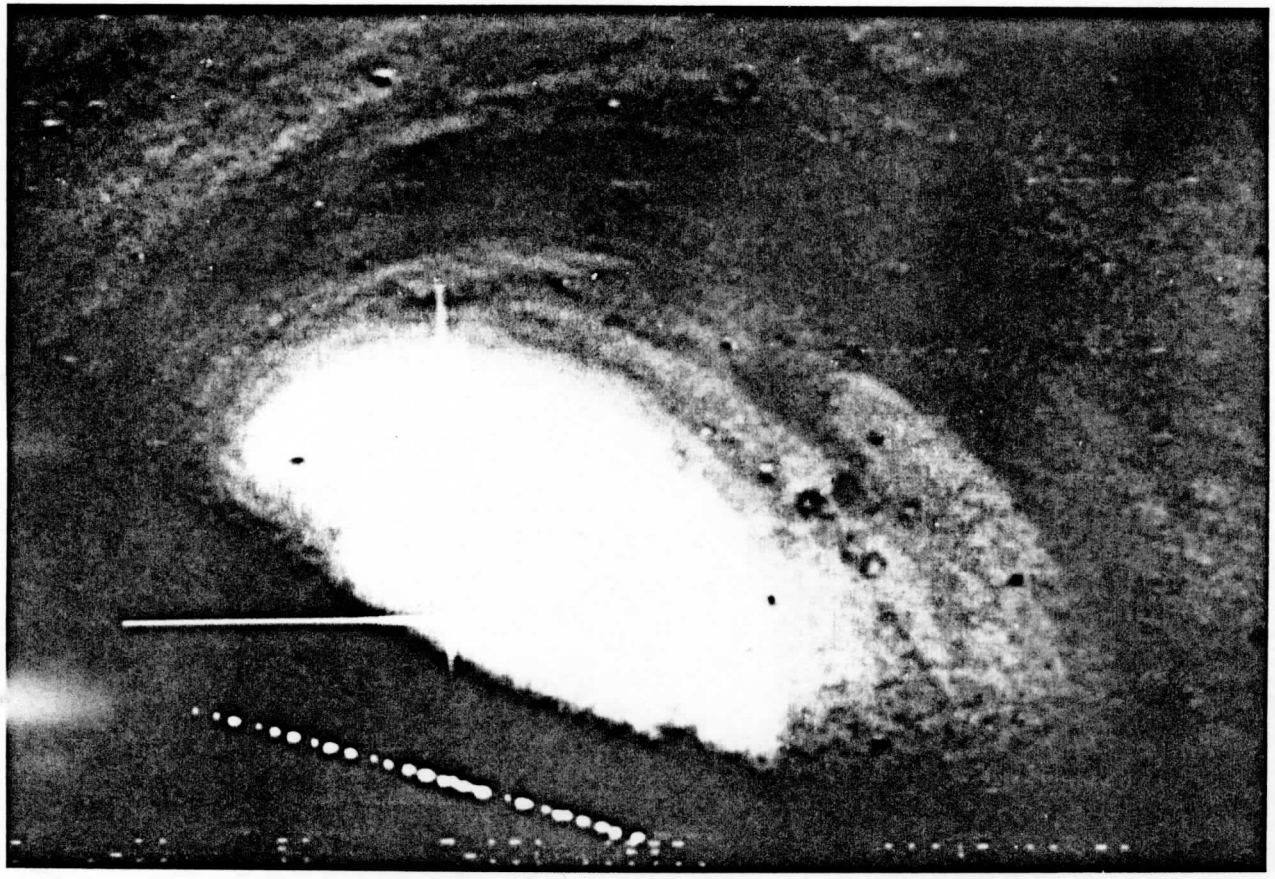

Figure 2

Figure 3

VENUS

POLAR STEREOGRAPHIC PROJECTION NORMALIZED VERSION

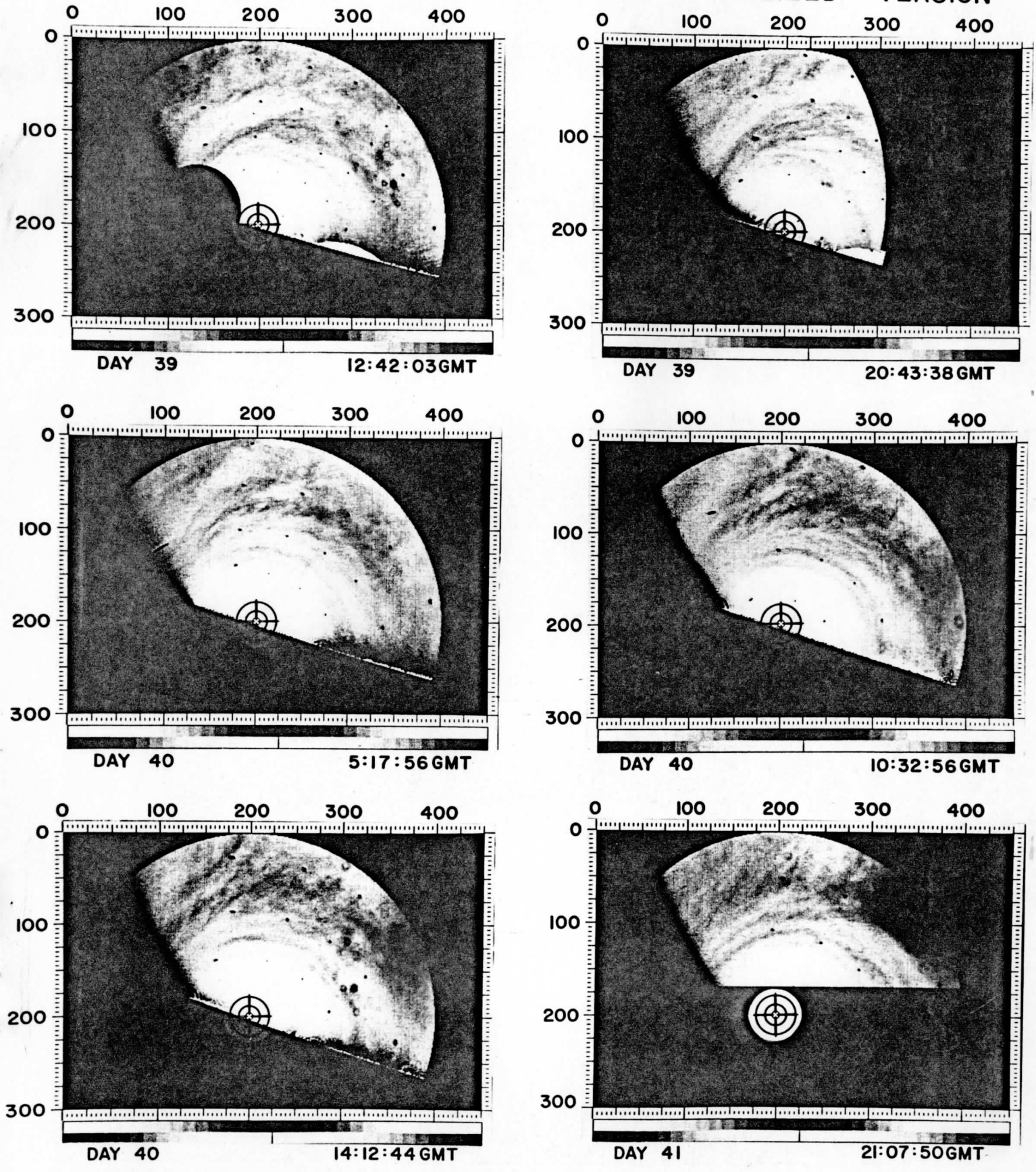

Figure 4

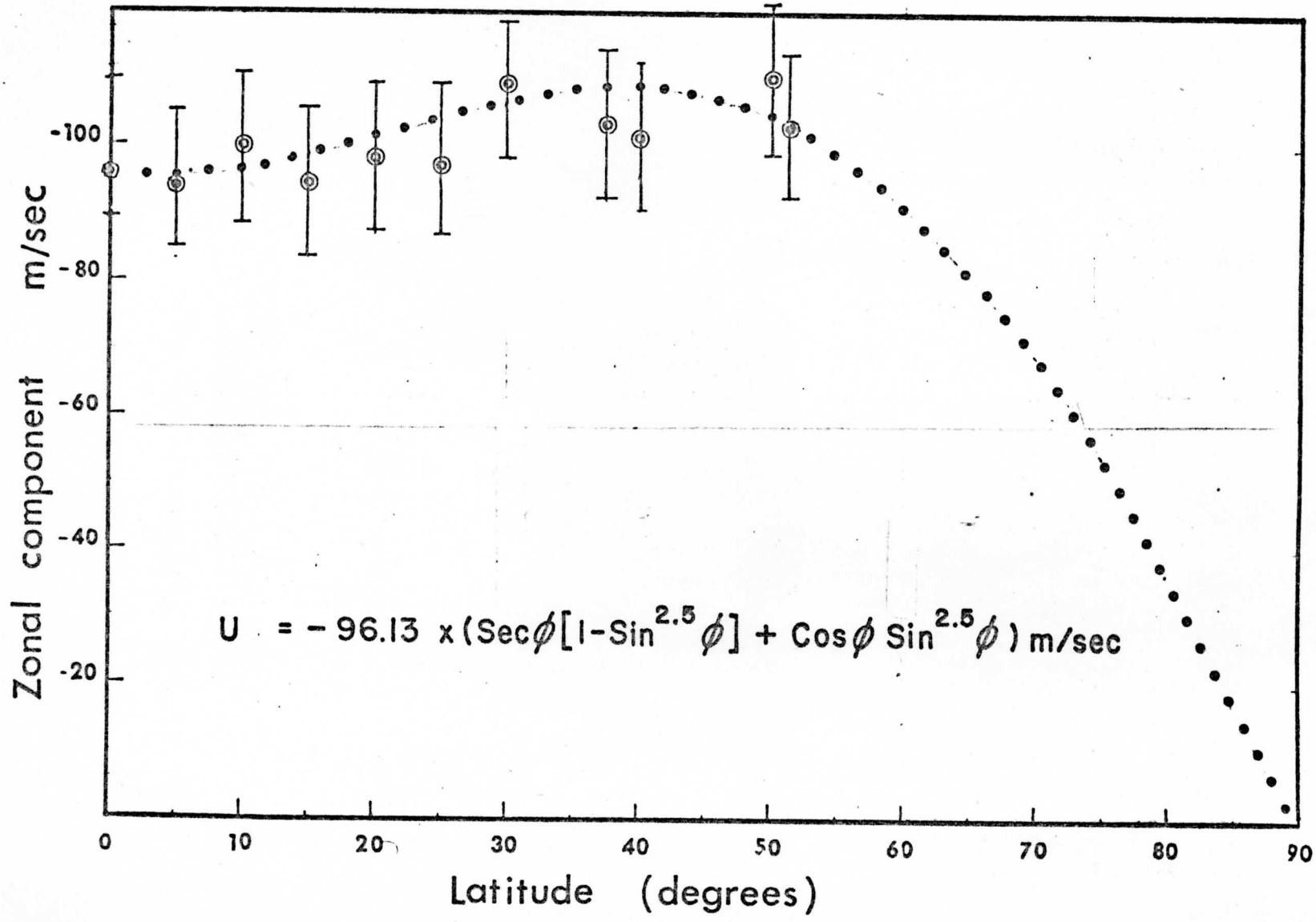

Figure 5 right

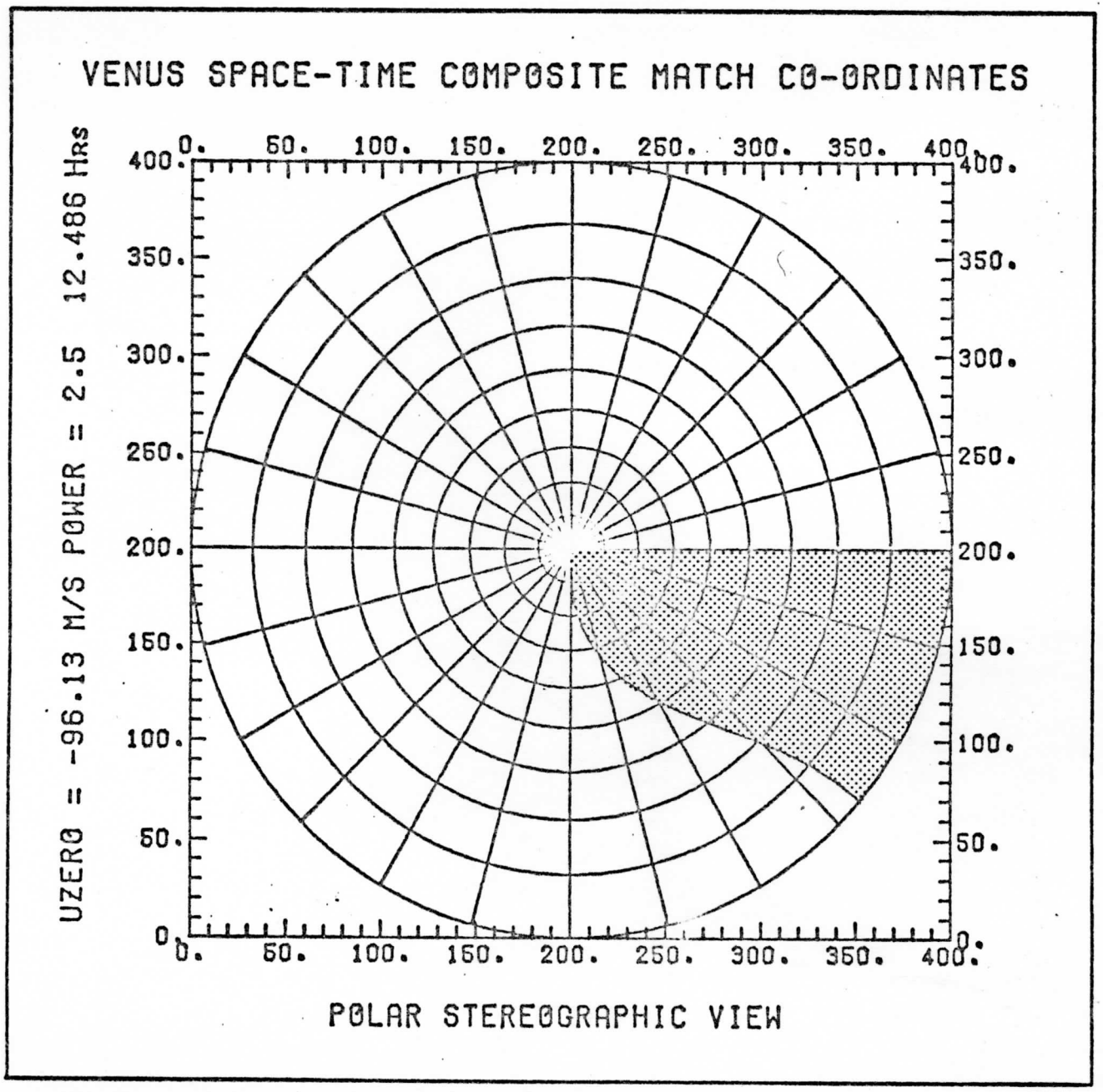

Figure 5 left

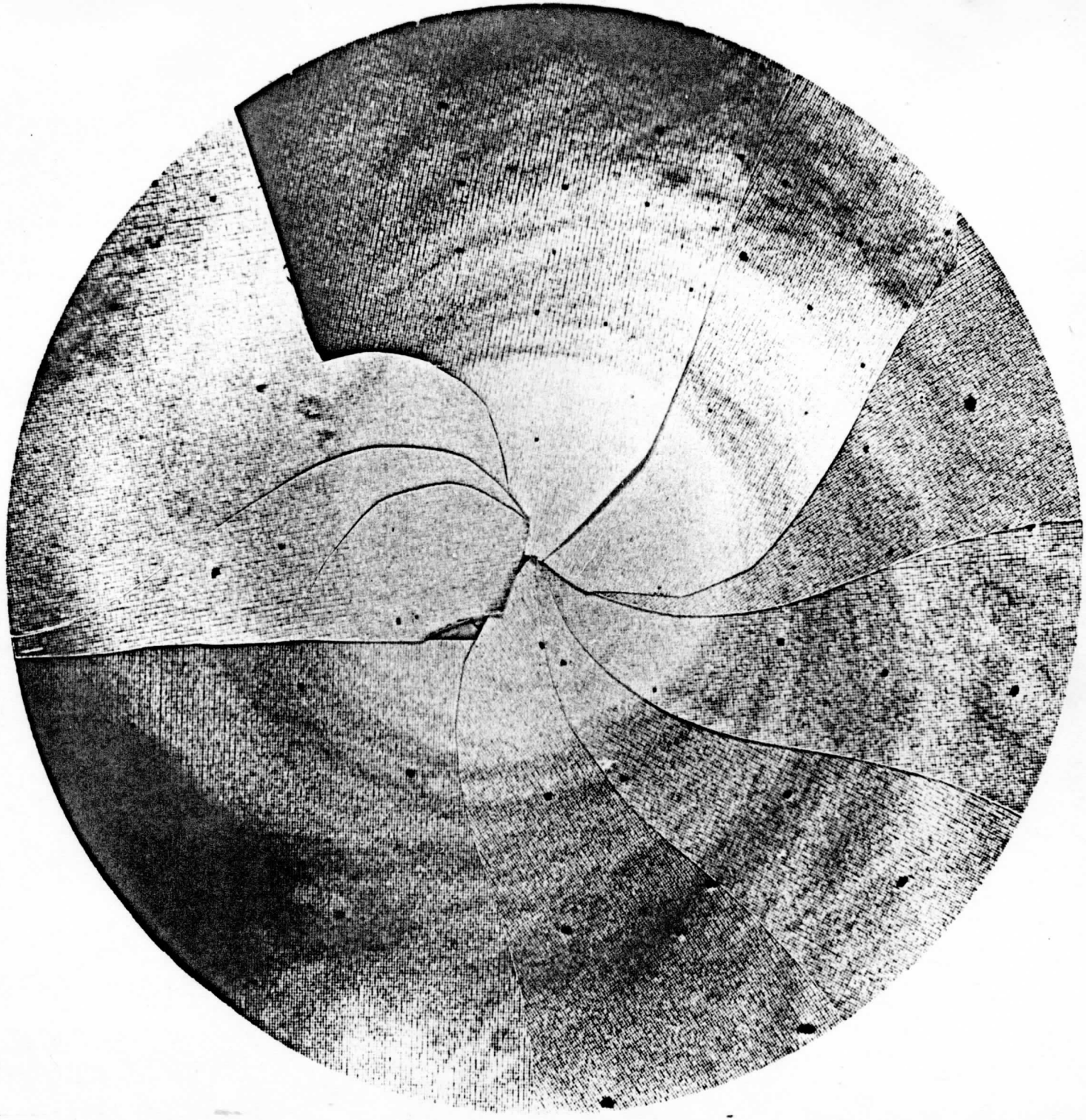

Figure 6

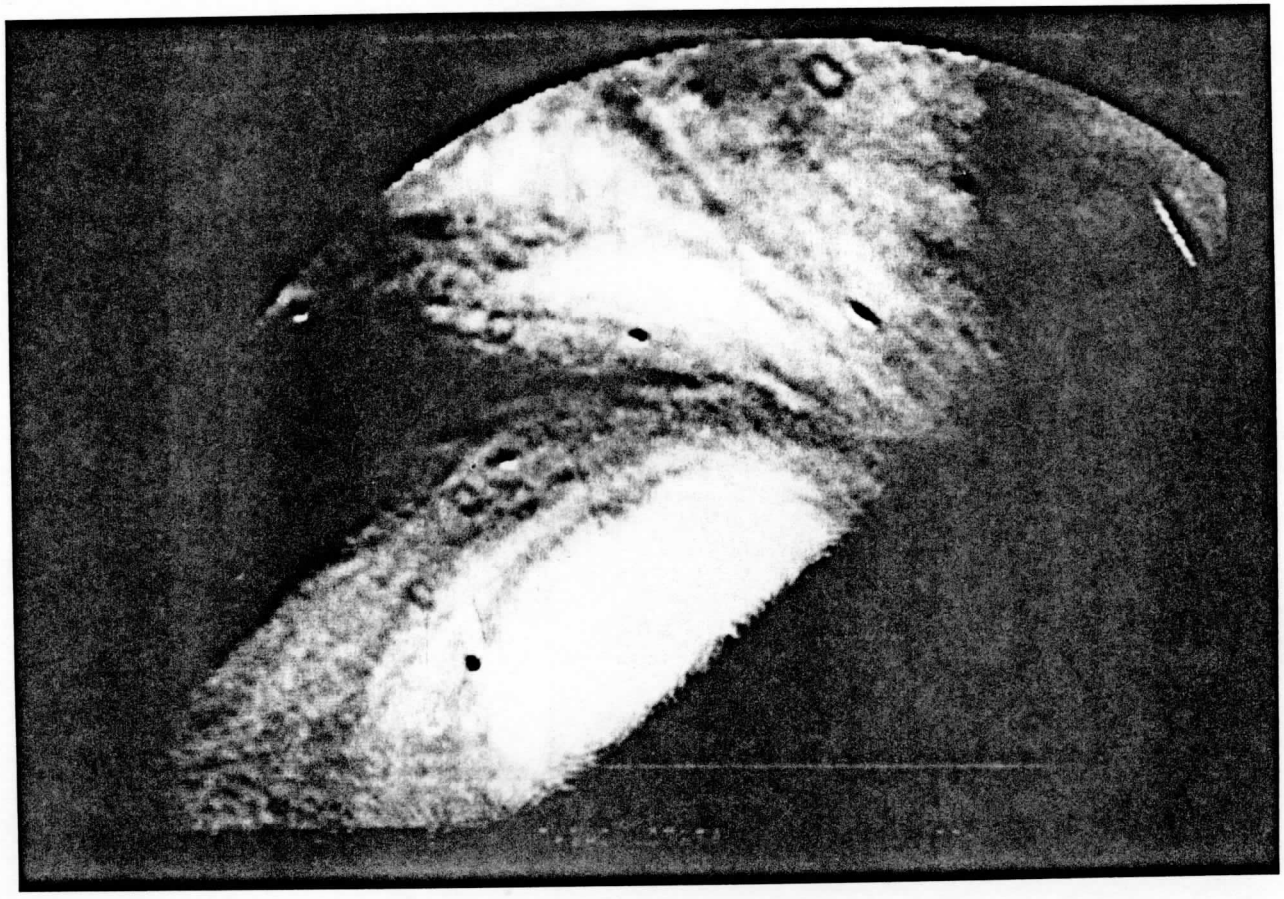

Figure 7

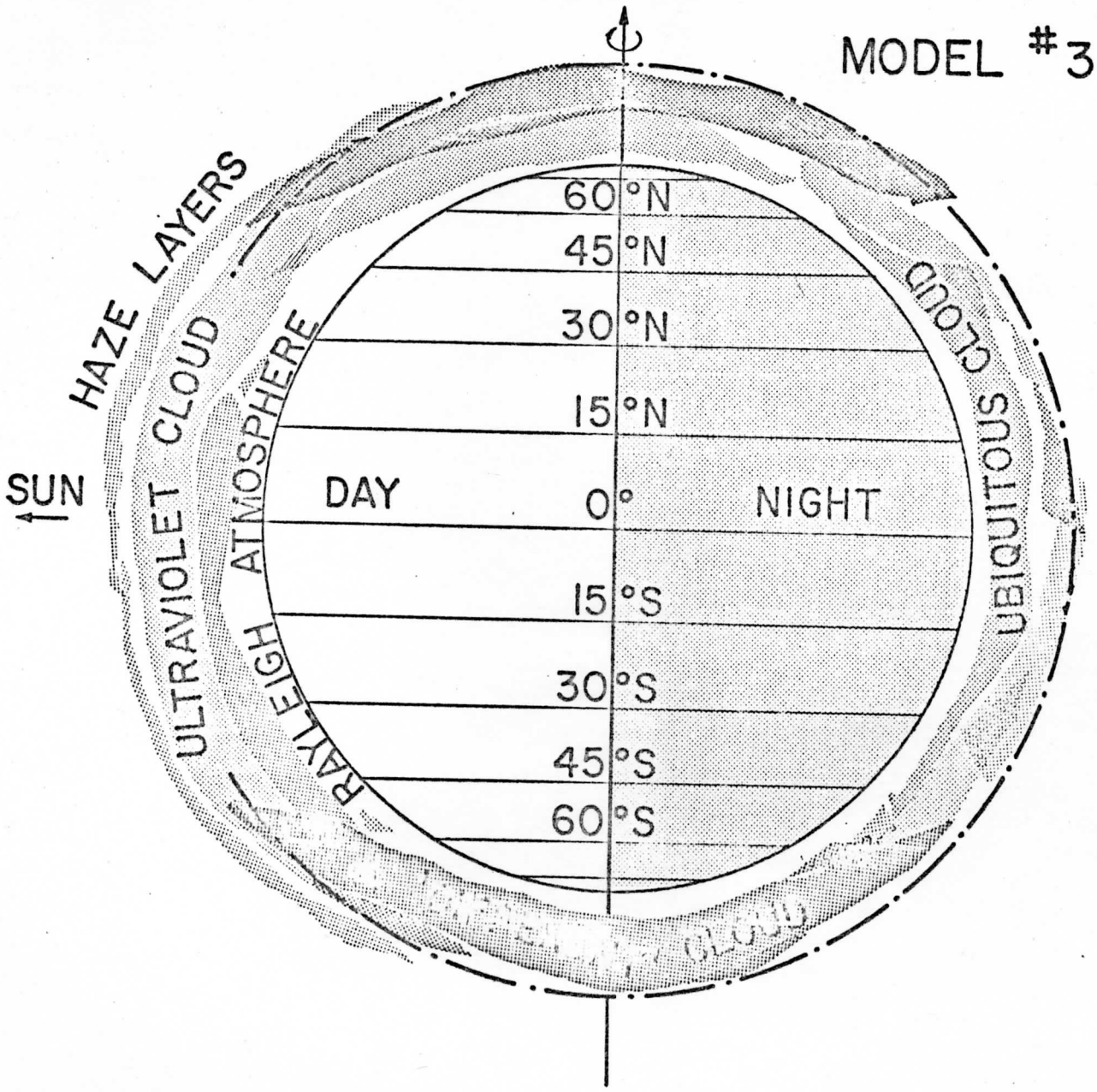
MODEL #3
HAZE LAYERS
ULTRAVIOLET CLOUD
RAYLEIGH ATMOSPHERE
UBIQUITOUS CLOUD
SUN
DAY
NIGHT
60°N
45°N
30°N
15°N
0°
15°S
30°S
45°S
60°S

Figure 8a

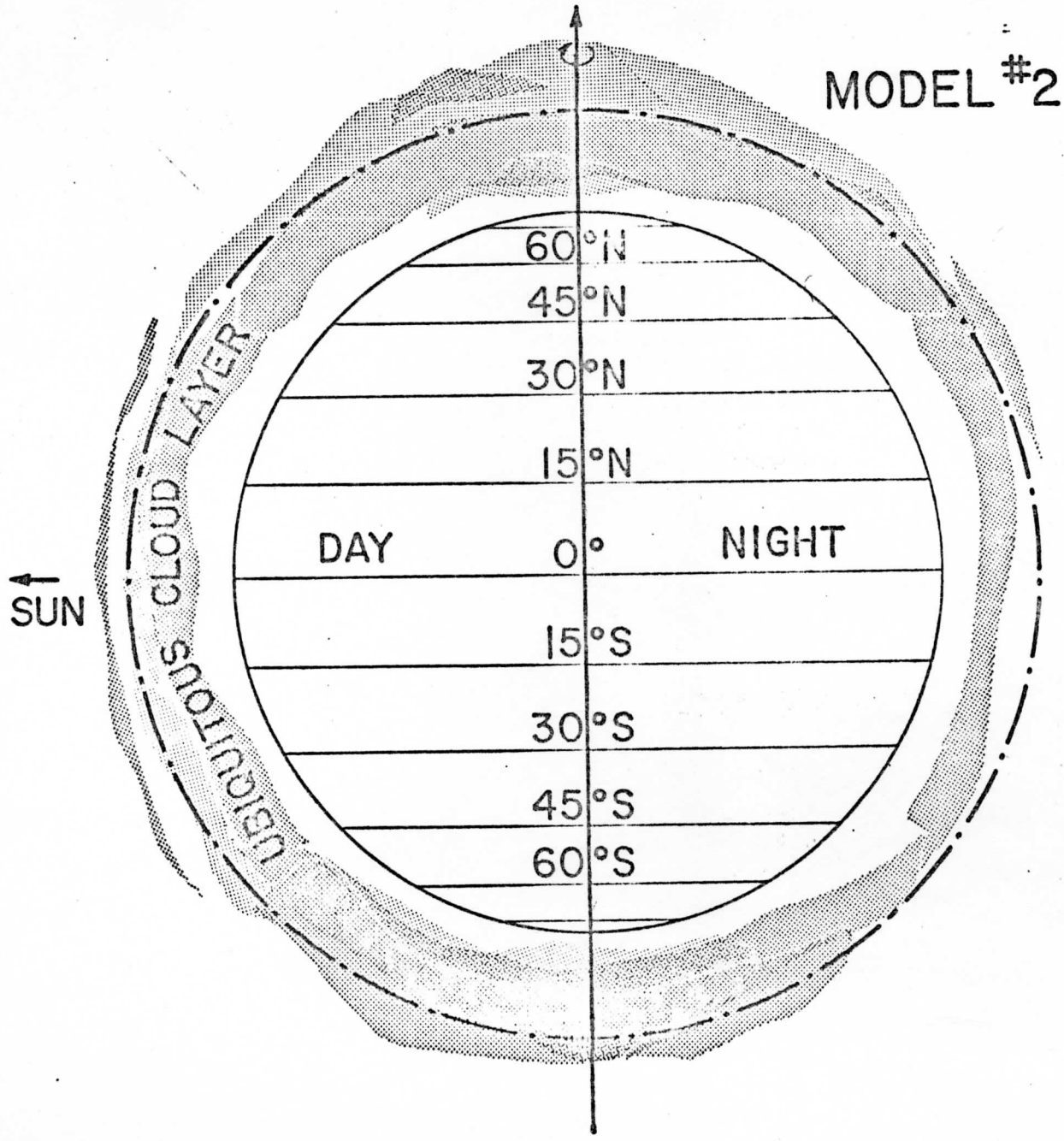
MODEL #2
60°N
45°N
30°N
15°N
DAY
0°
NIGHT
15°S
30°S
45°S
60°S
SUN
HOMOGENEOUS CLOUD LAYER

Figure 8b

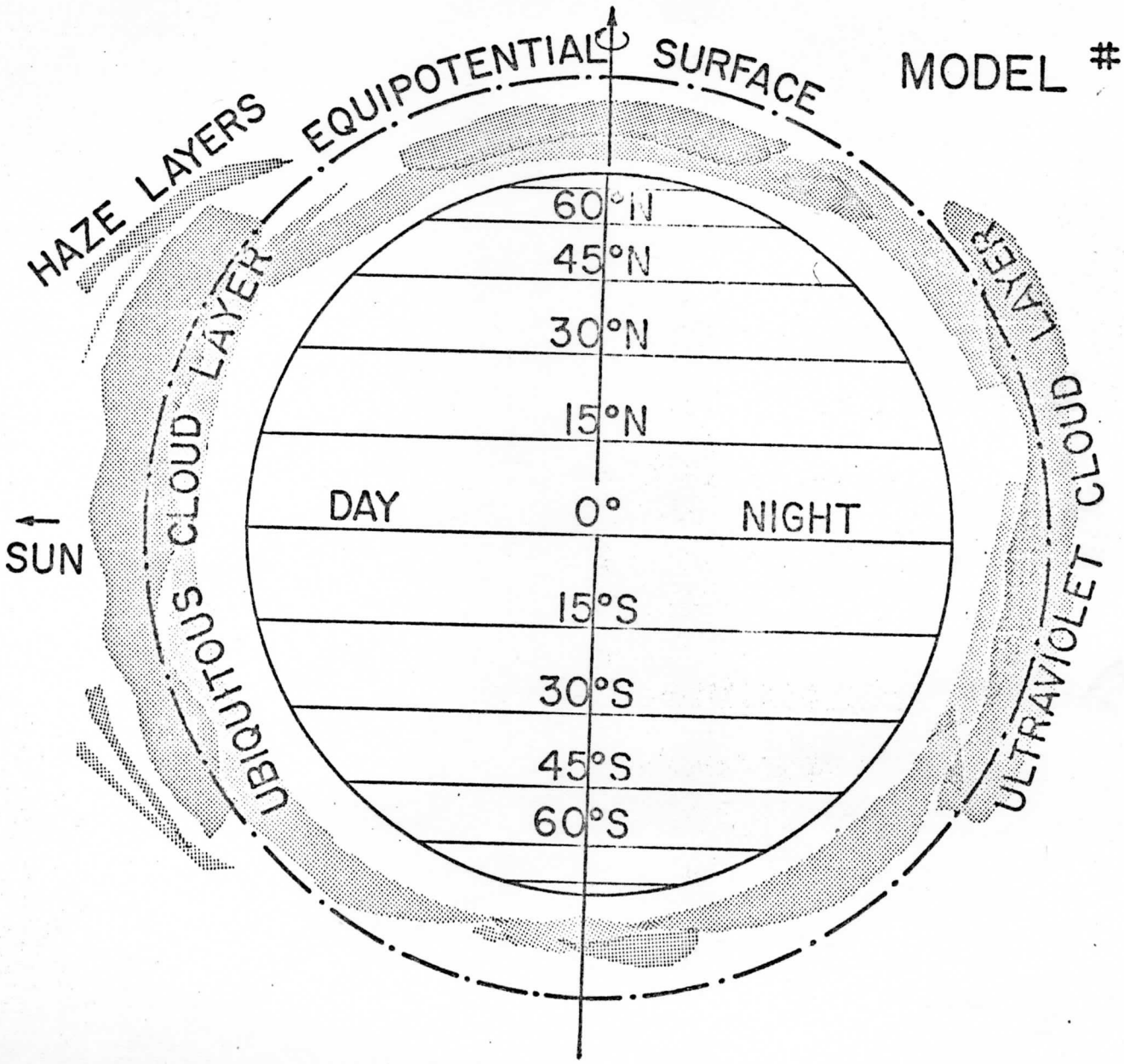
MODEL # 1
EQUIPOTENTIAL SURFACE
HAZE LAYERS
UBIQUITOUS CLOUD LAYER
ULTRAVIOLET CLOUD LAYER
60°N
45°N
30°N
15°N
DAY
0°
NIGHT
SUN
15°S
30°S
45°S
60°S

Figure 8c